

DIAMOND-BLACKFAN ANEMIA

Single-cell profiling of human bone marrow progenitors reveals mechanisms of failing erythropoiesis in Diamond-Blackfan anemia

Deena Iskander¹, Guanlin Wang^{2,3}, Elisabeth F. Heuston⁴, Chrysi Christodoulidou¹, Bethan Psaila³, Kanagaraju Ponnusamy¹, Hongwei Ren¹, Zeinab Mokhtari^{5,6}, Mark Robinson¹, Aristeidis Chaidos¹, Pritesh Trivedi⁷, Nikolaos Trasanidis¹, Alexia Katsarou¹, Richard Szydlo¹, Carmen G. Palii⁵, Mehmood H. Zaidi¹, Qais Al-Oqaily¹, Valentina S. Caputo^{1,8}, Anindita Roy^{3,9}, Yvonne Harrington¹⁰, Leena Karnik¹⁰, Kikkeri Naresh⁷, Adam J. Mead³, Supat Thongjuea², Marjorie Brand^{5,11}, Josu de la Fuente^{1,10}, David M. Bodine^{4*}, Irene Roberts^{3,9*}, Anastasios Karadimitris^{1*†}

Ribosome dysfunction underlies the pathogenesis of many cancers and heritable ribosomopathies. Here, we investigate how mutations in either ribosomal protein large (RPL) or ribosomal protein small (RPS) subunit genes selectively affect erythroid progenitor development and clinical phenotypes in Diamond-Blackfan anemia (DBA), a rare ribosomopathy with limited therapeutic options. Using single-cell assays of patient-derived bone marrow, we delineated two distinct cellular trajectories segregating with ribosomal protein genotypes. Almost complete loss of erythroid specification was observed in *RPS*-DBA. In contrast, we observed relative preservation of qualitatively abnormal erythroid progenitors and precursors in *RPL*-DBA. Although both DBA genotypes exhibited a proinflammatory bone marrow milieu, *RPS*-DBA was characterized by erythroid differentiation arrest, whereas *RPL*-DBA was characterized by preserved GATA1 expression and activity. Compensatory stress erythropoiesis in *RPL*-DBA exhibited disordered differentiation underpinned by an altered glucocorticoid molecular signature, including reduced *ZFP36L2* expression, leading to milder anemia and improved corticosteroid response. This integrative analysis approach identified distinct pathways of erythroid failure and defined genotype-phenotype correlations in DBA. These findings may help facilitate therapeutic target discovery.

INTRODUCTION

Somatic or germline ribosomal protein (RP) gene mutations underpin the pathogenesis of several cancers and inherited bone marrow failure syndromes (1). Diamond-Blackfan anemia (DBA) is a rare heritable ribosomopathy (2) characterized by anemia, multisystem congenital abnormalities, and cancer predisposition (3). Corticosteroids are the only widely used class of drugs in DBA (4), but fewer than half of patients respond (5, 6); the remainder require red cell transfusions or allogeneic bone marrow transplantation. About 75% of cases of DBA are caused by heterozygous mutations in individual genes encoding proteins that comprise the large 60S (*RPL*) or small

40S (*RPS*) ribosomal subunit (6, 7). Selective defects in erythropoiesis in DBA are associated with aberrant ribosome biogenesis and activation of p53-dependent apoptotic pathways (8). We previously used samples from individuals with DBA to elucidate the immunophenotypes of early and late erythroid progenitors (EPs), which correspond to functionally defined burst-forming unit (BFU-e) and colony-forming unit (CFU-e) erythroid (E) colonies, respectively (9, 10). Thus, hematopoiesis in DBA is a useful, accessible model for understanding erythropoiesis and the role of the ribosome in cell fate decisions and differentiation dynamics.

Impaired translation or transcription of the master erythroid-megakaryocyte (MK) transcription factor GATA1 (11) due to defective ribosome biogenesis (12) and excess heme toxicity (13, 14) has been suggested as a unifying mechanism of erythroid failure across DBA genotypes. However, inconsistent findings from human model cellular systems and cell lines (4, 14–16) are yet to be reconciled, and it remains unclear whether additional mechanisms may contribute to erythroid failure in DBA (17). Furthermore, although the diagnostic criteria of DBA include presentation in infancy with virtually no mature bone marrow erythroblasts (EBs) (3), atypical presentations in later life with milder hematological manifestations are not uncommon (18–22). The mechanisms underpinning these heterogeneous clinical phenotypes are yet to be elucidated.

Here, we delineate the cellular and molecular landscape of *RPS*-DBA and *RPL*-DBA using primary bone marrow samples from patients. To mitigate potential confounding effects of comparing different cellular differentiation stages in healthy and diseased tissue

¹Centre for Haematology, Department of Immunology and Inflammation, Imperial College London, London W12 0NN, UK. ²Medical Research Council (MRC) Weatherall Institute of Molecular Medicine (WIMM) Centre for Computational Biology, University of Oxford, Oxford OX3 9DS, UK. ³Medical Research Council (MRC) Molecular Haematology Unit, MRC Weatherall Institute of Molecular Medicine, NIHR Biomedical Research Centre, University of Oxford, Oxford OX3 9DS, UK. ⁴Hematopoiesis Section, National Human Genome Research Institute, National Institutes of Health, Bethesda, MD 20892-442, USA. ⁵Ottawa Hospital Research Institute, 501 Smyth Box 511, Ottawa, ON K1H 8L6, Canada. ⁶Department of Medicine II, Würzburg University Hospital, Interdisciplinary Center for Clinical Research (IZKF), Laboratory for Experimental Stem Cell Transplantation, Würzburg, Germany. ⁷Department of Histopathology, Imperial College Healthcare Trust, Du Cane Road, London W12 0HS, UK. ⁸School of Applied Sciences, London South Bank University, London SE1 0AA, UK. ⁹Department of Paediatrics, Children's Hospital, John Radcliffe, University of Oxford, Oxford OX3 9DU, UK. ¹⁰Department of Paediatrics, Imperial College Healthcare Trust, St Mary's Hospital, Praed Street, London W2 1NY, UK. ¹¹Department of Cellular and Molecular Medicine, University of Ottawa, 501 Smyth Road, Ottawa, ON K1H 8L6, Canada.

*Corresponding author. Email: a.karadimitris@imperial.ac.uk (A.K.); irene.roberts@paediatrics.ox.ac.uk (I.R.); tedyaz@nhgri.nih.gov (D.M.B.)

†Lead contact.

and to overcome limited EP numbers in DBA, we used single-cell transcriptomics [single-cell RNA sequencing (scRNA-seq)] of hematopoietic stem and progenitor cells (HSPCs) (23). Using this unbiased approach, we specifically aimed to elucidate the phenotypic and functional differences between *RPS*-DBA and *RPL*-DBA erythropoiesis, the mechanisms of erythroid failure, and their relationship with divergent clinical phenotypes.

RESULTS

Severe impairment of erythroid lineage specification is observed in bone marrow from patients with *RPS*-DBA but not *RPL*-DBA

To define the landscape of DBA hematopoiesis, we performed scRNA-seq of bone marrow CD34⁺ lineage (Lin)⁻ HSPCs using the 10x Genomics chromium platform (Fig. 1A). We studied six patients with red cell transfusion-dependent DBA (aged 2 to 19 years) with mutations in three of the four most common DBA genes [*RPS19* (*n* = 3), *RPL11* (*n* = 1), and *RPL5* (*n* = 2)] and three healthy donors (aged 3 to 17 years) (data file S1). High-quality sequencing data were obtained for all donors, and after quality control, 41,415 of 45,888 HSPCs were carried forward for analysis (table S1). All cells were integrated and subjected to donor correction by Harmony (24). Unsupervised clustering by the Louvain method identified 19 distinct clusters (Fig. 1B and fig. S1, A and B). We used the most highly expressed marker genes (data file S2) to assign cell lineage identity to clusters and confirmed their fidelity by projecting marker genes onto multiple published scRNA-seq datasets related to hematopoiesis (fig. S2) (25–29). Cell type annotation was further verified by calculating lineage gene scores using six gene sets comprising highly lineage-specific canonical markers (23, 30): E and EP; MK and MK progenitors (MKP); myeloid and monocyte/macrophage/neutrophil progenitors (MyP); lymphoid (Ly) and Ly progenitors (LyP); eosinophil, mast cell, and basophil progenitors (EoMBP); and hematopoietic stem cell/multipotent progenitor (HSC/MPP) (fig. S3A and data file S3). Differentiation trajectories were studied by ordering cells in gene expression space using force-directed graphs (FDGs) superimposed with lineage signature gene sets (Fig. 1C). This confirmed known lineage branching relationships from immature HSC/MPP to either committed LyP/MyP or EP/MKP/EoMBP (fig. S3B) (28, 31). Visualization by circos plots colored by donor type and enumeration of transcriptionally defined progenitor populations (Fig. 1B) revealed two divergent cellular patterns in DBA that segregated with genotype (Fig. 1D and fig. S3C): selective loss of EP and MKP in *RPS*-DBA but preservation of these progenitors in *RPL*-DBA, along the same cell state structure as normal bone marrow.

To independently validate the scRNA-seq findings, we used multiparameter flow cytometry of the bone marrow CD34⁺Lin⁻ compartment of 23 normal controls and 25 patients with DBA with six of the most common DBA genotypes (table S2 and data file S1) (6, 32). This confirmed the marked reduction in immunophenotypic CD38⁺ and CD38⁻ EP and MKP, defined as Lin⁻CD34⁺CD45RA⁻CD71⁺ (4, 23, 33), in *RPS*-DBA, whereas EP and MKP were largely preserved in *RPL*-DBA (Fig. 1, E and F). The frequencies of other transcriptionally defined HSPC subsets (Fig. 1D) or immunophenotypically defined granulocyte-macrophage progenitors, lymphoid-primed multipotent progenitors, or HSC/MPP (fig. S3D) (34) were not altered, and the frequency of CD34⁺ cells in bone marrow mononuclear

cells (BMMNCs) from all DBA genotypes was similar to control pediatric bone marrow (fig. S3E). Together, these findings suggest that, in *RPS*-DBA, there is depletion of EP and MKP downstream of the EP/MKP versus EoMBP fate decision point, whereas in *RPL*-DBA, EP and MKP are relatively preserved.

EP trajectories are distinct in primary human HSPCs isolated from patients with *RPS*-DBA and *RPL*-DBA

To refine lineage relationships within EP and MKP in more detail, we performed further Louvain subclustering of the 6380 EP and MKP cells in aggregate (Fig. 2, A and B). Inspection of the genes marking four EP and MKP subclusters (Fig. 2B and data file S4) showed that subcluster 1 was enriched for genes marking early erythroid development (*CSF2RB*); subcluster 2 for MKP genes; subcluster 3 for the erythroid differentiation hemoglobin (*HB*) genes and their *AHSP* chaperone (35); and subcluster 4 for erythroid and cell cycle control genes (*AURKB*).

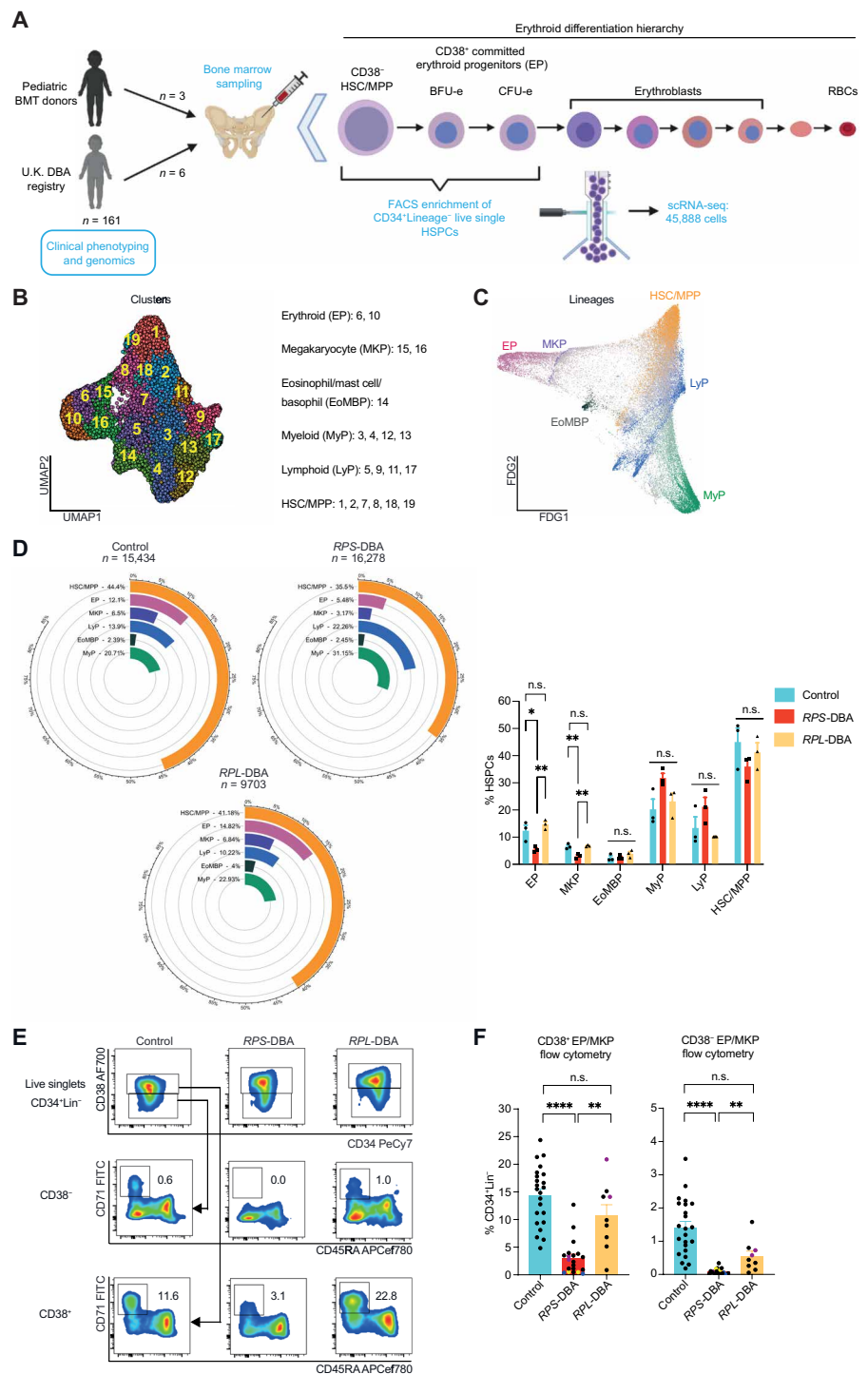
Next, we used previously published single-cell transcriptomic and proteomic data of murine and human HSPCs (31, 36) to better understand the developmental relationship between the EP and MKP clusters. We focused on expression of key E and MK transcription factors (Fig. 2C and fig. S4, A and B), specifically, *GATA2* as an early EP (EEP or BFU-e) marker down-regulated at the late EP (LEP or CFU-e) stage (9, 37), *GATA1* up-regulated from EEP to LEP and *KLF1* and *FLI1*, antagonizing one another to determine E versus MK cell fates (36). This allowed us to predict that, in normal bone marrow, cluster 1 corresponded to EEP (balanced *GATA1* and *GATA2* expression); cluster 2 to MKP; cluster 3 to LEP (higher expression of *GATA1* and *KLF1* and lower *GATA2*); and cluster 4 to the proliferative EP fraction (E cycling: higher expression of *AURKB* and *MKI67*), previously shown to precede irrevocable erythroid commitment (31, 38). This was supported by the differential expression patterns of additional genes, such as *CD34* in EEP and E cycling and *TFR2*, *TFR3* (*CD71*), *GYPB*, and *ENG* (*CD105*) in LEP (Fig. 2C). Expression of EP or MKP genes superimposed on FDGs (fig. S4A) further validated our subclustering analysis.

Next, we quantified the number of cells in each transcriptional subcluster in DBA bone marrow with reference to total CD34⁺ cells. All EP and MKP subclusters were depleted in *RPS*-DBA (Fig. 2D). By contrast, EP and MKP subcluster frequencies in *RPL*-DBA were similar to normal bone marrow, suggesting distinct erythroid cellular trajectories according to DBA genotype (Fig. 2D). To specifically address the transcriptional basis of these differences, we analyzed E and MK transcription factor expression. Compared to controls, *GATA2* (but not *GATA1* or *KLF1*) was increased in all *RPS*-DBA subclusters and *FLI1* expression was increased in EEP and LEP (Fig. 2C), consistent with block in erythroid commitment. In contrast, reduced expression of *FLI1* was identified in *RPL*-DBA EEP, E cycling, and MKP. Exploring this further by charting *FLI1* and *KLF1* coexpression in single EP or MKP cells (Fig. 2E) revealed prevailing expression of *KLF1* over *FLI1* in a higher fraction of EP and MKP in *RPL*-DBA, consistent with a predominant, *KLF1*-driven, erythroid program.

We corroborated these findings by measuring the frequency of immunophenotypic EEP, intermediate EP, and LEP (9, 38) in additional bone marrow samples. Although there was progressive reduction in all stages of EP development in *RPS*-DBA, these populations were preserved in *RPL*-DBA. This divergence was particularly notable in LEP, which were virtually absent in *RPS*-DBA (Fig. 2, F and G).

Fig. 1. Erythroid lineage specification is preserved in bone marrow isolated from patients with RPL-DBA but not RPS-DBA. (A) Study design for single-cell RNA sequencing (scRNA-seq) experiments showing source of DBA and healthy bone marrow from allogeneic bone marrow transplant (BMT) donors. Erythroid hierarchy depicted as follows: hematopoietic stem (HSC) and multipotent (MPP) cells, within the CD34⁺CD38⁻ bone marrow subfraction, mature into committed EEP (BFU-e) and LEP (CFU-e), within the CD34⁺CD38⁺ bone marrow subfraction. These then differentiate into CD34⁻ EB, which enucleate to form reticulocytes that egress into the peripheral blood and form red blood cells (RBCs).

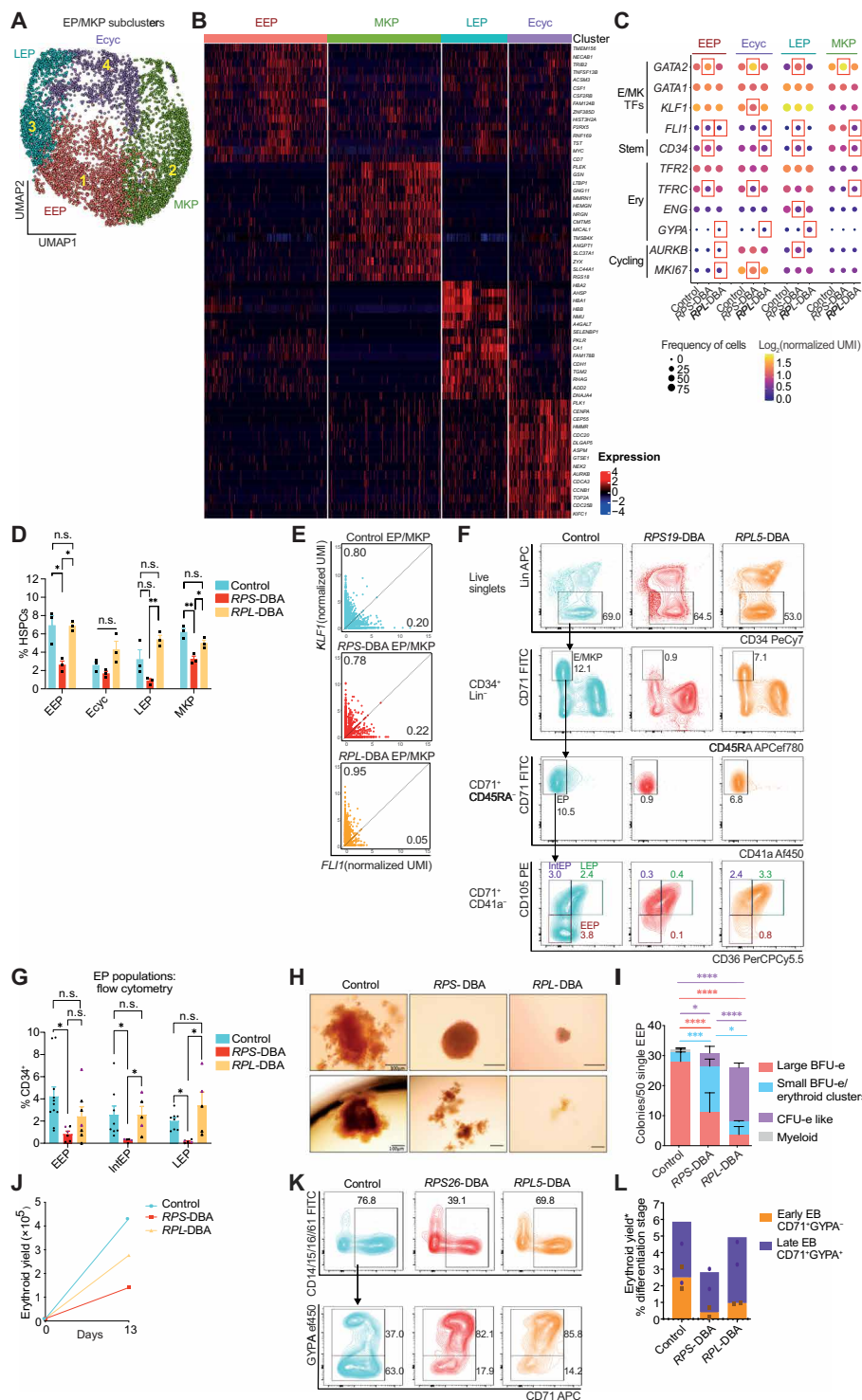
(B) Uniform Manifold Approximation and Projection (UMAP) embedding of 19 cell clusters generated by Louvain clustering of 41,415 CD34⁺Lineage⁻(Lin)⁻ HSPCs from nine donors in aggregate: control (15,434 cells; three donors) and DBA (25,981 cells; six donors, three RPS-DBA and three RPL-DBA). Cell type annotation of each cluster is also shown. (C) Force-directed graph (FDG) embedding of six major hematopoietic cell types in control and DBA cells is shown, colored by key marker gene sets (data file S3 and fig. S3A). Gray cells represent uncommitted cell types or cells expressing greater than one lineage gene set. (D) Circos plots (left) and a bar plot (right) depict proportions of cells in each of six cell types identified by scRNA-seq among total CD34⁺Lin⁻ cells by donor type. (E) The flow cytometry gating strategy used to identify CD71⁺CD45RA⁻ EP and MKP cells in the CD38⁻ immature and CD38⁺ mature subcompartments of bone marrow CD34⁺ cells is shown. Frequencies are shown as percent of CD34⁺Lin⁻ cells. AF700, Alexa Fluor 700; PE-Cy7, phycoerythrin-cyanine 7; FITC, fluorescein isothiocyanate; APC-ef780, allophycocyanin efluor 780. (F) Cumulative data show the frequency of BFU-e and MKP within CD34⁺Lin⁻CD71⁺CD38⁻ bone marrow subfraction and of BFU-e, CFU-e, and MKP within CD34⁺Lin⁻CD71⁺CD38⁺ bone marrow subfraction (n = 23 control, 20 RPS-DBA, and 9 RPL-DBA bone marrow samples). Colored symbols depict two bone marrow samples from the same patient collected at least 1 year apart. Bars show means ± SEM of biological replicates. *P < 0.05; **P < 0.01; ****P < 0.0001; n.s., not significant. Groups were compared by a one-way ANOVA with Holm-Sidak's correction (D) or a Kruskal-Wallis with Dunn's multiple comparisons test (F).



To determine the functional erythroid potential of RPS-DBA versus RPL-DBA EP, we plated stage-matched single EEP [purified by fluorescence-activated cell sorting (FACS)] in erythropoietin (Epo)-supported semisolid erythroid cultures. Although the clonogenic efficiency of DBA samples was normal, there were notable qualitative differences in colonies. In RPS-DBA, these mainly consisted of small BFU-e-forming loose clusters (E clusters) rather than the typical large BFU-E with tight bursts formed by normal control EEP, as previously described (9). By contrast, RPL-DBA EEP (Fig. 2, H and I) and total CD34⁺ (fig. S4C) generated highly abnormal, small CFU-e-like colonies of less than 100 cells. Giemsa staining of single erythroid colonies confirmed the presence of more mature EB in abnormal DBA colonies

versus normal BFU-e (fig. S4D), suggesting disordered differentiation. Commensurate with this, expression of the differentiation-associated gene *GYP A* was higher in RPL-DBA LEP than in their normal or RPS-DBA counterparts (Fig. 2C). Furthermore, in longitudinal Epo-supported liquid cultures, RPL-DBA bone marrow HSPCs generated a higher erythroid yield than RPS-DBA (Fig. 2J) with similar rates of apoptosis (fig. S4E) but with a higher fraction

Fig. 2. Features of the EP trajectory differentiate RPS-DBA and RPL-DBA primary human HSPCs. (A) A UMAP aggregate is shown of all control and DBA EP and MKP cells ($n = 6380$) depicting four distinct subclusters. (B) A heatmap is shown for the 15 top differentially expressed genes (row labels, right) for each of the four EP and MKP subclusters (color-coded columns). Labels across the top indicate cluster assignment according to their marker genes: early erythroid progenitors (EEP), cycling EP (Ecyc), late erythroid progenitors (LEP), and megakaryocyte progenitors (MKP). (C) A bubble plot shows the average expression of individual genes (depicted by color) and the fraction of cells expressing that gene (depicted by bubble size) within EP and MKP subclusters from control, RPS-DBA, or RPL-DBA bone marrow. Boxes highlight differentially expressed genes with $\log_2FC > 0.4$ and adjusted P value < 0.05 . TF, transcription factor; UMI, unique molecular identifier. (D) A bar plot depicting proportion of cells in each of four EP and MKP clusters among total $CD34^+Lin^-$ cells by donor type is shown. (E) Single-cell coexpression of *KLF1* and *FLI1* is shown for control, RPS-DBA, and RPL-DBA EP, and MKP cells. The diagonal marks cells with equal expression of both genes. The fraction of cells above and below the diagonal line is shown. (F) Representative flow cytometry plots show the gating strategy for $CD71^+CD41a^-$ erythroid progenitors (EP): $CD71^+CD36^-CD105^-$ early (EEP), $CD71^+CD36^+CD105^+$ intermediate (IntEP), and $CD71^+CD105^+CD36^+$ LEPs. Frequencies are shown as percent of total $CD34^+$ cells. (G) The frequency of EP subsets is shown as percent of $CD34^+$ bone marrow in control ($n = 11$ for EEP and $n = 8$ for Ecycling and LEP), RPS-DBA ($n = 6$ for EEP and $n = 5$ for Ecycling and LEP), and RPL-DBA ($n = 7$ for EEP and $n = 5$ for Ecycling and LEP) bone marrow. Purple symbols depict two bone marrow samples from the same patient collected at least 1 year apart. (H) Morphology of colonies generated on days 12 to 14 in methylcellulose medium from single-cell EEP FACS-purified ex vivo from control, RPS-DBA, and RPL-DBA bone marrow is shown. Images are representative of three independent experiments. Scale bars, 100 μm . (I) The frequency and type of hematopoietic colonies generated in methylcellulose from single-cell EEP FACS-purified ex vivo from control, RPS-DBA, and RPL-DBA bone marrow ($n = 3$) are shown. Significant differences in colony types are indicated. (J) Erythroid yield (total cell number multiplied by percent $CD71^+CD14/16/61^-$ cells) is shown from a longitudinal serum-free erythroid liquid culture of FACS-purified $CD34^+Lin^-$ HSPCs from control, RPS-DBA, and RPL-DBA bone marrow ($n = 2$). (K) Flow cytometry analysis of erythroid differentiation stage (characterized by Lin, CD71, and GYPA markers) is shown for EB on day 13 of culture of control, RPS-DBA, and RPL-DBA bone marrow HSPCs. (L) Cumulative data from two independent experiments show the fraction of early and late EB generated multiplied by erythroid yield from control, RPS-DBA, and RPL-DBA bone marrow HSPCs ($n = 2$). Plots show means \pm SEM of biological replicates. * $P < 0.05$; ** $P < 0.01$; *** $P < 0.001$; **** $P < 0.0001$. Groups were compared by a one-way ANOVA with Holm-Sidak's correction. (D), a Kruskal-Wallis with Dunn's multiple comparisons test (G), or a Fisher's exact test (I).



of more differentiated mature EB (Fig. 2, K and L, and fig. S4F), expressing higher amounts of Glycophorin A (GYPA) messenger RNA (mRNA) and protein, compared to control HSPCs (fig. S4, G and H). Furthermore, quantification of cell surface markers and

transcription factors using single-cell cytometry by time of flight (scCyTOF) in an independent RPL5-DBA bone marrow sample revealed lower expression [\log_2 fold change (FC) < -0.4] of CD34 (in MPP2 to PolyEB) and higher expression ($\log_2FC > 0.4$) of CD71 (in

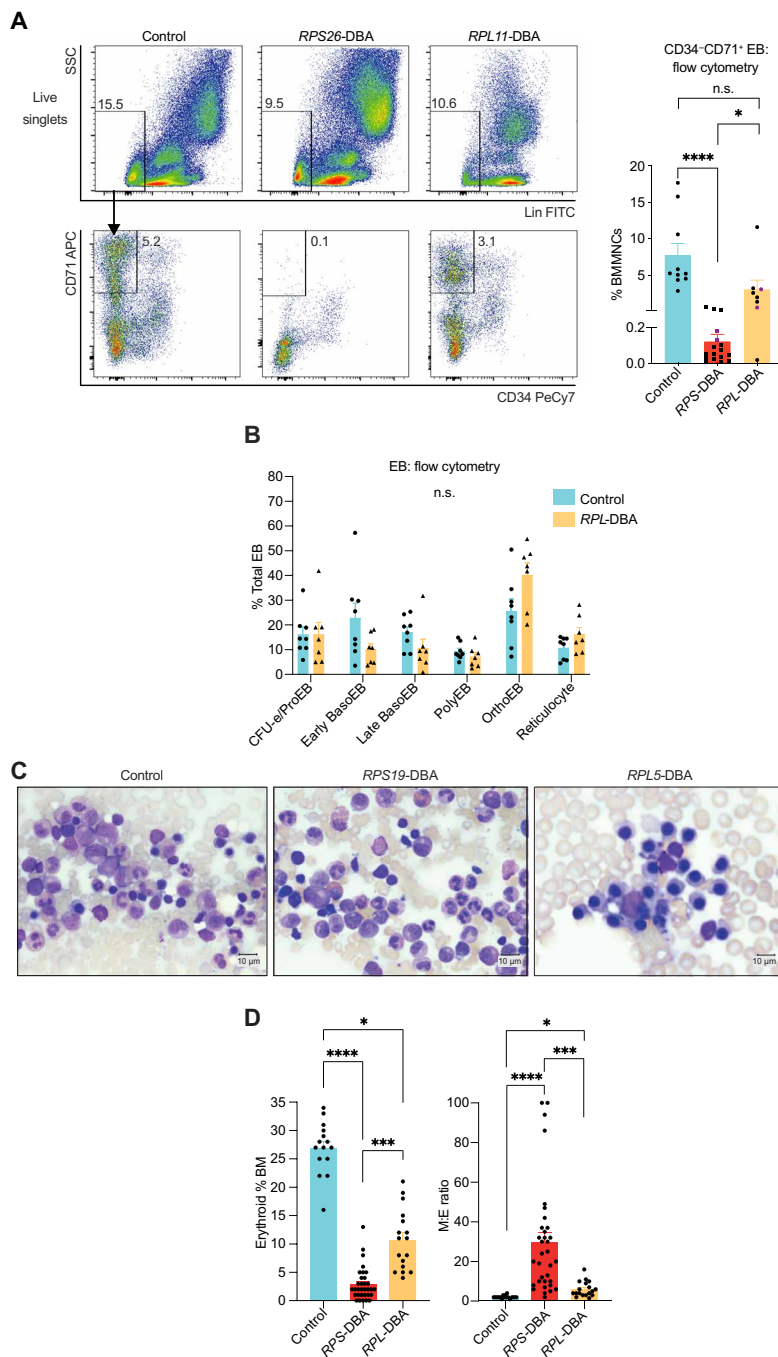


Fig. 3. Phenotypically normal mature EB are observed in *RPL*-DBA in vivo. (A) Representative flow cytometry plots (left) show the frequency of Lin⁻CD34⁻CD71⁺ EB within total BMMNCs. Cumulative data of EB frequencies within total BMMNCs are shown (right) in control ($n = 10$), *RPS*-DBA ($n = 17$), and *RPL*-DBA ($n = 8$) bone marrow. Purple symbols depict two samples from the same patient collected 2 years apart. SSC, side scatter. (B) Frequencies of EB subpopulations were measured by flow cytometry in total MNC derived from control ($n = 8$) and *RPL*-DBA ($n = 7$) bone marrow. (C) Representative morphological appearances are shown for bone marrow aspirates (stained with hematoxylin and eosin) from controls and patients with DBA with a *RPS19* and a *RPL5* mutation. Scale bars, 10 μ m. (D) EB frequencies in total nucleated cells and myeloid-to-erythroid lineage cell ratio (M:E ratio) were measured in bone marrow slide preparations from normal pediatric bone marrow controls ($n = 15$) and patients with *RPS*-DBA ($n = 32$; 34 for M:E) and *RPL*-DBA ($n = 17$; 18 for M:E). Plots show means \pm SEM of biological replicates. * $P < 0.05$; *** $P < 0.001$; **** $P < 0.0001$. Groups were compared by a Kruskal-Wallis with Dunn's multiple comparisons test.

EP and ProEB), CD36, and GYPA (in EP, ProEB, and PolyEB), compared with healthy control counterparts (fig. S5). GATA1 and KLF1 expression was not reduced compared with normal (fig. S5D), supportive of the scRNA-seq data (Fig. 2C). In summary, three complementary assays support the presence of distinct, genotype-associated patterns of erythroid failure in DBA from markedly reduced early erythroid specification in *RPS*-DBA to preservation of BFU-e that are functionally impaired with a distinct transition program through the erythroid differentiation hierarchy in *RPL*-DBA.

Phenotypically normal EB are observed in *RPL*-DBA in vivo

Given that absence of bone marrow EB is one of the required diagnostic criteria of DBA (3), we next investigated whether erythroid differentiation differed between *RPS*-DBA and *RPL*-DBA in vivo. First, we assessed the frequency of Lin⁻CD34⁻CD71⁺ EB in fresh DBA bone marrow samples (Fig. 3A). EB frequency in *RPS*-DBA bone marrow was lower than both normal controls and *RPL*-DBA. To define the in vivo defect more precisely, we used flow cytometry to measure the frequency of the six previously defined phenotypically distinct stages of EB maturation (39) on the basis of CD105 and GYPA expression (fig. S6, A and B). Although there were too few EB for analysis in *RPS*-DBA, we identified all the same stages of EB development in *RPL*-DBA as in control bone marrow (Fig. 3B), supporting relative preservation of the EP to EB developmental trajectory in *RPL*-DBA. We also compared differential cell counts from 52 bone marrow aspirates from patients with transfusion-dependent DBA (fig. S6C) and found that, although EB were reduced in both genotypes compared with controls, there was an about threefold higher erythroid cell frequency and lower myeloid:erythroid ratio in *RPL*-DBA versus *RPS*-DBA bone marrow (Fig. 3, C and D). These findings were consistent across six *RPS*-DBA and four *RPL*-DBA genotypes (fig. S6, D and E, table S2, and data file S1), confirming our finding of preservation of erythroid differentiation beyond the progenitor stage in *RPL*-DBA.

DBA is characterized by glucocorticoid pathway-deficient stress erythropoiesis and glucocorticoids induce *ZFP36L2*-mediated inhibition of erythroid differentiation

To investigate the molecular basis for these differences in erythroid differentiation, first, we confirmed that, in patients with DBA with loss-of-function mutations (data file S1), mRNA expression of the affected RP gene was selectively reduced to about 50% of normal (fig. S7A). We also found that expression of fetal hemoglobin (HbF; *HBG2*) and the fraction of cells expressing *HBG2* were higher in all

three EP populations from both DBA subtypes, compared with normal controls, confirming earlier studies (Fig. 4A) (40). Like *HBG2*, additional markers of stress erythropoiesis, such as *ERFE* and *GDF15* (41, 42), were up-regulated in DBA erythropoiesis (fig. S7B). Moreover, using the area under the curve (AUC_{Cell}) scoring method (43), we found enrichment in DBA EP of a set of genes (data file S3) up-regulated in murine fetal liver, the prototype for stress erythropoiesis (Fig. 4B) (31). Although stress erythropoiesis often occurs at the expense of the output of other lineages in murine models (31), we observed preserved myeloid progenitor frequency and function in *RPL*-DBA (fig. S3D and fig. S4C), consistent with our finding that the stress erythropoiesis signature is present in only a proportion of single cells (Fig. 4A and fig. S7B) and is insufficient to rescue either EP function or anemia in these patients.

To interrogate this further, we considered that exogenous glucocorticoids remain the only medical therapy for DBA. Stress erythropoiesis also requires an endogenous glucocorticoid-dependent transcriptional program that increases erythroid output by favoring EP expansion at the expense of differentiation (44, 45). Consistent with a state of disordered differentiation and as suggested by our *in vitro* data (Fig. 2, K and L, and fig. S4F), we found that expression of erythroid differentiation genes, such as *GYPA*, *AHSP*, and *HB*, was higher in *RPL*-DBA than control (Figs. 2C and 4C). Because transcription of *HBB* and *AHSP* is repressed by the glucocorticoid receptor in the presence of glucocorticoids (45), we hypothesized that the *RPL*-DBA differentiation pattern reflects a failure to appropriately up-regulate the endogenous glucocorticoid-dependent program of stress erythropoiesis in DBA. Consistent with this, using a set of genes up-regulated by glucocorticoids in murine EP (data file S3) (45, 46), we found a reduced glucocorticoid response in all DBA EP subclusters from both *RPL*-DBA and *RPS*-DBA, although the reduction was more pronounced in *RPL*-mutated EP (Fig. 4D). Expression of *ZFP36L2*, a glucocorticoid-responsive gene critical for glucocorticoid-mediated differentiation delay and subsequent enhanced erythroid output in murine fetal liver (46), was reduced in primary DBA cells (Fig. 4E).

To investigate the role of reduced *ZFP36L2* expression in impaired erythropoiesis, we partially knocked-out *RPL11* (residual *RPL11* mRNA, 33 to 48% of unedited controls; fig. S7, C and D) in erythroid K562 cells using clustered regularly interspaced short palindromic repeats (CRISPR)-Cas9 gene editing. Compared to unedited wild-type clones, *ZFP36L2* expression was reduced in *RPL11*-edited K562 cell clones (Fig. 4F) consistent with our data in primary DBA bone marrow cells. Next, as previously identified in murine erythroid cells (46), we found that dexamethasone treatment of *RPL11*-edited and control K562 clones resulted in a time-dependent loss of the cells coexpressing the erythroid differentiation markers *GYPA* and *CD71* (Fig. 4, G to I), commensurate with up-regulation of *ZFP36L2* expression (Fig. 4J). In accordance with this, RNA sequencing (RNA-seq) of *ex vivo* bone marrow stage-matched EB from a patient with *RPL5*-DBA, harvested before and after successful corticosteroid therapy, showed increased *ZFP36L2* but unchanged *RPL5*, *ADA*, and *HBG2* expression (Fig. 4K). Furthermore, lentiviral transduction of *ZFP36L2* complementary DNA (cDNA) into *RPL11*-edited K562 cells (fig. S7E) was sufficient to recapitulate the dexamethasone-induced loss of *GYPA* expression (fig. S7, F and G), resulting in a higher relative frequency of *CD71*⁺*GYPA*⁻ versus *CD71*⁺*GYPA*⁺ cells in both wild-type and *RPL11*-edited K562 cells (Fig. 4, L to N).

P53 activation and bone marrow inflammatory milieu in DBA

Next, we looked for additional pathways dysregulated in DBA and found negative enrichment of the heme pathway in *RPS*-DBA but not *RPL*-DBA EP and activation of p53 in both genotypes (Fig. 5, A and B). We also identified enrichment of inflammatory pathways, including tumor necrosis factor- α (TNF- α)-mediated signaling, interferon- α (IFN- α)-mediated signaling, and IFN- γ -mediated signaling (Fig. 5A), known instigators of stress erythropoiesis (47, 48). Inflammatory responses, IFN- α responses, and IFN- γ responses, but not p53 and TNF- α pathways, were particularly enriched in *RPS*-DBA compared with *RPL*-DBA (Fig. 5B). Inflammation and cytokine-mediated gene networks were enriched throughout the DBA HSPC compartment (fig. S8, A and B), suggesting a generalized bone marrow proinflammatory state linked to RP gene haploinsufficiency. In line with this, we found higher TNF- α and IFN- γ concentrations in DBA than control bone marrow plasma (Fig. 5C) as well as increased intracellular expression of both cytokines in DBA versus control *CD3*⁺ T cells and *CD3*⁻*CD56*⁺ natural killer (NK) cells, but not monocytes, after their *in vitro* activation (fig. S8, C and D).

To provide additional validation of the aberrant erythroid developmental pathways in *RPL*-DBA, we performed bulk RNA-seq of FACS-purified late basophilic EB from the bone marrow of three additional patients with *RPL*-DBA and three age-matched healthy donors (EB are virtually absent in *RPS*-DBA). As expected, expression of the mutated RP gene was selectively reduced by 50% (fig. S8E). Principal component analysis (Fig. 5D) showed clear partitioning of control and DBA samples, and differential gene expression analysis identified 1709 variable genes (Fig. 5E). As in *RPL*-DBA EP, gene set enrichment analysis (GSEA) and ingenuity pathway analysis revealed activation of p53, TNF- α , IFN- α , and IFN- γ inflammatory pathways in DBA EB (Fig. 5, F and G). Immunoproteasome and antigen presentation pathways, consistent with an active IFN- γ pathway, were also enriched, whereas ribosome biogenesis was decreased (Fig. 5F). Expression of the glucocorticoid-responsive gene *ZFP36L2* was decreased in *RPL*-DBA compared with control EB (Fig. 5H). Erythroid maturation markers, such as *HBA1*, *HBA2*, and *HBB*, were similar because of sorting of stage-matched populations (fig. S8E), and *HBG2* was increased (Fig. 5H). Therefore, although EB can develop in *RPL*-DBA, they display activation of the same pathological pathways identified in their upstream progenitors. Last, *eADA*, a purine metabolism enzyme used as a diagnostic biomarker in DBA, was up-regulated and highly expressed in *RPL*-DBA EB compared with their normal counterparts, matching the higher serum erythrocyte adenosine deaminase (eADA) activity in patients with *RPL*-DBA versus *RPS*-DBA (Fig. 5I) (6, 32).

Together, these findings provide *ex vivo* evidence of a proinflammatory bone marrow milieu in primary human DBA HSPC. Furthermore, although *RPL*-DBA EPs are relatively preserved in numbers, functionally, they appear to correspond to stress erythropoiesis that is deficient in its hallmark endogenous glucocorticoid-regulated program. This aberrant EP function leads to disordered differentiation and, in turn, reduced maintenance of the EP pool.

Preservation of GATA1 and its transcriptional program in *RPL*-DBA progenitors and precursors

GATA1 deficiency, due to reduced transcription (14), translation (4, 12), or increased caspase 3-mediated degradation (16), is proposed as a

Fig. 4. Glucocorticoid pathway–deficient stress erythropoiesis and ZFP36L2-mediated erythroid differentiation inhibition by glucocorticoids are observed in DBA. (A) Violin plots depicting the mean expression (yellow dot) and distribution (minimum to maximum) of *HBG2*, a stress erythropoiesis gene in control, *RPS*-DBA, and *RPL*-DBA EP subclusters (EEP, Ecycling, and LEP). The fraction of cells expressing *HBG2* is shown on the x axis.

(B) Mean expression (yellow dot) and distribution of AUCell score of stress erythropoiesis (SE) gene set is shown for control, *RPS*-DBA, and *RPL*-DBA EP subclusters. (C) A bubble plot shows the expression of erythroid differentiation genes in control, *RPS*-DBA, and *RPL*-DBA EP subclusters. (D) The AUCell score of glucocorticoid response genes in control, *RPS*-DBA, and *RPL*-DBA EP subclusters is shown by violin plots. (E) Violin plots depict the expression of *ZFP36L2* in control, *RPS*-DBA, and *RPL*-DBA EP subclusters. The fraction of cells expressing *ZFP36L2* is shown on the x axis. (F) *ZFP36L2* was measured by reverse transcription polymerase chain reaction (RT-PCR) in wild-type (wt, *n* = 6) and *RPL11* knockdown (kd, *n* = 3 or 4) K562 clones, normalized to wild-type and glyceraldehyde-3-phosphate dehydrogenase (*GAPDH*).

Data points represent RNA extracted at independent time points. (G) Erythroid differentiation of K652 cells was assessed by CD71 and GYPA expression by flow cytometry of untreated and dexamethasone (Dex)–treated wild-type and *RPL11* knockdown K562 clones. A representative of four independent experiments is shown. Numbers in the flow plots indicate the percent of live single cells. (H) FC of early (CD71⁺ GYPA⁻) and late (CD71⁺ GYPA⁺) EB in dexamethasone-treated wild-type K562 clones, normalized to untreated (*n* = 4). For early EB, the FC was calculated as (% CD71⁺ GYPA⁻ of dexamethasone-treated – % CD71⁺ GYPA⁻ of untreated) / % CD71⁺ GYPA⁻ of untreated. (I) FC of early (CD71⁺ GYPA⁻) and late (CD71⁺ GYPA⁺) EB in dexamethasone-treated *RPL11* knockdown K562 clones, normalized to untreated (*n* = 4). (J) *ZFP36L2* was measured by RT-PCR in dexamethasone-treated and untreated wild-type and *RPL11* knockdown K562 clones (*n* = 4), normalized to untreated and *GAPDH*. (K) *ZFP36L2*, *RPL5*, *ADA*, and *HBG2* expression was measured by RNA-seq of EB isolated from bone marrow of a patient with *RPL5*-DBA and purified by FACS 1 month before and 16 months after steroid therapy. Red line shows hemoglobin (Hb) concentration at time of bone marrow samplings. (L) Lentiviral transduction efficiency (% GFP⁺) 2 days after lentiviral transduction with mock (empty vector) or *ZFP36L2* cDNA. Plots are representative of three independent experiments. Numbers in the flow plots indicate the percent of live single cells. (M) Erythroid differentiation (represented by CD71 and GYPA expression) of wild-type and *RPL11* knockdown K562 clones is shown from 2 to 4 days after lentiviral transduction with mock (empty vector) or *ZFP36L2* cDNA. Plots are representative of three independent experiments. Numbers in the flow plots indicate the percent of live single cells. (N) FC of early (CD71⁺ GYPA⁻) and late (CD71⁺ GYPA⁺) EB in wild-type and *RPL11* knockdown K562 clones was quantified 2 to 4 days after lentiviral transduction with mock or *ZFP36L2* cDNA (*n* = 3 at day 2 and *n* = 2 at days 3 and 4). Plots show means ± SEM of replicates. **P* < 0.05; ***P* < 0.01; ****P* < 0.001; *****P* < 0.0001. Groups were compared by a Wilcoxon rank sum test (A, B, D, and E), an unpaired Student's *t* test (F), or a paired Student's *t* test (J).

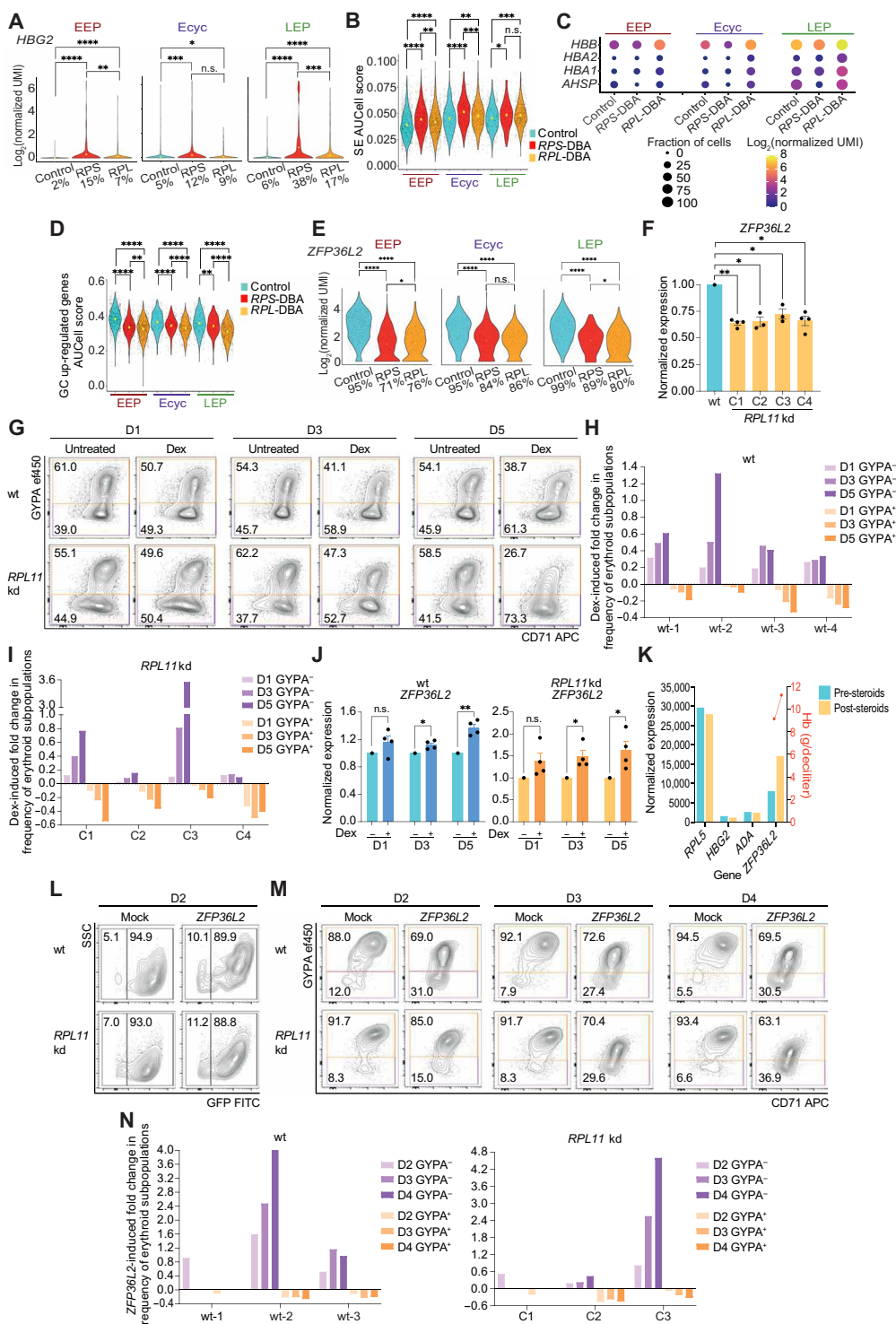
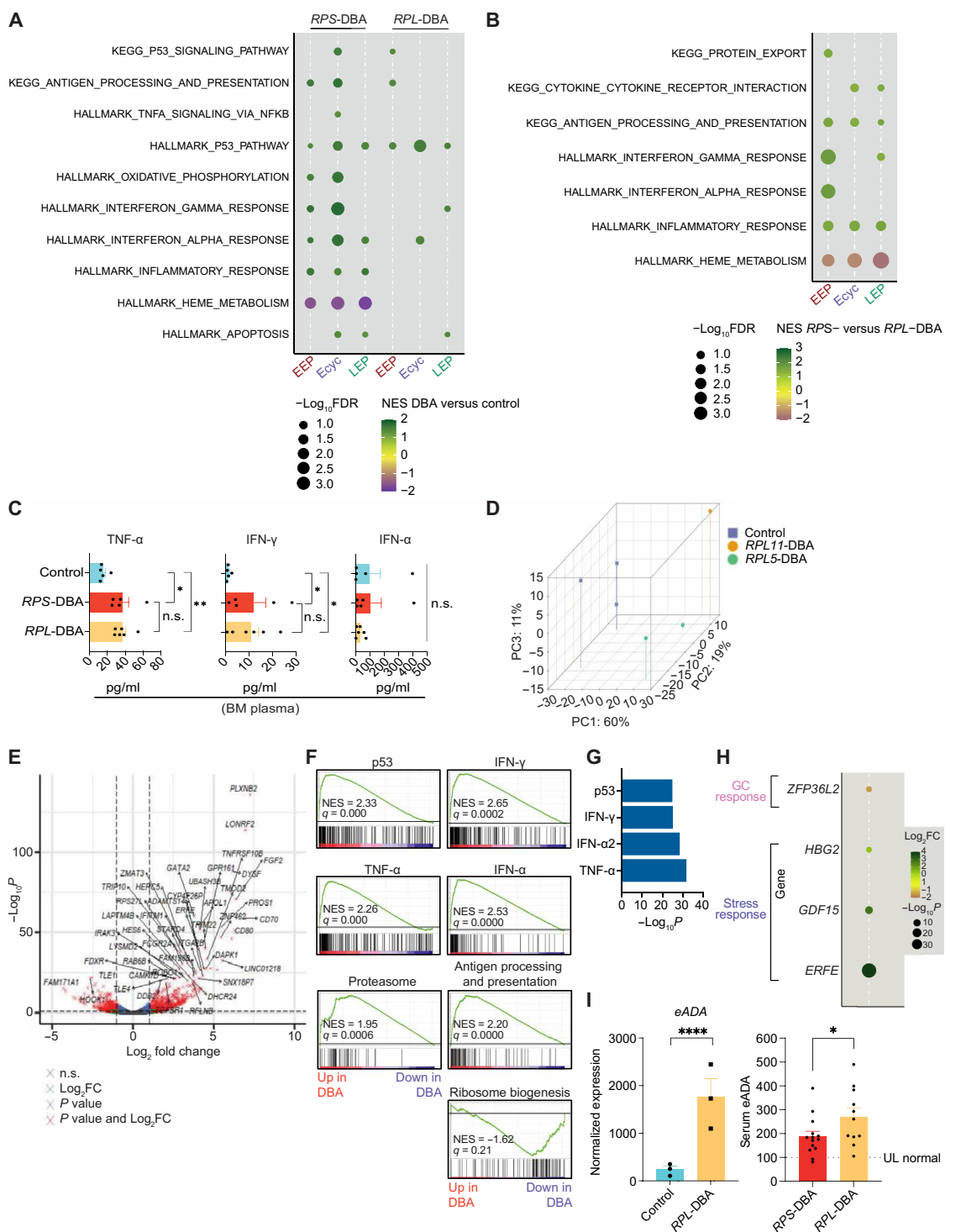


Fig. 5. P53 activation and bone marrow inflammatory milieu are increased in DBA.

(A) The bubble plot shows normalized enrichment score (NES) and false discovery rate ($-\log_{10}$ FDR) of significantly enriched (FDR q value < 0.25) pathways of interest on GSEA of differentially expressed genes (DEGs) between DBA and control EP subclusters. Pathways are from the Hallmark or Kyoto Encyclopedia of Genes and Genomes (KEGG) gene sets of Molecular Signatures Database. **(B)** The bubble plot shows enriched pathways between *RPS*-DBA and *RPL*-DBA EP subclusters. **(C)** The concentration of TNF- α , IFN- α , and IFN- γ in control, *RPS*-DBA, and *RPL*-DBA bone marrow plasma ($n = 5$ for control and *RPS*-DBA and $n = 6$ for *RPL*-DBA) was assessed by luminometry. **(D)** A principal component analysis (PCA) depiction of bulk RNA-seq data from stage-matched EB derived from three healthy pediatric controls and three patients with DBA is shown ($n = 1$ *RPL11* and $n = 2 *RPL5*), separated by principal component 1 (PC1), PC2, and PC3. **(E)** A volcano plot is shown, highlighting 1709 DEGs, of which 1101 are up-regulated. Thresholds (dash lines) are adjusted P value < 0.05 , and \log_2 FC ± 1 . Names of top 50 DEGs are shown. **(F)** GSEA plots show enrichment of Hallmark and KEGG gene sets in pre-ranked DEGs between control ($n = 3$) and *RPL*-DBA ($n = 3$) EB. Each bar represents a gene. The curve peak shows the NES, which reflects the degree to which a gene set is overrepresented at the top or bottom of the ranked list. **(G)** Ingenuity pathway analysis of DEG between *RPL*-DBA and control EB is shown highlighting the top four upstream regulators of the DBA transcriptome—p53, IFN- α , IFN- γ , and TNF- α . **(H)** The bubble plot depicts the \log_2 FC and $-\log_{10}$ adjusted P value of *ZFP36L2* and three stress erythropoiesis genes, quantified by bulk RNA-seq in *RPL*-DBA ($n = 3$) and control ($n = 3$) EB. All genes have \log_2 FC > 0.6 and adjusted P values < 0.05 . **(I)** eADA mRNA was quantified by bulk RNA-seq of FACS-purified EB from control and *RPL*-DBA ($n = 3$) bone marrow (left). Adjusted P value is shown. Peripheral blood red blood cell eADA activity (nmol/mg Hb/hour) is shown (right), in patients with *RPS*-DBA ($n = 14$) and *RPL*-DBA ($n = 11$) who are treatment independent or steroid-treated but are not receiving blood transfusions. UL normal, upper limit of normal. Plots show means \pm SEM of biological replicates. $*P < 0.05$; $**P < 0.01$; $****P < 0.0001$. Groups were compared by a Kruskal-Wallis test (C) or a Mann-Whitney U test (I, right).$



Downloaded from <https://www.science.org> on September 09, 2021

unifying mechanism for selective erythroid arrest in DBA. However, such studies were mostly performed in cultured cells, cell lines, or whole bone marrow containing both erythroid and nonerythroid cells. We had the opportunity to investigate the role of GATA1 *ex vivo* at single-cell resolution in *RPS*-DBA and *RPL*-DBA, not confounded by steroid therapy. First, we performed GSEA of our transcriptome data against three GATA1 genes sets (12, 49). This identified a depleted transcription factor database (TRANSFAC) or early GATA1 transcriptional signature in *RPS*-DBA EP (Fig. 6A and fig. S9A), consistent with the severe, early erythroid specification defect. By contrast, *RPL*-DBA EP and EB were enriched for the GATA1 transcriptional program throughout their developmental trajectory (Fig. 6A and fig. S9A). In *RPL*-DBA LEP and EB, the late but not early GATA1 signature was enriched in line with their altered differentiation trajectory (fig. S9A). In addition, expression of *GATA1short* and *GATA1full-length* isoforms was unchanged in *RPL*-DBA compared with control EB (Fig. 6B). This suggests that DBA caused by *RPL* haploinsufficiency is unlikely to be underpinned by unbalanced GATA1 isoform abundance, as is the case in patients with DBA-like disease with germline *GATA1* mutations that preserve *GATA1short* (50).

To elucidate the effect of *RPS* or *RPL* haploinsufficiency on GATA1 protein expression in primary DBA bone marrow cells, we stained bone marrow sections from seven patients with *RPL5/11*-DBA, four patients with *RPS19/24/26*-DBA, and three healthy controls, with an antibody specific for *GATA1full-length* (Fig. 6, C to E, and fig. S9, B to D). In *RPS*-DBA, most GATA1⁺ cells were negative for the erythroid marker Glycophorin C (GYPC) and morphologically corresponded to nonerythroid precursors (Fig. 6C). Overall, GATA1 expression was higher in *RPL*-DBA versus *RPS*-DBA EB and only marginally lower in *RPL*-DBA compared with control erythroid cells (Fig. 6E). Combined cell surface and intracellular staining followed by flow cytometry (Fig. 6F) or CyTOF (fig. S9E) showed a similar pattern of GATA1 expression in *RPL5*-DBA and control primary EP and EB. Together, these findings show that, in the preserved EP and precursors of *RPL*-DBA, GATA1 expression and its transcriptional program are largely intact.

The distinct clinical phenotype of *RPL*-DBA

Because our data suggested a milder cellular and functional defect in *RPL*-DBA than *RPS*-DBA *ex vivo*, we next investigated the clinical and hematological correlates of these differences by analyzing the characteristics of the UK DBA registry (5) with documented *RPL* ($n = 44$) and *RPS* ($n = 62$) mutations (table S2). In line with our transcriptomic and functional data, patients with *RPL*-DBA presented with anemia at an older age (regardless of sex) and with a higher hemoglobin concentration, than those with *RPS*-DBA (Fig. 7, A and B; fig. S10, A to C; and data file S5). Furthermore, a higher proportion of patients with *RPL*-DBA were initially corticosteroid responsive (Fig. 7C, fig. S10D, and data file S5), although long-term steroid dependence was not increased (Fig. 7D and fig. S10E) and rates of spontaneous or steroid-induced remission were not different between genotypes (fig. S10F). We also confirmed previous observations (51) of a higher rate of indel genetic variants (fig. S10G) and congenital anomalies (fig. S10H) in *RPL*-DBA compared with *RPS*-DBA, as well as associations between *RPL5* and cleft palate and *RPL11* and congenital thumb anomalies (Fig. 7D and fig. S10I) (51). Together, these genotype-phenotype correlations validate the clinical and biological relevance of the distinct erythroid developmental

pathways identified in our transcriptomic and functional studies (fig. S11).

DISCUSSION

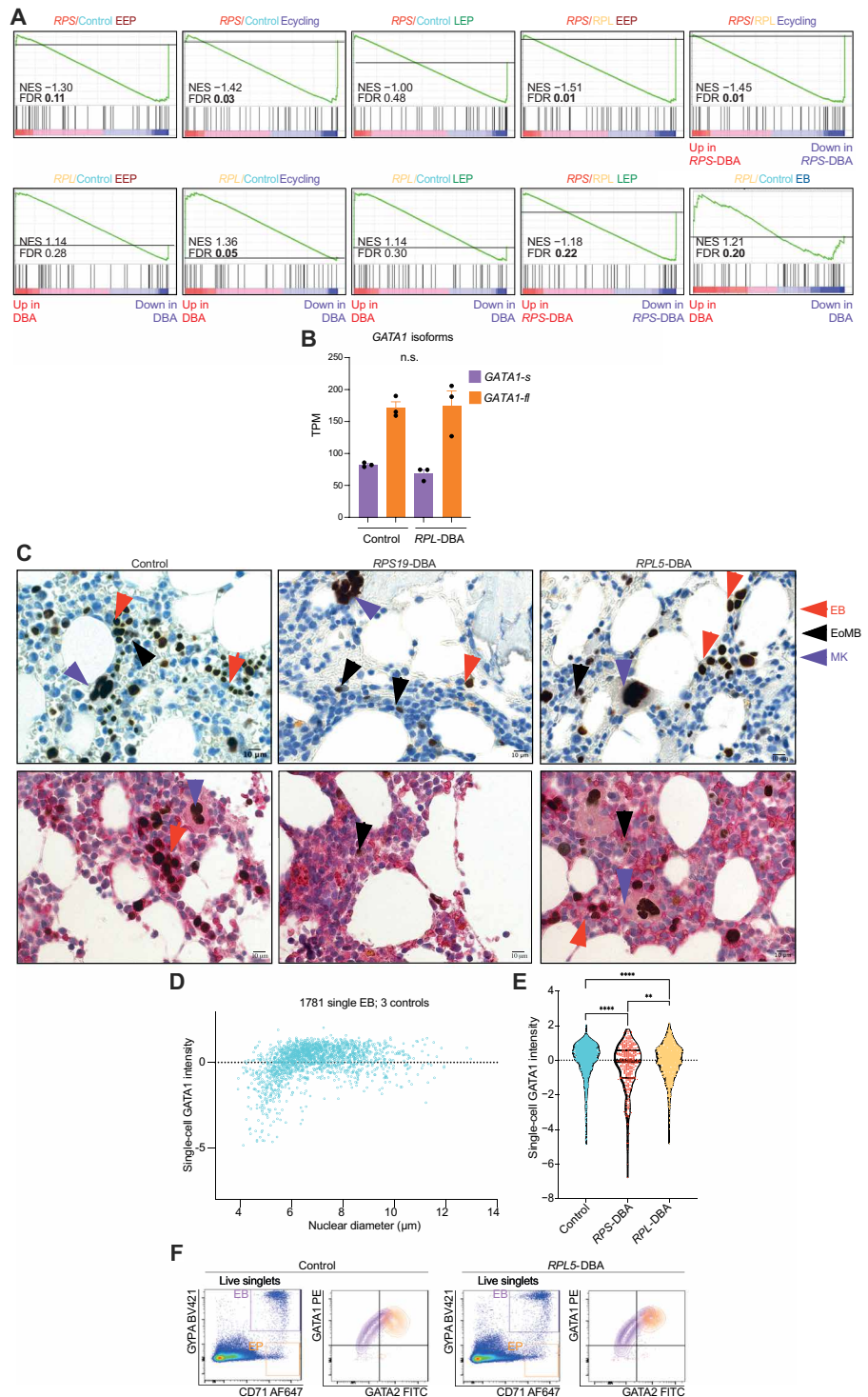
Here, we applied complementary molecular and functional single-cell analyses to dissect the cellular and molecular mechanisms underlying impaired erythropoiesis in DBA, the prototypic ribosomopathy. We identify two distinct patterns of erythroid failure that segregate with underlying genotype: a severe defect in early erythroid specification in *RPS*-DBA with a consequent almost complete lack of erythroid precursors, contrasting with relatively preserved erythroid cells throughout their developmental trajectory in *RPL*-DBA, but with disordered EP differentiation.

Our data point to a previously unrecognized role of stress erythropoiesis in the pathogenesis of erythroid failure in DBA. DBA EP and EB exhibit many of the molecular hallmarks of stress erythropoiesis, including overexpression of *GDF15* and *HBG2*, the orchestrator and signature gene of stress erythropoiesis, respectively (40, 41). However, the endogenous glucocorticoid-dependent transcriptional signature appears to be defective in DBA-associated stress erythropoiesis. These results derived from primary DBA bone marrow erythroid cells mirror the anemia associated with accelerated erythroid differentiation under conditions of stress in mice lacking expression of the glucocorticoid receptor (*NR3C1*) (44). Similarly, our transcriptional and cellular data indicate that erythroid differentiation is disordered in *RPL*-DBA, thereby providing a mechanism by which exogenously administered glucocorticoids exert their therapeutic effects in patients with DBA, which is by blocking erythroid differentiation to maintain the EP pool, a cellular mechanism reported for normal erythropoiesis in response to glucocorticoids (52, 53).

A role for the RNA binding protein *ZFP36L2* in mediating glucocorticoid-induced delayed erythroid differentiation has been previously reported (46). In this regard, our finding of reduced *ZFP36L2* expression in DBA erythroid cells and *ZFP36L2*-mediated inhibition of erythroid differentiation in *RPL11*-deficient K562 cells, a surrogate model of human *RPL*-DBA haploinsufficient erythropoiesis, supports a pivotal role for *ZFP36L2* in the pathogenesis of erythroid failure in DBA. We hypothesize that restoration of the ability to up-regulate critical glucocorticoid-dependent genes, such as *ZFP36L2*, underpins the therapeutic effect of glucocorticoids in DBA. Thus, glucocorticoids improve the quality of stress erythropoiesis rather than restore steady state-like erythropoiesis. In line with this, eADA and HbF markers usually remain elevated in steroid-treated DBA (Fig. 4K) (3). Conversely, our observation that reduced *ZFP36L2* promotes erythroid differentiation may be exploited in other pathologic states characterized by excessive stress erythropoiesis but blocked erythroid differentiation, such as β -thalassemia and polycythemia rubra vera, where accelerated maturation (by macrophage depletion for example) ameliorates pathological erythropoiesis and anemia (54).

As well as aberrant stress erythropoiesis, in all DBA genotypes, we demonstrate activation of P53 (8). Although the only other published transcriptomic data from DBA bone marrow did not show P53 pathway enrichment, the three patients studied were in clinical remission (4, 55). Inhibition of P53 was recently shown to be beneficial in *RPS* models of DBA erythropoiesis (8). Our data further support therapeutic targeting of this pathway in *RPL*-DBA.

Fig. 6. GATA1 and its transcriptional program are preserved in RPL-DBA. (A) GSEA is shown against a TRANSFAC-derived GATA1 gene set (12) of DEG between control and DBA subgroups at different erythroid stages (scRNA-seq for EP and bulk RNA-seq for EB). Significant FDRs of <0.25 are highlighted in bold face. (B) Full-length and short GATA1 transcript isoform abundance were determined by transcript analysis of bulk RNA-seq of stage-matched EB from healthy control and RPL-DBA bone marrow (*n* = 3). TPM, transcripts per million. (C) Top: Representative images show GATA1 expression assessed by immunohistochemistry of healthy control, RPS-DBA, and RPL-DBA bone marrow sections. GATA1 expression is shown by brown staining in EB (identified by their unilobar round nuclei), MK (large multilobe nuclei), and EoMB (bilobed/horseshoe nuclei and granular cytoplasm). Expression is weaker in EoMB compared with EB or MK cells and decreases in late EB relative to early/intermediate EB. Bottom: Costaining for GATA1 and the erythroid-specific marker Glycophorin C (GYPC) to distinguish EB (GYPC⁺ red membrane or cytoplasmic rim) from EoMB or MK (GYPC⁻). Scale bars, 10 μm. (D) The correlation between GATA1 expression and nuclear diameter in control bone marrow is shown. (E) Violin plots show single-cell GATA1 expression, measured in bone marrow EB from control (*n* = 1781 cells; three donors), RPS-DBA (*n* = 286; four donors), and RPL-DBA (*n* = 1179; seven donors). Distribution is from the 5th percentile to the 95th percentile. Dotted line shows mean expression of all samples, and the y axis shows number of SDs that each data point differs from mean (Z score). (F) Representative plots show GATA1 and GATA2 expression measured by intracellular flow cytometry in control and RPL5-DBA bone marrow EP (CD71^{hi}GYPA⁻) and EB (CD71 + GYPA⁺). Quadrants in GATA1 versus GATA2 plot were set using fluorescence-minus-one plus isotype controls. AF647, Alexa Fluor 647; BV421, Brilliant Violet 421. Groups were compared by a Mann-Whitney *U* test (B) or a Kruskal-Wallis with Dunn's multiple comparisons test (E). ***P* < 0.01, *****P* < 0.0001.



Our work also identifies activation of IFN- α , IFN- γ , and TNF- α inflammatory pathways in both RPS-DBA and RPL-DBA HSPCs, potential triggers that could incite and sustain stress erythropoiesis (47, 48, 56). Although inflammatory signatures are more prominent in RPS-DBA than RPL-DBA EP, they are pervasive and detected in the progenitors of several blood lineages. This is consistent with a bone marrow inflammatory milieu in vivo, supported by detection of elevated IFN- γ and TNF- α in DBA bone marrow plasma. Inflammatory signature imprints were previously reported in mature red blood cells from patients with DBA (57) and in zebrafish RPL11 morpholinos (58). Here, we show enrichment in specific hematopoietic lineages and ubiquitously within the bone marrow environment. Both cell intrinsic and extrinsic defects might trigger inflammatory responses. For instance, RP haploinsufficiency and, in turn, aberrant ribosomal RNA (rRNA) biogenesis may generate rRNA species that trigger cellular RNA sensors and an intrinsic IFN response. Specific for

erythropoiesis, association between EB and proinflammatory EB island macrophages (54) or nonspecifically activated T or NK cells might lead to excess inflammatory cytokine production that further impairs already intrinsically compromised DBA erythropoiesis (59). We identified increased secretion of these cytokines by activated T and NK cells in DBA compared with controls, suggesting that targeted anti-inflammatory agents should be investigated in DBA,

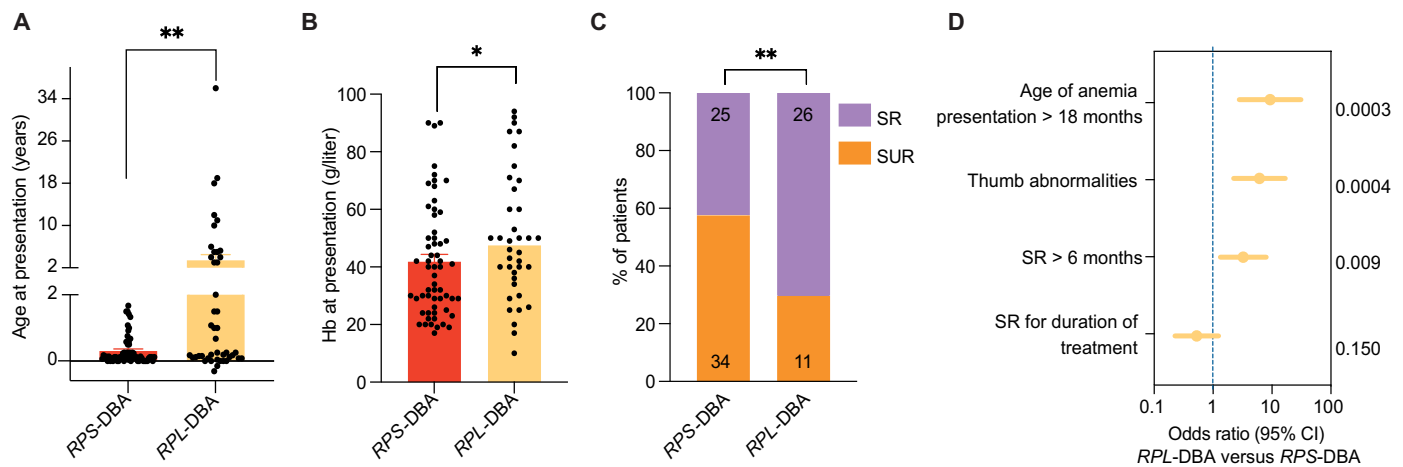


Fig. 7. RPL-DBA has a distinct clinical phenotype from RPS-DBA. (A) Age at presentation with anemia is plotted according to RPS-DBA ($n = 62$) or RPL-DBA ($n = 44$) genotype. Dots depict data points for individual patients. (B) Hemoglobin concentration (g/liter) at presentation is shown, according to RPS-DBA ($n = 59$) or RPL-DBA ($n = 38$) genotype. (C) The fraction of steroid-responsive (SR) cases (transfusion-independent for greater than 6 months) versus steroid-unresponsive (SUR) cases is shown according to RPS-DBA ($n = 59$) or RPL-DBA ($n = 37$) genotype. Numbers of cases are shown in the bars. (D) Odds ratio and 95% confidence intervals (CI) of specific clinical features and outcomes in RPL-DBA versus RPS-DBA are shown. P values are shown on the right. Bars in A and B show mean \pm SEM of biological replicates. Continuous variables were compared across genotypes using a Mann-Whitney U test (A and B). Frequencies of cases were compared across genotypes using a Pearson chi-square test (C). All variables significant on univariate analysis were tested by binary logistic or multiple linear regression, as appropriate. P values shown refer to regression analyses. * $P < 0.05$; ** $P < 0.01$.

including TNF- α inhibitors that are known to be beneficial in anemia associated with chronic inflammation (60). Reduced expression of *ZFP36L2* might also modulate inflammatory activation of lymphoid and myeloid cells in DBA bone marrow given its known anti-inflammatory effects (61, 62), providing another potential mechanism through which glucocorticoids exert their therapeutic effects in DBA. These findings may also have wider implications for other heritable ribosomopathies, such as Shwachman-Diamond syndrome, and for acute leukemia, juvenile myelomonocytic leukemia, or myelodysplastic syndromes (MDS), such as 5q-MDS associated with somatic *RPS14* haploinsufficiency (63). Like DBA, these disorders are associated with a proinflammatory bone marrow milieu (64, 65) and, in turn, an increased risk of preleukemic and leukemic transformation (66, 67).

GATA1 insufficiency has been suggested as a mechanism of erythroid failure in DBA, and the rate of GATA1 translation is dictated by its engagement with the ribosome (4). In B cells derived from patients with DBA, profiling of polysome-associated mRNA transcripts showed that translation defects of the *BCAT1* transcript, which has a long 5' untranslated region, were more severe in RPS19 than RPL11 cells (68). Consistent with this, we found reduced GATA1 transcriptional activity in RPS-DBA EP, suggestive of GATA1 protein reduction. In RPL-DBA, however, we show a GATA1 mRNA and protein expression pattern that is appropriate for the stage of erythroid development as well as an apparently robust GATA1-regulated transcriptional program. Thus, our data suggest that strategies to increase GATA1 translation are more likely to be effective in RPS-DBA, whereas therapies such as glucocorticoids that delay erythroid differentiation (52, 53) and specifically modulate the glucocorticoid target *ZFP36L2* are likely to be more effective in RPL-DBA.

Last, data from our large cohort of patients with DBA show that individuals with RPL genotypes are more likely to exhibit a milder

hematological phenotype appearing later in life and show improved initial corticosteroid responses. This is consistent with our findings of relative preservation in RPL-DBA of the EP populations that are targeted by glucocorticoids (38, 69), coupled with stress erythropoiesis deficient in the normal endogenous glucocorticoid response pathway. Furthermore, these findings complement the diagnostic value of identified genetic variants and allow more precise prediction of the disease course in patients. Despite the milder hematological phenotype in RPL-DBA, some nonhematological manifestations, such as congenital abnormalities, are more severe in RPL-DBA and, irrespective of genotype, patients with DBA have a higher risk of malignancy at a younger age than the normal population (32, 70). The paradox of attenuated hematological features but more severe skeletal defects associated with RPL-DBA genotypes highlights the diverse biological consequences of ribosome dysfunction (32, 71).

Our study has several limitations. This work is limited to the study of HSPC and erythroid precursors and does not include mature myeloid compartments or stromal cells, also potential sources of inflammatory cytokines in DBA bone marrow. Future scRNA-seq and functional studies could address, for example, the potential role of erythroblastic island macrophages in erythroid failure in the two DBA subgroups. Investigation of larger numbers of patients with distinct genotypes within each of the RPS-DBA and RPL-DBA subgroups is needed to further refine genotype-phenotype correlations. Last, the precise mechanisms by which glucocorticoid response pathways are impaired in the face of RP gene haploinsufficiency remain to be addressed.

In summary, we present unbiased charting at single-cell resolution of erythropoiesis in patients with DBA. Our data delineate developmental trajectories and, in turn, elucidate how these shape clinical phenotypes and therapeutic responses, according to genotypes. Furthermore, we provide access to a unique single-cell transcriptomic dataset from pediatric HSPCs in a ribosomopathy,

providing cell intrinsic and extrinsic pathogenetic insights, including candidate therapeutic targets for failing erythropoiesis, such as P53 and *ZFP36L2*. Last, our study is a paradigm of the power of single-cell analysis in deciphering phenotypes and cellular and molecular mechanisms, paving the way for precision-based approaches in rare heritable diseases.

MATERIALS AND METHODS

Study design

The overall objective of this study was to integrate clinical, cellular, and transcriptomic data from a large cohort of patients with DBA to elucidate genotype-phenotype correlations. Only patients who met the diagnostic criteria of DBA (3) with confirmed pathogenic RP gene mutations were included. The number of biological replicates was determined by primary sample availability and is specified in the figure legends. Outliers are included.

Patient details

Human bone marrow samples (data file S1) were collected after written informed consent, in accordance with the Declaration of Helsinki under a study approved by the National Research Ethics Committee (REC reference 12/LO/0426). Where possible, control and disease samples were age- and sex-matched. Healthy donor pediatric bone marrow was collected from sibling donors; samples carrying α - or β -thalassemia or sickle cell trait were used in selected experiments (excluding RNA-seq) given the limited supply of pediatric bone marrow and the importance of age matching (72). At least one true hematologically normal individual was included in the control group in each experiment.

BMMNC isolation and CD34⁺ cell selection

BMMNCs were isolated by Ficoll-Hypaque (Sigma-Aldrich) density centrifugation as per the manufacturer's instructions and used for flow cytometric analysis, subjected to CD34⁺ selection or cryopreserved, as determined by downstream experiments. CD34⁺ cells were isolated magnetically from BMMNCs using the MiniMACS Separator kit (Miltenyi Biotec Ltd.) as per the manufacturer's instructions. The typical purity and yield of the selected population was >95% after two column passages.

Flow cytometry, FACS, and CyTOF

Cells were suspended in RoboSep, incubated with FcR blocker (Miltenyi Biotec) for 5 min at room temperature and then stained with a panel of up to 13 commercial fluorophore-conjugated monoclonal antibodies (table S3) for 20 min at 4°C. After washing, cells were stained with 4',6-diamidino-2-phenylindole [Sigma-Aldrich; 1 μ l/100 μ l of stock (5 ng/ml)] or Brilliant Violet (BV) 510 Live/Dead Fixable Stain (BD Biosciences) for dead cell exclusion, before data acquisition on a four-laser BD LSRFortessa or BD Fusion flow cytometer. Data were acquired using FACSDiva software v8.0.1 and analyzed using FlowJo software (v10.5.3, Tree Star). Cell doublets and nonviable cells were excluded. Gates were set with fluorescein-minus-one plus immunoglobulin isotype controls or, where cell numbers were limiting, with unstained controls. For cell sorting, cells were passed through a 70- μ m mesh cell strainer before sorting on a BD FACS Aria III (scRNA-seq), BD Fusion (bulk RNA-seq and cell culture), or Sony MA900 (K562). The sort purity was assessed by recovery of sorted cells and was consistently >95%. To measure

apoptosis, cells were stained with an antibody against annexin V in Annexin V Binding Buffer (BioLegend), as per the manufacturer's instructions. For intracellular flow cytometry and scCyTOF, see Supplementary Materials and Methods and tables S3 and S4.

scRNA-seq (10x Chromium)

Cells were thawed, stained with flow antibodies (table S3), and sorted as described in the method above. CD34⁺Lin⁻ cells (12×10^3 to 15×10^3) were sorted into 2 μ l of phosphate-buffered saline (PBS) and 0.05% UltraPure bovine serum albumin followed by adjustment of the cell number/volume to the target for loading onto the 10x Chromium Controller. Processing was performed as per the Chromium Single Cell 3' library and Gel Bead Kits (10x Genomics) v2 or v3. Pre-amplified cDNA was subjected to library preparation and multiplexing and then sequenced on a HiSeq 2500, NextSeq 550, or Novaseq 6000 (table S1) by the National Institutes of Health Intramural Sequencing Center Comparative Sequencing Program. All scRNA-seq analyses were performed using customized pipelines [SingCellaR, package available from <https://github.com/supatt-lab/SingCellaR>, as previously described (23); code is deposited on Zenodo (10.5281/zenodo.5167626)]. Analyses are detailed in Supplementary Materials and Methods.

In vitro liquid erythroid culture

Total CD34⁺Lin⁻ or FACS-isolated EEP subpopulations were cultured in 96-well round- or flat-bottom plates, and concentration was maintained at less than 2×10^6 /ml by partial medium changes every 2 to 3 days. Base medium consisted of stemspan (STEMCELL Technologies), penicillin/streptomycin (100 U/ml; Sigma-Aldrich), stem cell factor (100 ng/ml; PeproTech), interleukin-3 (IL-3) (10 ng/ml; PeproTech), lipids (40 μ g/ml; Sigma-Aldrich), L-glutamine (25 ng/ml; Sigma-Aldrich), and IL-6 (10 ng/ml; PeproTech). The concentration of Epo (Bio-Techne) was increased from 0.5 to 3 to 4 U/ml on day 7. The cultures were incubated at 37°C with 5% CO₂ for up to 14 days.

Methocult assay

Single EEP or 500 CD34⁺ cells were FACS-sorted into 100 μ l or 1 ml of H4034 medium (STEMCELL Technologies) in each well of a flat-bottomed 96-well plate or a 24-well plate, respectively. Cultures were incubated at 37°C with 5% CO₂ for 14 days. Colonies were photographed using an inverted microscope (Evos XL Core) and scored by morphological assessment according to established criteria (73). Specifically, dense colonies of EB in "bursts" were counted on days 12 to 14 as BFU-e, whereas small uni- or bicentric clusters of EB were counted on day 7 as "CFU-e-like." BFU-e colonies with abnormal morphology or color were termed "erythroid clusters" (9). On day 14, selected colonies were plucked and cytospun to allow morphological examination of their cellular composition.

Microscopy using cytopins

FACS-sorted or cultured cells were suspended in RoboSep, at a concentration of 2×10^4 to 5×10^4 cells per 200 μ l. Cells were cyto-centrifuged at 400 rpm for 5 min onto Superfrost slides, using a Shandon Cytospin 2 (Thermo Fisher Scientific). Slides were air-dried, fixed in 100% methanol, and stained with working solutions of May-Grünwald-Giemsa (Sigma-Aldrich). Cytopins were photographed using a Nikon Eclipse E400 inverted microscope and camera.

Bulk RNA-seq

RNA was extracted using the NucleoSpin RNA XS kit (Macherey-Nagel). Directional mRNA libraries were prepared using the NEBNext Poly(A) mRNA Magnetic Isolation Module, NEBNext Directional RNA First and Second Strand Synthesis Modules, and the NEBNext Ultra II DNA Library Prep Kit for Illumina (New England Biolabs), as per the manufacturer's version 1.5 protocol. For further details, see Supplementary Materials and Methods.

Bone marrow plasma

Bone marrow aspirate (1 to 2 ml) was collected in an EDTA tube (BD Biosciences) and spun at 1500g at 4°C for 12 min. The upper plasma layer was aspirated, spun at 4°C, and then stored immediately at -80°C. Analysis of bone marrow plasma cytokines and chemokines was performed by Eve Technologies using the Human Cytokine Array (HD42) Discovery Assay.

Clinical registry data

Clinical and laboratory data were collected prospectively and uniformly from 161 patients with presumed DBA notified to St Mary's Hospital, Imperial College Healthcare Trust, London, UK over a 7-year period (2013 to 2020). Missing data were collected retrospectively. Fifteen of 161 patients were excluded from the study because there was insufficient data available to fulfill the diagnostic criteria for DBA (3). Targeted next-generation sequencing (7) or whole-exome sequencing was used to screen for RP gene and *GATA1* mutations (table S2).

Statistical analyses

Data aggregation and statistical analyses were performed using GraphPad Prism (v8.1.0) and SPSS (version 26, IBM Corp.) for experimental and clinical registry data, respectively. Unless otherwise stated, bar plots show means \pm SE of the mean and a two-tailed *P* value of less than 0.05 was considered significant. Statistical tests used, numbers and types of replicates, and *P* value thresholds are described in the legends. Differences in continuous variables between two groups were assessed using the Student's *t* test (parametric), Mann-Whitney *U* test (nonparametric), or Wilcoxon rank test (nonparametric), and comparisons between more than two groups were assessed using the Kruskal-Wallis test (nonparametric) or the one-way analysis of variance (ANOVA) test (parametric), with Dunn or Holm-Sidak multiple comparisons tests, respectively. Normality of data was assessed by the Shapiro-Wilk test (data file S6). Fisher's exact or Pearson chi-square test was used to compare proportions of categorical variables. For clinical registry data, all variables found to be significant in univariate analyses were included in a multivariate stepwise logistic or linear regression analysis for binary and continuous variables, respectively.

SUPPLEMENTARY MATERIALS

www.science.org/doi/10.1126/scitranslmed.abf0113

Materials and Methods

Figs. S1 to S11

Tables S1 to S5

Data files S1 to S6

References (74–83)

[View/request a protocol for this paper from Bio-protocol.](#)

REFERENCES AND NOTES

- K. R. Kampen, S. O. Sulima, S. Vereecke, K. de Keersmaecker, Hallmarks of ribosomopathies. *Nucleic Acids Res.* **48**, 1013–1028 (2020).
- L. Luzzatto, A. Karadimitris, Dyskeratosis and ribosomal rebellion. *Nat. Genet.* **19**, 6–7 (1998).
- A. Vlachos, S. Ball, N. Dahl, B. P. Alter, S. Sheth, U. Ramenghi, J. Meerpohl, S. Karlsson, J. M. Liu, T. Leblanc, C. Paley, E. M. Kang, E. J. Leder, E. Atsidaftos, A. Shimamura, M. Bessler, B. Glader, J. M. Lipton; Participants of Sixth Annual Daniella Maria Arturi International Consensus Conference, Diagnosing and treating Diamond Blackfan anaemia: Results of an international clinical consensus conference. *Br. J. Haematol.* **142**, 859–876 (2008).
- R. K. Khajuria, M. Munschaer, J. C. Ulirsch, C. Fiorini, L. S. Ludwig, S. K. McFarland, N. J. Abdulhay, H. Specht, H. Keshishian, D. R. Mani, M. Jovanovic, S. R. Ellis, C. P. Fulco, J. M. Engreitz, S. Schütz, J. Lian, K. W. Gripp, O. K. Weinberg, G. S. Pinkus, L. Gehrke, A. Regev, E. S. Lander, H. T. Gazda, W. Y. Lee, V. G. Panse, S. A. Carr, V. G. Sankaran, Ribosome levels selectively regulate translation and lineage commitment in human hematopoiesis. *Cell* **173**, 90–103.e19 (2018).
- D. Iskander, I. Roberts, C. Rees, R. Szydlo, M. Alkian, M. Neale, Y. Harrington, P. Kelleher, A. Karadimitris, J. de la Fuente, Impaired cellular and humoral immunity is a feature of Diamond-Blackfan anaemia; experience of 107 unselected cases in the United Kingdom. *Br. J. Haematol.* **186**, 321–326 (2019).
- J. C. Ulirsch, J. M. Verboon, S. Kazerounian, M. H. Guo, D. Yuan, L. S. Ludwig, R. E. Handsaker, N. J. Abdulhay, C. Fiorini, G. Novese, E. T. Lim, A. Cheng, B. B. Cummings, K. R. Chao, A. H. Beggs, C. A. Genetti, C. A. Sieff, P. E. Newburger, E. Niewiadomska, M. Matysiak, A. Vlachos, J. M. Lipton, E. Atsidaftos, B. Glader, A. Narla, P. E. Gleizes, M. F. O'Donohue, N. Montel-Lehry, D. J. Amor, S. A. McCarroll, A. H. O'Donnell-Luria, N. Gupta, S. B. Gabriel, D. G. MacArthur, E. S. Lander, M. Lek, L. Da Costa, D. G. Nathan, A. A. Korostelev, R. Do, V. G. Sankaran, H. T. Gazda, The genetic landscape of Diamond-Blackfan Anemia. *Am. J. Hum. Genet.* **103**, 930–947 (2018).
- G. Gerrard, M. Valgañón, H. E. Foong, D. Kasperaviciute, D. Iskander, L. Game, M. Müller, T. J. Aitman, I. Roberts, J. de la Fuente, L. Foroni, A. Karadimitris, Target enrichment and high-throughput sequencing of 80 ribosomal protein genes to identify mutations associated with Diamond-Blackfan anaemia. *Br. J. Haematol.* **162**, 530–536 (2013).
- A. M. Taylor, E. R. Macari, I. T. Chan, M. C. Blair, S. Doulatov, L. T. Vo, D. M. Raiser, K. Siva, A. Basak, M. Pirouz, A. N. Shah, K. McGrath, J. M. Humphries, E. Stillman, B. P. Alter, E. Calo, R. I. Gregory, V. G. Sankaran, J. Flygare, B. L. Ebert, Y. Zhou, G. Q. Daley, L. I. Zon, Calmodulin inhibitors improve erythropoiesis in Diamond-Blackfan anemia. *Sci. Transl. Med.* **12**, eabb5831 (2020).
- D. Iskander, B. Psaila, G. Gerrard, A. Chaidos, H. En Foong, Y. Harrington, L. C. Karnik, I. Roberts, J. de la Fuente, A. Karadimitris, Elucidation of the EP defect in Diamond-Blackfan anemia by characterization and prospective isolation of human EPs. *Blood* **125**, 2553–2557 (2015).
- Y. Mori, J. Y. Chen, J. V. Pluvinae, J. Seita, I. L. Weissman, Prospective isolation of human erythroid lineage-committed progenitors. *Proc. Natl. Acad. Sci. U.S.A.* **112**, 9638–9643 (2015).
- S. H. Orkin, L. I. Zon, Hematopoiesis: An evolving paradigm for stem cell biology. *Cell* **132**, 631–644 (2008).
- L. S. Ludwig, H. T. Gazda, J. C. Eng, S. W. Eichhorn, P. Thiru, R. Ghazvinian, T. I. George, J. R. Gotlib, A. H. Beggs, C. A. Sieff, H. F. Lodish, E. S. Lander, V. G. Sankaran, Altered translation of *GATA1* in Diamond-Blackfan anemia. *Nat. Med.* **20**, 748–753 (2014).
- Z. Yang, S. B. Keel, A. Shimamura, L. Liu, A. T. Gerds, H. Y. Li, B. L. Wood, B. L. Scott, J. L. Abkowitz, Delayed globin synthesis leads to excess heme and the macrocytic anemia of Diamond Blackfan anemia and del(5q) myelodysplastic syndrome. *Sci. Transl. Med.* **8**, 338ra67 (2016).
- S. Rio, M. Gastou, N. Karboul, R. Derman, T. Suriyun, H. Manceau, T. Leblanc, J. El Benna, C. Schmitt, S. Azouzi, J. Larghero, Z. Karim, A. Maclas-Garcia, J. J. Chen, O. Hermine, G. Courtois, H. Puy, L. Gouya, N. Mohandas, L. Da Costa, Regulation of globin-heme balance in Diamond-Blackfan anemia by HSP70/*GATA1*. *Blood* **133**, 1358–1370 (2019).
- K. A. O'Brien, J. E. Farrar, A. Vlachos, S. M. Anderson, C. A. Tsujiura, J. Lichtenberg, L. Blanc, E. Atsidaftos, A. Elkahlon, X. An, S. R. Ellis, J. M. Lipton, D. M. Bodine, Molecular convergence in ex vivo models of Diamond-Blackfan anemia. *Blood* **129**, 3111–3120 (2017).
- M. Gastou, S. Rio, M. Dussiot, N. Karboul, H. Moniz, T. Leblanc, M. Sevin, P. Gonin, J. Larghero, C. Garrido, A. Narla, N. Mohandas, W. Vainchenker, O. Hermine, E. Solary, L. Da Costa; French Society of Hematology (SFH); French Society of Immunology and Hematology (SHIP), The severe phenotype of Diamond-Blackfan anemia is modulated by heat shock protein 70. *Blood Adv.* **1**, 1959–1976 (2017).
- A. R. Migliaccio, L. Varricchio, Concise review: Advanced cell culture models for Diamond Blackfan anemia and other erythroid disorders. *Stem Cells* **36**, 172–179 (2018).
- A. Narla, D. Yuan, S. Kazerounian, C. LaVasseur, J. C. Ulirsch, J. Narla, B. Glader, V. G. Sankaran, H. Gazda, A novel pathogenic mutation in RPL11 identified in a patient diagnosed with diamond Blackfan anemia as a young adult. *Blood Cells Mol. Dis.* **61**, 46–47 (2016).

19. E. Flores Ballester, J. J. Gil-Fernández, M. Vázquez Blanco, J. M. Mesa, J. de Dios García, A. T. Tamayo, C. Burgaleta, Adult-onset Diamond-Blackfan anemia with a novel mutation in the exon 5 of RPL11: Too late and too rare. *Clin. Case Rep.* **3**, 392–395 (2015).
20. C. M. Carlston, Z. A. Afify, J. C. Palumbos, H. Bagley, C. Barbagelata, W. L. Wooderchak-Donahue, R. Mao, J. C. Carey, Variable expressivity and incomplete penetrance in a large family with non-classical Diamond-Blackfan anemia associated with ribosomal protein L11 splicing variant. *Am. J. Med. Genet. A* **173**, 2622–2627 (2017).
21. O. Steinberg-Shemer, S. Keel, O. Dgany, T. Walsh, S. Noy-Lotan, T. Krasnov, J. Yacobovich, P. Quarello, U. Ramenghi, M. C. King, A. Shimamura, H. Tamary, Diamond Blackfan anemia: A nonclassical patient with diagnosis assisted by genomic analysis. *J. Pediatr. Hematol. Oncol.* **38**, e260–e262 (2016).
22. M. Sonoda, M. Ishimura, Y. Ichimiya, E. Terashi, K. Eguchi, Y. Sakai, H. Takada, A. Hama, H. Kanno, T. Toki, E. Ito, S. Ohga, Atypical erythroblastosis in a patient with Diamond-Blackfan anemia who developed del(20q) myelodysplasia. *Int. J. Hematol.* **108**, 228–231 (2018).
23. B. Psaila, G. Wang, A. Rodriguez-Meira, R. Li, E. F. Heuston, L. Murphy, D. Yee, I. S. Hitchcock, N. Sousos, J. O'Sullivan, S. Anderson, Y. A. Senis, O. K. Weinberg, M. L. Calicchio, D. Iskander, D. Royston, D. Milojkovic, I. Roberts, D. M. Bodine, S. Thongjuea, A. J. Mead, Single-cell analyses reveal megakaryocyte-biased hematopoiesis in myelofibrosis and identify mutant clone-specific targets. *Mol. Cell* **78**, 477–492.e8 (2020).
24. I. Korsunsky, N. Millard, J. Fan, K. Slowikowski, F. Zhang, K. Wei, Y. Baglaenko, M. Brenner, P.-r. Loh, S. Raychaudhuri, Fast, sensitive and accurate integration of single-cell data with Harmony. *Nat. Methods* **16**, 1289–1296 (2019).
25. D.-M. Popescu, R. A. Botting, E. Stephenson, K. Green, S. Webb, L. Jardine, E. F. Calderbank, K. Polanski, I. Goh, M. Efremova, M. Acres, D. Maunder, P. Vegh, Y. Gitton, J.-E. Park, R. Rento-Tormo, Z. Miao, D. Dixon, R. Rowell, D. McDonald, J. Fletcher, E. Poyner, G. Reynolds, M. Mather, C. Moldovan, L. Mamanova, F. Greig, M. D. Young, K. B. Meyer, S. Lisgo, J. Bacardit, A. Fuller, B. Millar, B. Innes, S. Lindsay, M. J. T. Stubbington, M. S. Kowalczyk, B. Li, O. Ashenberg, M. Tabaka, D. Dionne, T. L. Tickle, M. Slyper, O. Rozenblatt-Rosen, A. Filby, P. Carey, A.-C. Villani, A. Roy, A. Regev, A. Chédotal, I. Roberts, B. Göttgens, S. Behjati, E. Laurenti, S. A. Teichmann, M. Haniffa, Decoding human fetal liver haematopoiesis. *Nature* **574**, 365–371 (2019).
26. L. Velten, S. F. Haas, S. Raffel, S. Blaszkiewicz, S. Islam, B. P. Hennig, C. Hirche, C. Lutz, E. C. Buss, D. Nowak, T. Boch, W.-K. Hofmann, A. D. Ho, W. Huber, A. Trumpp, M. A. Essers, L. M. Steinmetz, Human haematopoietic stem cell lineage commitment is a continuous process. *Nat. Cell Biol.* **19**, 271–281 (2017).
27. I. Tirosh, B. Izar, S. M. Prakadan, M. H. Wadsworth, D. Treacy, J. J. Trombetta, A. Rotem, C. Rodman, C. Lian, G. Murphy, M. Fallahi-Sichani, K. Dutton-Regester, J. R. Lin, O. Cohen, P. Shah, D. Lu, A. S. Genshaft, T. K. Hughes, C. G. K. Ziegler, S. W. Kazer, A. Gaillard, K. E. Kolb, A. C. Villani, C. M. Johannessen, A. Y. Andreev, E. M. Van Allen, M. Bertagnolli, P. K. Sorger, R. J. Sullivan, K. T. Flaherty, D. T. Frederick, J. Jané-Valbuena, C. H. Yoon, O. Rozenblatt-Rosen, A. K. Shalek, A. Regev, L. A. Garraway, Dissecting the multicellular ecosystem of metastatic melanoma by single-cell RNA-seq. *Science* **352**, 189–196 (2016).
28. R. Drissen, N. Buza-Vidas, P. Woll, S. Thongjuea, A. Gambardella, A. Giustacchini, E. Mancini, A. Zriwil, M. Lutteropp, A. Grover, A. Mead, E. Sitnicka, S. E. W. Jacobsen, C. Nerlov, Distinct myeloid progenitor-differentiation pathways identified through single-cell RNA sequencing. *Nat. Immunol.* **17**, 666–676 (2016).
29. H. Chen, L. Albergante, J. Y. Hsu, C. A. Lareau, G. Lo Bosco, J. Guan, S. Zhou, A. N. Gorban, D. E. Bauer, M. J. Aryee, D. M. Langenau, A. Zinovyev, J. D. Buenrostro, G.-C. Yuan, L. Pinello, Single-cell trajectories reconstruction, exploration and mapping of omics data with STREAM. *Nat. Commun.* **10**, 1903 (2019).
30. J. D. Buenrostro, M. R. Corces, C. A. Lareau, B. Wu, A. N. Schep, M. J. Aryee, R. Majeti, H. Y. Chang, W. J. Greenleaf, Integrated single-cell analysis maps the continuous regulatory landscape of human hematopoietic differentiation. *Cell* **173**, 1535–1548.e16 (2018).
31. B. K. Tusi, S. L. Wolock, C. Weinreb, Y. Hwang, D. Hidalgo, R. Zilionis, A. Waisman, J. R. Huh, A. M. Klein, M. Socolovsky, Population snapshots predict early haematopoietic and erythroid hierarchies. *Nature* **555**, 54–60 (2018).
32. P. Quarello, E. Garelli, A. Carando, R. Cillario, A. Brusco, E. Giorgio, D. Ferrante, P. Corti, M. Zecca, M. Luciani, F. Pierri, M. C. Putti, M. E. Cantarini, P. Farruggia, A. Barone, S. Cesaro, G. Russo, F. Fagioli, I. Dianzani, U. Ramenghi; AIEOP working group on Diamond Blackfan Anaemia, A 20-year long term experience of the Italian Diamond-Blackfan Anaemia Registry: *RPS* and *RPL* genes, different faces of the same disease? *Br. J. Haematol.* **190**, 93–104 (2020).
33. F. Notta, S. Zandi, N. Takayama, S. Dobson, O. I. Gan, G. Wilson, K. B. Kaufmann, J. McLeod, E. Laurenti, C. F. Dunant, J. D. McPherson, L. D. Stein, Y. Dror, J. E. Dick, Distinct routes of lineage development reshape the human blood hierarchy across ontogeny. *Science* **351**, aab2116 (2016).
34. S. Doulatov, F. Notta, E. Laurenti, J. E. Dick, Hematopoiesis: A human perspective. *Cell Stem Cell* **10**, 120–136 (2012).
35. V. Viprakasit, V. S. Tanphaichitr, W. Chinchang, P. Sangkla, M. J. Weiss, D. R. Higgs, Evaluation of alpha hemoglobin stabilizing protein (AHSP) as a genetic modifier in patients with β thalassemia. *Blood* **9**, 3296–3299 (2004).
36. C. G. Palli, Q. Cheng, M. A. Gillespie, P. Shannon, M. Mazurczyk, G. Napolitani, N. D. Price, J. A. Ranish, E. Morrissey, D. R. Higgs, M. Brand, Single-cell proteomics reveal that quantitative changes in co-expressed lineage-specific transcription factors determine cell fate. *Cell Stem Cell* **24**, 812–820.e5 (2019).
37. N. Suzuki, N. Suwabe, O. Ohneda, N. Obara, S. Imagawa, X. Pan, H. Motohashi, M. Yamamoto, Identification and characterization of 2 types of erythroid progenitors that express GATA-1 at distinct levels. *Blood* **102**, 3575–3583 (2003).
38. R. J. Ashley, H. Yan, N. Wang, J. Hale, B. M. Dulmovits, J. Papoin, M. E. Olive, N. D. Udeshi, S. A. Carr, A. Vlachos, J. M. Lipton, L. Da Costa, C. Hillyer, S. Kinet, N. Taylor, N. Mohandas, A. Narla, L. Blanc, Steroid resistance in Diamond Blackfan anemia associates with p57Kip2 dysregulation in erythroid progenitors. *J. Clin. Invest.* **130**, 2097–2110 (2020).
39. J. A. García-Vela, I. Martín Rubio, J. Marquet, M. A. Alvarez Juárez, CD105 expression in early erythroid precursors. *Am. J. Hematol.* **92**, E155–E156 (2017).
40. B. P. Alter, P. S. Rosenberg, T. Day, S. Menzel, N. Giri, S. A. Savage, S. L. Thein, Genetic regulation of fetal haemoglobin in inherited bone marrow failure syndromes. *Br. J. Haematol.* **162**, 542–546 (2013).
41. S. Hao, J. Xiang, D. C. Wu, J. W. Fraser, B. Ruan, J. Cai, A. D. Patterson, Z. C. Lai, R. F. Paulson, Gdf15 regulates murine stress erythroid progenitor proliferation and the development of the stress erythropoiesis niche. *Blood Adv.* **3**, 2205–2217 (2019).
42. L. Kautz, G. Jung, E. V. Valore, S. Rivella, E. Nemeth, T. Ganz, Identification of erythroferone as an erythroid regulator of iron metabolism. *Nat. Genet.* **46**, 678–684 (2014).
43. S. Aibar, C. B. González-Blas, T. Moerman, V. A. Huynh-Thu, H. Imrichova, G. Hulselmans, F. Rambow, J. C. Marine, P. Geurts, J. Aerts, J. Van Den Oord, Z. K. Atak, J. Wouters, S. Aerts, SCENIC: Single-cell regulatory network inference and clustering. *Nat. Methods* **14**, 1083–1086 (2017).
44. A. Bauer, F. Tronche, O. Wessely, C. Kellendonk, H. M. Reichardt, P. Steinlein, G. Schütz, H. Beug, The glucocorticoid receptor is required for stress erythropoiesis. *Genes Dev.* **13**, 2996–3002 (1999).
45. A. Kolbus, M. Blázquez-Domingo, S. Carotta, W. Bakker, S. Luedemann, M. Von Lindern, P. Steinlein, H. Beug, Cooperative signaling between cytokine receptors and the glucocorticoid receptor in the expansion of erythroid progenitors: Molecular analysis by expression profiling. *Blood* **102**, 3136–3146 (2003).
46. L. Zhang, L. Prak, V. Rayon-Estrada, P. Thiru, J. Flygare, B. Lim, H. F. Lodish, ZFP36L2 is required for self-renewal of early burst-forming unit erythroid progenitors. *Nature* **499**, 92–96 (2013).
47. L. F. Bennett, C. Liao, M. D. Quickel, B. S. Yeoh, M. Vijay-Kumar, P. Hankey-Giblin, K. S. Prabhu, R. F. Paulson, Inflammation induces stress erythropoiesis through heme-dependent activation of SPI-C. *Sci. Signal.* **12**, eaap7336 (2019).
48. R. F. Paulson, B. Ruan, S. Hao, Y. Chen, Stress erythropoiesis is a key inflammatory response. *Cell* **9**, 634 (2020).
49. M. J. Weiss, C. Yu, S. H. Orkin, Erythroid-cell-specific properties of transcription factor GATA-1 revealed by phenotypic rescue of a gene-targeted cell line. *Mol. Cell. Biol.* **3**, 1642–1651 (1997).
50. V. G. Sankaran, R. Ghazvinian, R. Do, P. Thiru, J.-A. Vergilio, A. H. Beggs, C. A. Sieff, S. H. Orkin, D. G. Nathan, E. S. Lander, H. T. Gazda, Exome sequencing identifies GATA1 mutations resulting in Diamond-Blackfan anemia. *J. Clin. Invest.* **122**, 2439–2443 (2012).
51. H. T. Gazda, M. R. Sheen, A. Vlachos, V. Choesmel, M.-F. O'Donohue, H. Schneider, N. Darras, C. Hasman, C. A. Sieff, P. E. Newburger, S. E. Ball, E. Niewiadomska, M. Matysiak, J. M. Zaucha, B. Glader, C. Niemeyer, J. J. Meerpohl, E. Atsidaftos, J. M. Lipton, P.-E. Gleizes, A. H. Beggs, Ribosomal protein L5 and L11 mutations are associated with cleft palate and abnormal thumbs in Diamond-Blackfan anemia patients. *Am. J. Hum. Genet.* **83**, 769–780 (2008).
52. S. E. Sjögren, K. Siva, S. Soneji, A. J. George, M. Winkler, P. Jaako, M. Wlodarski, S. Karlsson, R. D. Hannan, J. Flygare, Glucocorticoids improve erythroid progenitor maintenance and dampen Trp53 response in a mouse model of Diamond-Blackfan anaemia. *Br. J. Haematol.* **171**, 517–529 (2015).
53. H. Li, A. Natarajan, J. Ezike, M. I. Barrasa, Y. Le, Z. A. Feder, H. Yang, C. Ma, S. Markoulaki, H. F. Lodish, Rate of progression through a continuum of transit-amplifying progenitor cell states regulates blood cell production. *Dev. Cell* **49**, 118–129.e7 (2019).
54. P. Ramos, C. Casu, S. Gardenghi, L. Breda, B. J. Crielgaard, E. Guy, M. F. Marongiu, R. Gupta, R. L. Levine, O. Abdel-Wahab, B. L. Ebert, N. Van Rooijen, S. Ghaffari, R. W. Grady, P. J. Giardina, S. Rivella, Macrophages support pathological erythropoiesis in polycythemia vera and β -thalassemia. *Nat. Med.* **19**, 437–445 (2013).
55. H. T. Gazda, A. T. Kho, D. Sanoudou, J. M. Zaucha, I. S. Kohane, C. A. Sieff, A. H. Beggs, Defective ribosomal protein gene expression alters transcription, translation, apoptosis, and oncogenic pathways in Diamond-Blackfan anemia. *Stem Cells* **24**, 2034–2044 (2006).

56. R. F. Paulson, L. Shi, D. C. Wu, Stress erythropoiesis: New signals and new stress progenitor cells. *Curr. Opin. Hematol.* **18**, 139–145 (2011).
57. E. N. Pesciotta, H.-S. Lam, A. Kossenkov, J. Ge, L. C. Showe, P. J. Mason, M. Bessler, D. W. Speicher, In-depth, label-free analysis of the erythrocyte cytoplasmic proteome in Diamond Blackfan anemia identifies a unique inflammatory signature. *PLOS ONE* **10**, e0140036 (2015).
58. N. Danilova, M. Wilkes, E. Bibikova, M.-Y. Youn, K. M. Sakamoto, S. Lin, Innate immune system activation in zebrafish and cellular models of Diamond Blackfan anemia. *Sci. Rep.* **8**, 5165 (2018).
59. I. C. Macdougall, A. C. Cooper, Hyporesponsiveness to erythropoietic therapy due to chronic inflammation. *Eur. J. Clin. Invest.* **35**, 32–35 (2005).
60. G. Weiss, T. Ganz, L. T. Goodnough, Anemia of inflammation. *Blood* **133**, 40–50 (2019).
61. F. Salerno, S. Engels, M. van den Biggelaar, F. P. J. van Alphen, A. Guislain, W. Zhao, D. L. Hodge, S. E. Bell, J. P. Medema, M. von Lindern, M. Turner, H. A. Young, M. C. Wolkers, Translational repression of pre-formed cytokine-encoding mRNA prevents chronic activation of memory T cells. *Nat. Immunol.* **19**, 828–837 (2018).
62. K.-T. Wang, H.-H. Wang, Y.-Y. Wu, Y.-L. Su, P.-Y. Chiang, N.-Y. Lin, S.-C. Wang, G.-D. Chang, C.-J. Chang, Functional regulation of Zfp3611 and Zfp3612 in response to lipopolysaccharide in mouse RAW264.7 macrophages. *J. Inflamm.* **12**, 42 (2015).
63. R. K. Schneider, M. Schenone, M. V. Ferreira, R. Kramann, C. E. Joyce, C. Hartigan, F. Beier, T. H. Brümendorf, U. Germing, U. Platzbecker, G. Büsche, R. Knüchel, M. C. Chen, C. S. Waters, E. Chen, L. P. Chu, C. D. Novina, R. C. Lindsley, S. A. Carr, B. L. Ebert, Rps14 haploinsufficiency causes a block in erythroid differentiation mediated by S100A8 and S100A9. *Nat. Med.* **22**, 288–297 (2016).
64. J. Vadakekolathu, M. D. Minden, T. Hood, S. E. Church, S. Reeder, H. Altmann, A. H. Sullivan, E. J. Viboch, T. Patel, N. Ibrahimova, S. E. Warren, A. Arruda, Y. Liang, T. H. Smith, G. A. Foulds, M. D. Bailey, J. Gowen-MacDonald, J. Muth, M. Schmitz, A. Cesano, A. G. Pockley, P. J. M. Valk, B. Löwenberg, M. Bornhäuser, S. K. Tasian, M. P. Rettig, J. K. Davidson-Moncada, J. F. DiPersio, S. Rutella, Immune landscapes predict chemotherapy resistance and immunotherapy response in acute myeloid leukemia. *Sci. Transl. Med.* **12**, eaaz0463 (2020).
65. O. Dufva, P. Pölonen, O. Brück, M. A. I. Keränen, J. Klievink, J. Mehtonen, J. Huuhtanen, A. Kumar, D. Malani, S. Siitonen, M. Kankainen, B. Ghimire, J. Lahtela, P. Mattila, M. Vähä-Koskela, K. Wennerberg, K. Granberg, S. K. Leivonen, L. Meriranta, C. Heckman, S. Leppä, M. Nykter, O. Lohi, M. Heinäniemi, S. Mustjoki, Immunogenomic landscape of hematological malignancies. *Cancer Cell* **38**, 380–399.e13 (2020).
66. A. J. Warren, Molecular basis of the human ribosomopathy Shwachman-Diamond syndrome. *Adv. Biol. Regul.* **67**, 109–127 (2018).
67. L. Dong, W. M. Yu, H. Zheng, M. L. Loh, S. T. Bunting, M. Pauly, G. Huang, M. Zhou, H. E. Broxmeyer, D. T. Scadden, C. K. Qu, Leukemo-genic effects of Ptpn11 activating mutations in the stem cell microenvironment. *Nature* **539**, 304–308 (2016).
68. T. C. Pereboom, A. Bondt, P. Pallaki, T. D. Klason, Y. J. Goos, P. B. Essers, M. J. Groot Koerkamp, H. T. Gazda, F. C. Holstege, L. D. Costa, A. W. MacInnes, Translation of branched-chain aminotransferase-1 transcripts is impaired in cells haploinsufficient for ribosomal protein genes. *Exp. Hematol.* **42**, 394–403.e4 (2014).
69. J. Flygare, V. R. Estrada, C. Shin, S. Gupta, H. F. Lodish, HIF1 α synergizes with glucocorticoids to promote BFU-E progenitor self-renewal. *Blood* **117**, 3435–3444 (2011).
70. A. Vlachos, P. S. Rosenberg, E. Atsidaftos, J. Kang, K. Onel, R. N. Sharaf, B. P. Alter, J. M. Lipton, Increased risk of colon cancer and osteogenic sarcoma in Diamond-Blackfan anemia. *Blood* **132**, 2205–2208 (2018).
71. E. W. Mills, R. Green, Ribosomopathies: There's strength in numbers. *Science* **358**, eaan2755 (2017).
72. W. W. Pang, S. L. Schrier, I. L. Weissman, Age-associated changes in human hematopoietic stem cells. *Semin. Hematol.* **54**, 39–42 (2017).
73. F. D. Goldman, G. Aubert, A. J. Klingelutz, M. Hills, S. R. Cooper, W. S. Hamilton, A. J. Schlueter, K. Lambie, C. J. Eaves, P. M. Lansdorp, Characterization of primitive hematopoietic cells from patients with dyskeratosis congenita. *Blood* **111**, 4523–4531 (2008).
74. L. Gilles, A. D. Arslan, C. Marinaccio, Q. J. Wen, P. Arya, M. McNulty, Q. Yang, J. C. Zhao, K. Konstantinoff, T. Lasho, A. Pardanani, B. Stein, I. Plo, S. Sundaravel, A. Wickrema, A. Migliaccio, S. Gurbuxani, W. Vainchenker, L. C. Platanius, A. Tefferi, J. D. Crispino, Downregulation of GATA1 drives impaired hematopoiesis in primary myelofibrosis. *J. Clin. Invest.* **127**, 1316–1320 (2017).
75. H. H. Kampinga, J. Hageman, M. J. Vos, H. Kubota, R. M. Tanguay, E. A. Bruford, M. E. Cheetham, B. Chen, L. E. Hightower, Guidelines for the nomenclature of the human heat shock proteins. *Cell Stress Chaperones* **14**, 105–111 (2009).
76. A. Dobin, C. A. Davis, F. Schlesinger, J. Drenkow, C. Zaleski, S. Jha, P. Batut, M. Chaisson, T. R. Gingeras, STAR: Ultrafast universal RNA-seq aligner. *Bioinformatics* **29**, 15–21 (2013).
77. Y. Liao, G. K. Smyth, W. Shi, The Subread aligner: Fast, accurate and scalable read mapping by seed-and-vote. *Nucleic Acids Res.* **41**, e108–e108 (2013).
78. M. I. Love, W. Huber, S. Anders, Moderated estimation of fold change and dispersion for RNA-seq data with DESeq2. *Genome Biol.* **15**, 550 (2014).
79. B. Li, C. N. Dewey, RSEM: Accurate transcript quantification from RNA-Seq data with or without a reference genome. *BMC Bioinformatics* **12**, 323 (2011).
80. H. M. Wain, E. A. Bruford, R. C. Lovering, M. J. Lush, M. W. Wright, S. Povey, Guidelines for human gene nomenclature. *Genomics* **79**, 464–470 (2002).
81. I. Boria, E. Garelli, H. T. Gazda, A. Aspesi, P. Quarello, E. Pavesi, D. Ferrante, J. J. Meerpohl, M. Kartal, L. Da Costa, A. Proust, T. Leblanc, M. Simansour, N. Dahl, A.-S. Fröjmark, D. Pospisilova, R. Cmejla, A. H. Beggs, M. R. Sheen, M. Landowski, C. M. Buros, C. M. Clinton, L. J. Dobson, A. Vlachos, E. Atsidaftos, J. M. Lipton, S. R. Ellis, U. Ramenghi, I. Dianzani, The ribosomal basis of Diamond-Blackfan anemia: Mutation and database update. *Hum. Mutat.* **31**, 1269–1279 (2010).
82. J. M. Schwarz, D. N. Cooper, M. Schuelke, D. Seelow, MutationTaster2: Mutation prediction for the deep-sequencing age. *Nat. Methods* **11**, 361–362 (2014).
83. B. Psaila, A. J. Mead, Single-cell approaches reveal novel cellular pathways for megakaryocyte and erythroid differentiation. *Blood* **133**, 1427–1435 (2019).

Acknowledgments: We are grateful to the patients with DBA and their families, the Pediatric Hematology team (St Mary's Hospital), and the John Goldman Centre for Cellular Therapy, Hammersmith Hospital. We also acknowledge the London Institute of Medical Sciences/ National Institute of Health Imperial Biomedical Research Centre (NIHR BRC) Flow Cytometry Facility; S. Rothery (Facility for Imaging by Light Microscopy, Imperial College London); N. Ashley (Medical Research Council Weatherall Institute of Molecular Medicine Single Cell Genomics Facility); A. Young (NISC Comparative Sequencing Program) and D. Carragher (Ottawa Hospital Research Institute Proteomics Core/CyTOF Facility) for technical expertise; and E. Chalmers and Z. Rooke for clinical registry data. **Funding:** This work was supported by an NIHR Academic Clinical Lectureship (to D.I.), Academy of Medical Sciences Starter Grant (to D.I.), British Society of Haematology Early Stage grant (to D.I.), Blood Cancer UK Clinical Research Fellowship (to D.I.), and DBA UK Research Award (to D.I.); Cancer Research UK Advanced Clinician Scientist Fellowship (to B.P.); National Institute of Diabetes and Digestive and Kidney Diseases, NIH (2R01DK098449 to M.B.); National Human Genome Research Institute Intramural funds (to D.M.B.); and Imperial NIHR BRC (to A. Karadimitris). **Author contributions:** D.I. conceived, performed, and analyzed experiments (sample processing, scRNA-seq, bulk RNA-seq, cell culture, flow cytometry, GATA1 immunohistochemistry, and CRISPR-Cas9); performed bioinformatic analyses (scRNA-seq and bulk RNA-seq); collected and analyzed clinical registry data; and wrote the manuscript. G.W. and E.F.H. developed and performed bioinformatic analyses. M.R. and N.T. contributed to bioinformatic analysis of bulk RNA-seq data, and Z.M. analyzed CyTOF data. C.C. performed and analyzed experiments (sample processing, cell culture, flow cytometry, GATA1 immunohistochemistry, and CRISPR-Cas9) and contributed to preparation of manuscript figures. B.P., K.P., H.R., C.G.P., Q.A.-O., M.H.Z., and A. Katsarou performed experiments as follows: scRNA-seq (B.P.), CRISPR-Cas9 (K.P., H.R., and Q.A.-O.), CyTOF (C.G.P.), flow cytometry (M.H.Z.), and sample processing (A. Katsarou). P.T. and K.N. performed immunohistochemistry. R.S. contributed to statistical analysis. A.J.M., M.B., J.d.I.F., and D.M.B. provided resources and expertise. V.S.C., K.P., and A.R. provided methodology and expertise. A.C. and S.T. designed bioinformatic pipelines. J.d.I.F. and L.K. contributed clinical samples. I.R. and D.M.B. helped to design the project, interpreted data, and edited the manuscript. A. Karadimitris conceived the project, designed experiments, interpreted data, and wrote the manuscript. All authors read and approved the submitted manuscript. **Competing interests:** A. Karadimitris provides consulting for Gilead Greece. J.d.I.F. is on the advisory board of bluebird bio, CRISPR Therapeutics/VERTEX, Novartis, Beam Therapeutics, and Jazz; has received speaker fees from Jazz; and has received a research grant from bluebird bio. A.J.M. provides consulting for Novartis, Celgene/BMS, Abbvie, CTI, and Gilead; has received speaker fees from Novartis; and has received research funding from Novartis and Celgene/BMS. B.P. provides consulting for Constellation and has received speaker fees from Novartis. All other authors declare that they have no competing interests. **Data and materials availability:** All data associated with this study are present in the paper or the Supplementary Materials. The raw RNA-seq datasets generated during the current study are available at the NCBI GEO DataSets under the accession codes GSE156441 and GSE181830. CyTOF data are available at flow repository under accession code FR-FCM-Z3QN, and code is available at Zenodo (10.5281/zenodo.5167626) and GitHub (https://github.com/guanlinW/Iskander_et_al_DBA_2021).

Submitted 18 October 2020
Accepted 13 August 2021
Published 8 September 2021
10.1126/scitranslmed.abf0113

Citation: D. Iskander, G. Wang, E. F. Heuston, C. Christodoulidou, B. Psaila, K. Ponnusamy, H. Ren, Z. Mokhtari, M. Robinson, A. Chaidos, P. Trivedi, N. Trasanidis, A. Katsarou, R. Szydlow, C. G. Pali, M. H. Zaidi, Q. Al-Oqaily, V. S. Caputo, A. Roy, Y. Harrington, L. Karnik, K. Nares, A. J. Mead, S. Thongjuea, M. Brand, J. de la Fuente, D. M. Bodine, I. Roberts, A. Karadimitris, Single-cell profiling of human bone marrow progenitors reveals mechanisms of failing erythropoiesis in Diamond-Blackfan anemia. *Sci. Transl. Med.* **13**, eabf0113 (2021).

Single-cell profiling of human bone marrow progenitors reveals mechanisms of failing erythropoiesis in Diamond-Blackfan anemia

Deena IskanderGuanlin WangElisabeth F. HeustonChrysi ChristodoulidouBethan PsailaKanagaraju PonnusamyHongwei RenZeinab MokhtariMark RobinsonAristeidis ChaidosPritesh TrivediNikolaos TrasanidisAlexia KatsarouRichard SzydloCarmen G. PaliMehmood H. ZaidiQais Al-OqailyValentina S. CaputoAnindita RoyYvonne HarringtonLeena KarnikKikkeri NareshAdam J. MeadSupat ThongjueaMarjorie BrandJosu de la FuenteDavid M. Bodinelrene RobertsAnastasios Karadimitris

Sci. Transl. Med., 13 (610), eabf0113. • DOI: 10.1126/scitranslmed.abf0113

Redefining ribosomopathies

Diamond-Blackfan anemia (DBA) is a rare ribosomopathy with limited therapeutic options. DBA is characterized by mutations in either the ribosomal protein large (RPL) or ribosomal protein small (RPS) subunit genes, but it is not fully understood how these two types of DBA differ. To address this, Iskander *et al.* used single-cell profiling of bone marrow progenitors isolated from individuals with *RPS*-DBA or *RPL*-DBA. The authors found that *RPS*-DBA is characterized by loss of erythroid specification, whereas *RPL*-DBA was characterized by preservation of erythroid progenitors, although the cells were qualitatively abnormal. These findings, together with data suggesting differences in glucocorticoid responsiveness, will help develop targeted treatments for *RPL*-DBA and *RPS*-DBA.

View the article online

<https://www.science.org/doi/10.1126/scitranslmed.abf0113>

Permissions

<https://www.science.org/help/reprints-and-permissions>

Use of think article is subject to the [Terms of service](#)

Supplementary Materials for

Single-cell profiling of human bone marrow progenitors reveals mechanisms of failing erythropoiesis in Diamond-Blackfan anemia

Deena Iskander *et al.*

Corresponding author: Anastasios Karadimitris, a.karadimitris@imperial.ac.uk;
Irene Roberts, irene.roberts@paediatrics.ox.ac.uk; David M. Bodine, tedyaz@nhgri.nih.gov

Sci. Transl. Med. **13**, eabf0113 (2021)
DOI: 10.1126/scitranslmed.abf0113

The PDF file includes:

Materials and Methods
Figs. S1 to S11
Tables S1 to S5
References (74–83)

Other Supplementary Material for this manuscript includes the following:

Data files S1 to S6

Supplementary Materials

Materials and Methods

Single-cell RNA sequencing (scRNA-seq) analyses

Matrices were obtained of each individual sample by aligning FASTQ files to the human reference genome (GRCh38 3.0.0) using Cell Ranger software (version 3.0.1) from 10x Genomics. Quality control (QC) parameters used for filtering cells are outlined in **table S1**. In total, 41,415 CD34⁺Lineage(Lin)⁻ cells (25,981 from Diamond-Blackfan anemia (DBA) donors and 15,434 cells from healthy donors) from all 9 donors were included in analyses. 1,239 highly variable genes were identified in the aggregate of 9 samples, 8 mitochondrial and heat shock protein genes (75) were removed, leaving 1,231 highly variable genes for subsequent analyses. Donor and batch effects were regressed out using the Harmony method (24). The first 30 principal components (PCs) were used (based on elbowplot visualization) to run Uniform Manifold Approximation and Projection (UMAP) analysis combined with Louvain clustering. Nineteen clusters were identified initially and superimposed on the two-dimensional UMAP, as shown in **Fig. 1B**. Differentially expressed genes of up to 100 genes per cluster are shown in **data file S2**. Lineage signature gene sets (**data file S3**) were designed and used to verify the lineage identity of clusters as previously described (23). Differentiation trajectories were inferred from Force Directed Graphs (FDG) based on the fa2 package. To examine erythroid progenitor (EP) and megakaryocyte progenitor (MKP) heterogeneity, cells from the original clusters 6, 10, 15 and 16 ($n=6380$) were extracted. After normalization, 20 PCs were used for analysis and 1,496 highly variable genes were identified after removing 10 mitochondrial and heat shock protein genes. Clustering analysis initially identified nine sub-clusters of EP/MKP cells. Marker genes were inspected as described above and clusters with similar transcriptional profiles were merged to give four major EP/MKP subclusters (**Fig. 2, A and B; data file S4**). All heatmaps show scaled (z score) expression values.

To assess differences between transcriptomes, differentially expressed genes (DEG) analyses were performed in the 6 cell lineage types and in EP/MKP subclusters, by pairwise comparisons as follows: *RPS*-DBA versus control, *RPL*-DBA versus control and *RPS*-DBA versus *RPL*-DBA. Genes were ranked according to scores calculated by multiplying the Log₂ fold change in expression by the -log₁₀ of the adjusted p-value [false discovery rate (FDR) values]. All genes were used as background. Gene lists were subjected to Gene Set Enrichment Analysis (GSEA) using available software (<http://software.broadinstitute.org/gsea/index.jsp>) with 'Run GSEAPreranked' and default parameters, against the Hallmark and Kyoto Encyclopedia of Genes and Genomes (KEGG) gene sets, that were downloaded from MSigDB

(<http://www.broadinstitute.org/gsea/msigdb/collections.jsp>). In addition, customized gene sets were used from the published literature for GATA1 upregulated targets (12, 49). GSEA pathways with an FDR q-value < 0.25 were regarded as significant.

The stress erythropoiesis gene set (**data file S3**) comprises genes most significantly upregulated in murine fetal liver P2 EPs compared with bone marrow (31) (fetal liver erythropoiesis is analogous to stress erythropoiesis), as well as *HBG2*, *ERFE* and *GDF15* (40–42). The glucocorticoid (GC) target gene set was compiled by mining the literature for genes upregulated in murine fetal liver in response to glucocorticoids (45, 46) (as limited human data available) and expressed in the EP/MKP dataset [Log₂Normalized unique molecular identifier (UMI) >0]. The Area Under the Curve (AUCell) package (43) was used to calculate each individual cell's AUCell score for specific gene sets. One-tailed Wilcoxon rank-sum test was used to compare AUCell scores and gene expression between groups.

Intracellular flow cytometry

For GATA transcription factor analysis, after extracellular staining, mononuclear cells were washed, fixed, and permeabilized using the Transcription Factor Buffer Set (BD Pharmingen), following the manufacturer's protocol, then incubated with GATA1 and GATA2 antibodies [or Immunoglobulin (Ig) isotypes] at 4°C for 50 minutes, washed and run on an LSR Fortessa flow cytometer.

For intracellular tumor necrosis factor (TNF)- α and interferon (IFN)- γ quantification, the CD34⁺ or mononuclear cell fraction of control and DBA bone marrow were incubated at 37°C for 5 hours with Cell Stimulation Cocktail (Invitrogen) containing phorbol 12-myristate 13-acetate (PMA), ionomycin, brefeldin A and monensin (Cell Stimulation Cocktail; Life Technologies) or brefeldin A (GolgiPlug; BD Biosciences) alone, washed, and stained with extracellular antibodies as described in the main text materials and methods section. Samples were then fixed and permeabilized using the eBioscience Intracellular Fixation & Permeabilization Buffer Set per manufacturer's protocol, followed by incubating with TNF- α and IFN- γ antibodies at room temperature for 20 minutes, washing and acquisition on an LSR Fortessa flow cytometer. See **table S3** for details of antibodies used.

CyTOF

Thawed bone marrow mononuclear cell (BMMNC) samples were counted, and viability measured by trypan blue exclusion. Up to 5 million cells per sample were aliquoted for staining. For viability staining, cells were washed with phosphate buffered saline (PBS) and then incubated in 300 μ l of 2.5 μ M cisplatin solution for 5 minutes at room temperature. Residual cisplatin was quenched by washing cells twice in Cell Staining Buffer (Fluidigm). Next, cells were incubated with the surface-

staining cocktail for 30 minutes at 4°C (**table S4**). Cells were washed with PBS and then fixed using 2% methanol-free formaldehyde solution (Thermo Fisher Scientific) for 30 minutes at room temperature. Subsequently, samples were permeabilized using the Nuclear Antigen Staining kit (Fluidigm), according to the manufacturer's protocol, followed by incubation with the intracellular-staining cocktail (**table S4**) for 30 minutes at 4°C. Finally, samples were washed with PBS and then resuspended in a 1.6% formaldehyde solution containing 125nM iridium1 191/193 (Fluidigm). Cells were incubated overnight, washed with Cell Staining Buffer, Cell Acquisition Solution (Fluidigm) and then resuspended at a concentration of 5×10^5 cells per ml in Cell Acquisition Solution containing a 5:1 dilution of EQ Normalization beads (Fluidigm). The samples were acquired on a Helios Mass Cytometer equipped with a wide-bore sample injector at an event rate of 300-500 events per second. After acquisition, repeat acquisitions of the same sample were concatenated, then normalized using the Fluidigm software. Normalized fcs files were exported for high dimensional analysis.

GATA1 immunohistochemistry (IHC) staining and imaging

GATA1 IHC was performed on archived bone marrow paraffin 1mm sections, as previously described (74) using an anti-GATA1 full length antibody (D52H6, Cell Signaling Technology). Automated staining was performed in a Leica BOND-III Automated IHC Stainer as follows: deparaffinization and treatment with 3% hydrogen peroxide to quench endogenous peroxidase activity, antigen retrieval using EDTA (0.001 mol/L), pH 8.0 (Invitrogen) at 96°C for 30 minutes, washing in Tris buffer (Covance), incubation with GATA1 antibody at a 1:200 dilution for 20 minutes at room temperature, incubation for 30 minutes with a horseradish peroxidase (HRP)-labelled polymer conjugated to goat anti-rabbit Ig antibody (PowerVision; Leica Microsystems), staining with diaminobenzidine (DAB; Dako) as a chromogen, enhancement with 1% copper sulphate solution, washing, counterstaining with Mayer's hematoxylin (Sigma-Aldrich), dehydration, and mounting.

Analysis was blinded to minimize observation bias. Image acquisition was automated by using the Zeiss Axio Observer Inverted Widefield Microscope (63 x objective). Ten to 15 images were acquired from each stained trephine to ensure sampling of distinct, non-overlapping areas of tissue. Images were analyzed with Fiji (ImageJ 1.43j, National Institutes of Health). GATA1- positive cells were identified in each image using a custom-made automated image analysis pipeline in Fiji, similar to previously published method (4). Specifically, nuclei were segmented by blue intensity to create a binary mask followed by cell separation using the binary watershed command. The binary mask was processed to create regions of interest (yellow outlines: **Fig. 6C**), based on size and circularity to exclude GATA1⁺ megakaryocyte and GATA1⁺ myeloid cells. Each enumerated cell was manually verified to ensure designation to the correct hematopoietic lineage. The raw data

images were used for measuring DAB staining using the Fiji plugin “color deconvolution” with the built-in vector “H DAB”. Diameter (mm) and mean intensity, ranging from 0 (total white) to 255 (deep brown), were measured per cell using the region of interest (ROI) mask superimposed on the DAB only image.

For selected samples with sufficient stored material, an additional bone marrow section was co-stained for GATA1 and Glycophorin C (GYPC), a cell membrane marker of erythroblasts, using a monoclonal mouse anti-human GYPC antibody (clone RET40f, Dako) at a 1:150 dilution. A red stain (Leica bond polymer red detection kit; Leica Biosystems) was used as a chromogen. GYPC positive erythroid cells were identified visually by their deep red perinuclear staining.

Bulk RNA-sequencing

To prepare double stranded DNA libraries for RNA-sequencing, 1×10^3 - 8×10^4 cells (according to availability in individual samples) were purified by fluorescence- activated cell sorting (FACS) into lysis buffer (NucleoSpin RNA XS kit, Macherey-Nagel), vortexed, snap frozen on dry ice and stored at -80°C . On thawing, RNA was extracted, and quality assessed using the Agilent RNA 6000 Pico Kit (Agilent Bioanalyzer), accepting RNA Integrity numbers (RIN) of >7 . First, mRNA was isolated from total RNA using oligo-dT selection and fragmented (NEBNext Poly(A) mRNA Magnetic Isolation Module), followed by first and second strand cDNA synthesis (NEBNext Directional RNA First and Second Strand Synthesis Modules). Directionality was achieved by addition of Actinomycin D (Sigma-Aldrich). Double-stranded complementary DNA (ds cDNA) was purified and stored at -20°C until End Prep of the cDNA library, adaptor ligation and polymerase chain reaction (PCR) enrichment, using a unique Truseq barcode for each sample [NEBNext Ultra II DNA Library Prep Kit for Illumina, NEBNext Multiple Oligos for Illumina Primer (Index Primers Set 1)]. Following optimization, 13-16 PCR cycles were performed for 1-10 ng total input RNA. The PCR reaction was purified, eluted in $15 \mu\text{l}$ 10 mM TrisHCl, then stored at -20°C . cDNA library quality was assessed using the Agilent DNA high sensitivity (HS) Kit (Agilent Bioanalyzer). In cases where an adaptor-dimer peak was visible at 128 base pairs (bp), a repeat clean-up step was performed using Agencourt AMPure XP Beads (Beckman Coulter). Libraries were quantified by the Qubit dsDNA HS Assay Kit (Thermo Fisher Scientific) and equimolar concentrations pooled for sequencing on the Illumina HiSeq 2500 platform.

After demultiplexing, paired-end 100 bp raw reads obtained from RNA-seq experiments were subjected to quality control using FAST-QC software then aligned using “STAR 2.5.3a” (76) against the GRCh38 human reference genome, employing the default settings. Post-alignment QC was performed using Picard and Sequence Alignment/Map (SAM) tools. Raw counts at the gene level were obtained using the “Rsubread” Bioconductor package (77). Data normalization and differential expression analysis across different groups were performed using the “DESeq2”

Bioconductor package (78). A combined fold change of 0.6 (Log₂ scale) and P_{adj} 0.05 cutoff was applied to obtain significantly up- or down-regulated genes. Log₂ fold change values were Z-score standardized, clustered and visualized as heatmaps within the R environment. Gene networks and upstream regulators were identified through the use of Ingenuity Pathways Analysis (Ingenuity Systems, www.ingenuity.com). GSEA was performed on genes preranked by Log₂ fold change. To perform isoform analysis, the BLUEPRINT consortium method was employed (http://dcc.blueprint-epigenome.eu/#/md/rna_seq_grch38). In brief, alignment to the transcriptome was performed using “STAR 2.5.3a” and transcripts were quantified using the RNA-Seq by Expectation Maximization (RSEM) package (79).

Cell lines

K562 and 293T cells were obtained from the American Type Culture Collection (ATCC) and cultured in Dulbecco’s Modified Eagle Medium (DMEM) high glucose medium (Sigma-Aldrich) and Roswell Park Memorial Institute Medium 1640 (RPMI-1640) respectively, supplemented with 20% fetal bovine serum (FBS), 1% penicillin/streptomycin, and 2 mM L-glutamine, with or without 1 μM Dexamethasone (3.3mg/mL, Panpharma).

CRISPR/Cas9 genome editing and lentiviral transduction

Ribonucleoprotein comprising Cas9 and single guide RNA (Synthego) was used to knockdown *RPL11* in the K562 cell line. *ZFP36L2* cDNA open reading frame (Genscript) was introduced by lentiviral transduction (**table S5**). A single guide RNA (sgRNA) sequence (5'-UCCCUGUUGCAGCAGGAUCA-3') with 2'-O-methyl-3'-phosphorothiate modifications targeting exon 2 of *RPL11* (Synthego) was pre-complexed with *Streptococcus pyogenes* Cas9 nuclease (Synthego) at a molar ratio of 3:1 (sgRNA: Cas9) to form a ribonucleoprotein (RNP). Negative control comprised Cas9 without sgRNA. Transient transfection of K562 with RNP was performed using the Neon Transfection System (Thermo Fisher Scientific), per the manufacturer’s protocol. Electroporated cells were cultured for 3 days then sorted as single cells and expanded for 3 weeks. Clones were harvested for genomic DNA extraction using the Monarch Genomic DNA Purification Kit (New England Biolabs) per the manufacturer’s protocol.

Sanger sequencing

RPL11 exon 2 was amplified using forward (5'-TCCGAGCTGTCTTCTCCCT-3') and reverse (5'-TGTCTCCACTCTCCCAACA-3') primers and the Qiagen Fast Cycling PCR Master Mix 2x, as per manufacturer’s protocol. PCR products were purified (Monarch PCR & DNA Cleanup Kit;

New England Biolabs) and subjected to Sanger sequencing (Genewiz), then analyzed using the Interference of CRISPR Edits (ICE) tool (v2.0, Synthego).

Reverse Transcription Polymerase Chain Reaction (RT-PCR)

RNA was extracted using the Nucleospin RNA isolation kit (Macherey-Nagel) and cDNA synthesized using the RevertAid RT Reverse Transcription Kit or the Superscript III First Strand Kit (Thermo Fisher Scientific), as per manufacturer's protocol. RT-PCR was performed using TaqMan Fast Advanced Master Mix, probes as listed in **table S5**, and StepOnePlus Real-Time PCR system (Applied Biosystems). Each cDNA sample was run in triplicate. Gene expression was calculated using the $\Delta\Delta C_t$ method, with normalization of each sample to glyceraldehyde-3-phosphate dehydrogenase (*GAPDH*) then dexamethasone (Dex)-treated to untreated, *ZFP36L2* to mock or DBA to control.

Lentiviral transduction of K562

ZFP36L2 cDNA open reading frame (clone ID OHu05808) was amplified from the pcDNA3.1+/C-(K) DYK vector (GenScript) using Phusion Hot Start II High-Fidelity PCR Master Mix (Thermo Fisher Scientific) with forward (5'-TTTAGAATTCATGTCGACCA-3') and reverse (5'-TTAAGGCCTTCAGTCGTCGGAG-3') primers. Restriction enzymes EcoRI and StuI were used for cloning into the LeGO-iG2-IRES-EGFP vector (gift from Boris Fehse lab, AdDEGne plasmid #27341). 293T cells were transfected with psPAX2, pMD2.G alongside LeGO-iG2. Viral supernatant was harvested 48 hours post-transfection, concentrated by ultracentrifugation at 23,000g for 120 minutes at 4°C and stored at -80°C. To calculate viral titer [transducing units (TU) per ml], green fluorescent protein (GFP) expression was assessed by flow cytometry 5 days post-transduction of serial dilutions of virus. To transduce K562, non-coated 96-well flat bottom plates were pre-treated with retronectin 50 µg/ml (Takara) for 12 hours at 4°C followed by blocking with PBS plus 2% bovine serum albumin for 30 minutes at room temperature and washing with PBS plus 25 mM HEPES [4-(2-hydroxyethyl)-1-piperazineethanesulfonic acid; Sigma-Aldrich]. 8×10^5 K562 cells were transduced with either mock (empty vector) or *ZFP36L2* lentivirus using a multiplicity of infection of 2 to 5. Analysis was performed on days 2 to 4 post-transduction.

Clinical registry mutation analysis

RP mutations identified in patients included in this study are shown in **table S2**. Pathogenicity was assigned to variants as per the Association for Clinical Genomic Science (ACGS) criteria; clearly pathogenic [CPV], likely pathogenic [LPV], variant of unknown significance [VUS], unlikely pathogenic variant (UPV) and clearly not pathogenic (80). CPV are previously documented as pathogenic in the Leiden Open (source) Variant Database (LOVD) (81) or are new null variants

(nonsense, frameshift, canonical ± 1 or 2 splice sites, initiation codon, frameshift or whole allele deletions) in known DBA genes (genes known to harbor variants that cause DBA). Some mutations are missense mutations and non-canonical splice site defects classified as likely deleterious through multiple in silico platforms, such as the Mutation Taster for functional prediction (82). Mutations in RP genes not previously implicated in DBA or variants of unclear pathogenicity in known DBA genes were classified as VUS and not included in the study, pending further validation studies.

Supplementary Figures

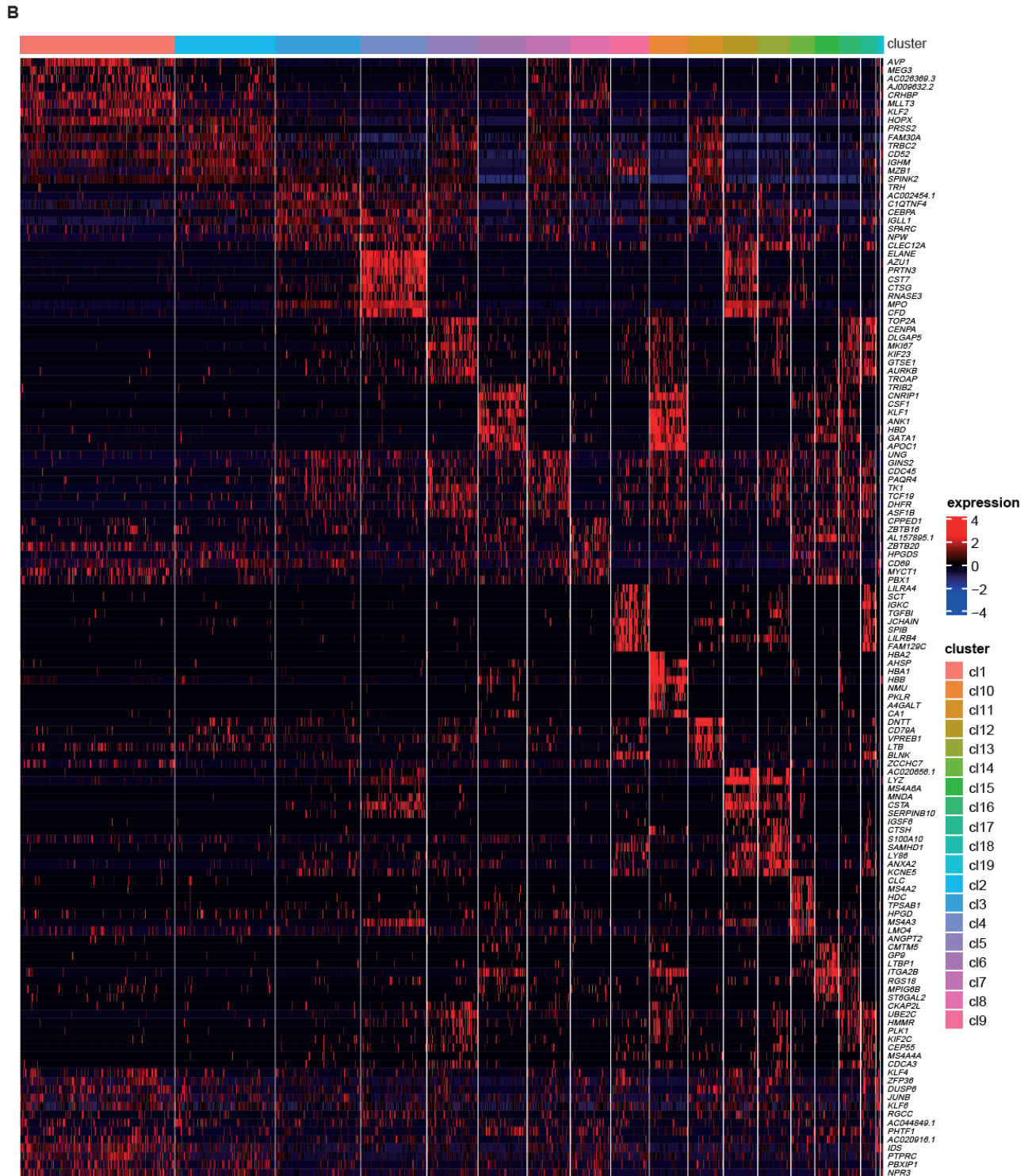
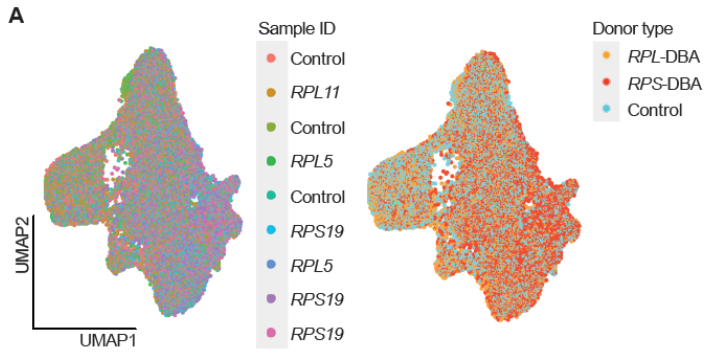


Fig. S1. ScRNA-seq of CD34⁺Lin⁻ hematopoietic stem and progenitor cells (HSPCs) and cell type annotation.

- A) Aggregate of 41,415 cells from 9 individual donors, after regression of donor effect. Single cells are colored by sample ID (left) and donor type (healthy control, *RPS*-DBA or *RPL*-DBA, right).
- B) The heatmap shows the top 8 top upregulated genes in 19 clusters generated by Louvain community-detection clustering method. Legend shows Z-score of expression.

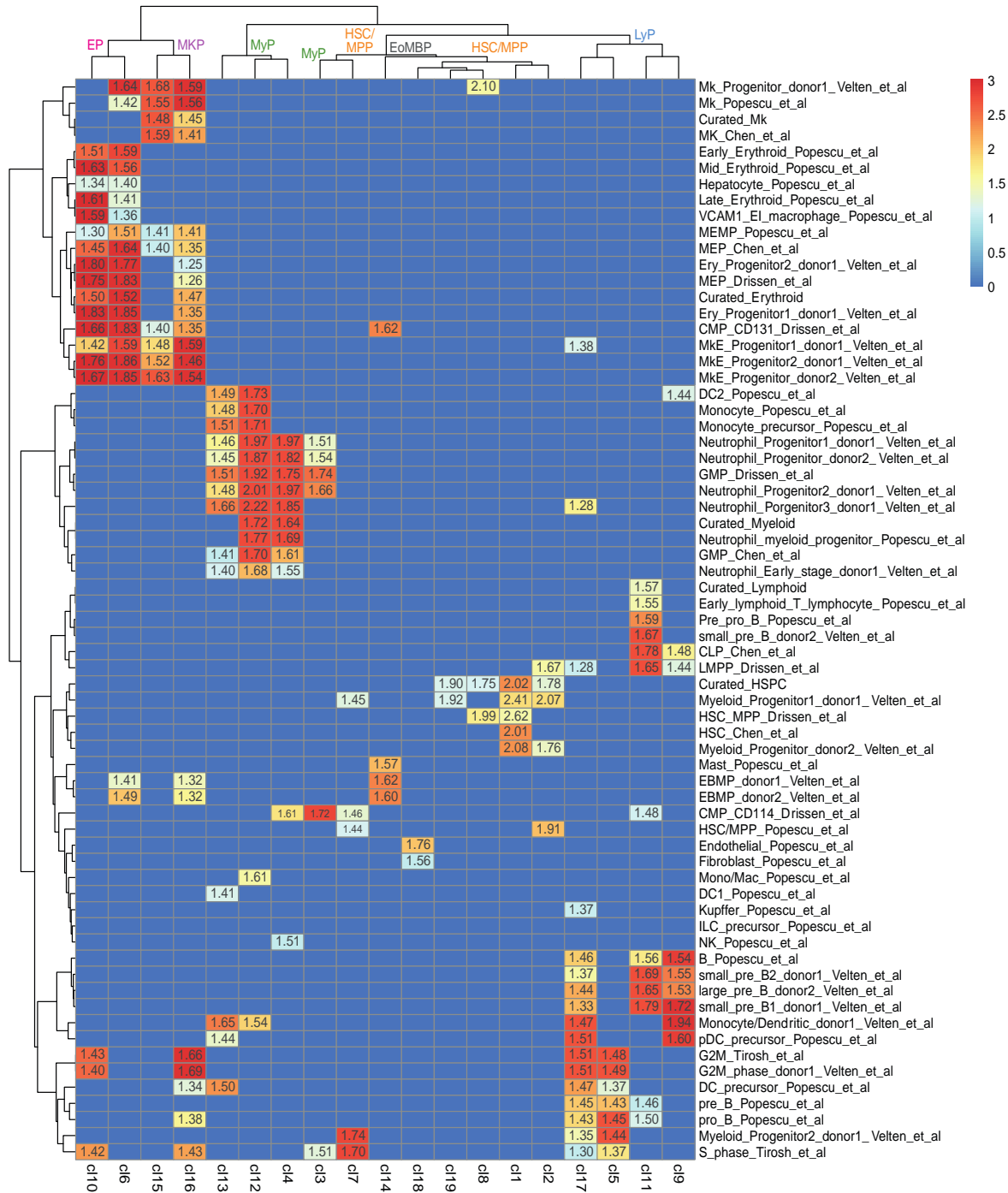


Fig. S2. Verification of hematopoietic lineage identity of Louvain clusters.

The heatmap shows partitioning of Louvain clusters (columns, ranked 1 to 19) according to upregulated expression of gene sets marking specific hematopoietic stem and progenitor cell populations (rows), derived from published scRNA-seq datasets (25–29). Legend shows Z-score of expression.

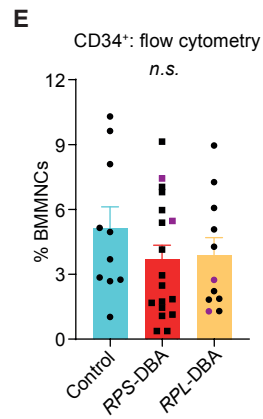
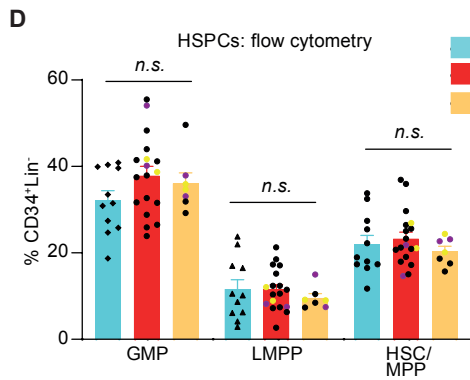
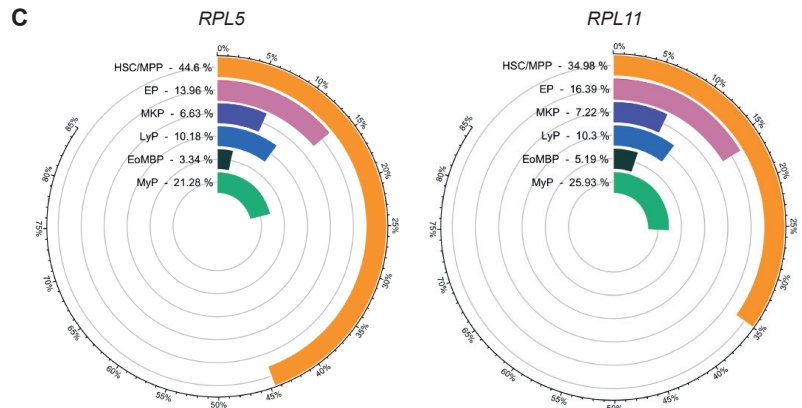
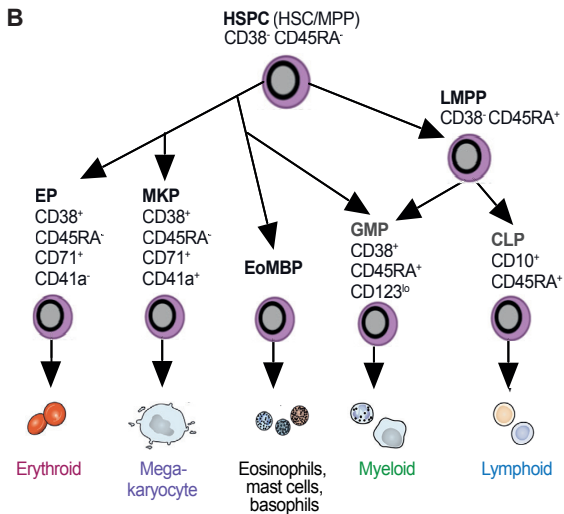
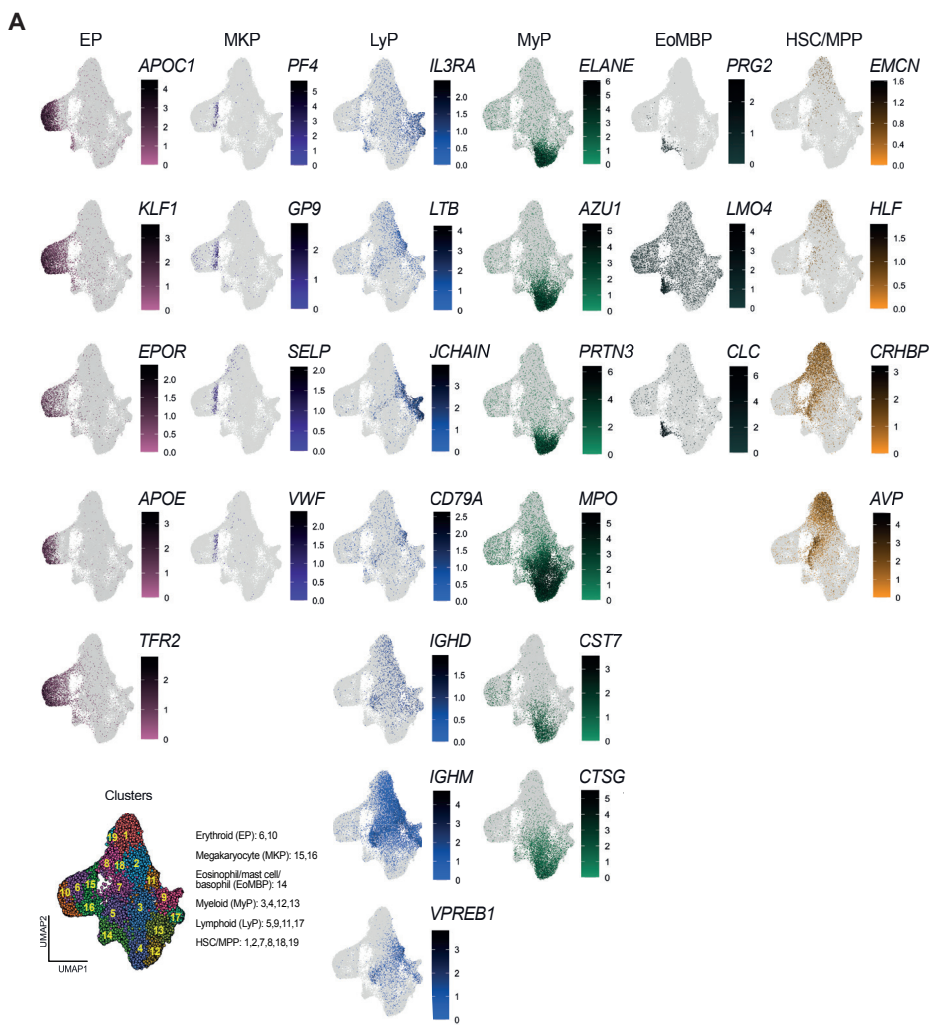


Fig. S3. Quantification of HSPC subsets.

- A)** UMAP plots of all CD34⁺Lin⁻ cells are shown embedded by expression of each gene used in the respective lineage gene signature set. Color gradients correspond to logarithmic-transformed expression. Abbreviations: HSC: hematopoietic stem cells; MPP: multipotent progenitors; EP: erythroid progenitors; LyP; lymphoid progenitors; MKP: megakaryocyte progenitors; MyP: myeloid progenitors; EoMBP: eosinophil/mast cell/basophil progenitors. UMAP embedded by Louvain clusters is shown at the bottom left for reference.
- B)** A schematic of recently revised model of the human hematopoietic hierarchy is shown (28, 83) in which undifferentiated HSPCs, including HSC and MPP split into 2 branches: one branch encompassing EP, MKP and EoMBP, and the other branch comprising lymphoid-primed multipotent progenitors (LMPP). The latter specify further into common lymphoid (CLP) and granulocytic-macrophage (GMP) progenitors (34).
- C)** Circos plots depict lineages of CD34⁺Lin⁻ cells according to *RPL5* or *RPL11* genotype.
- D)** Frequencies of HSC/MPP, LMPP and GMP are expressed as percent of CD34⁺Lin⁻ cells, as measured by flow cytometry in CD34⁺ cells isolated from healthy control ($n=11$), *RPS*-DBA ($n=18$) and *RPL*-DBA ($n=7$) fresh bone marrow. Immunophenotypes were defined as shown in **fig. S3B**.
- E)** Frequencies of CD34⁺ cells are expressed as percent of BMMNCs isolated from healthy control ($n=10$), *RPS*-DBA ($n=18$) and *RPL*-DBA ($n=11$) fresh bone marrow.

Plots show mean \pm SEM of biological replicates. *n.s.*, not significant. Groups were compared by a Kruskal-Wallis with Dunn's multiple comparisons test.

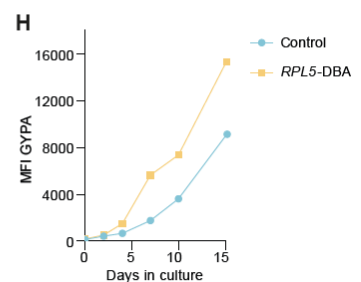
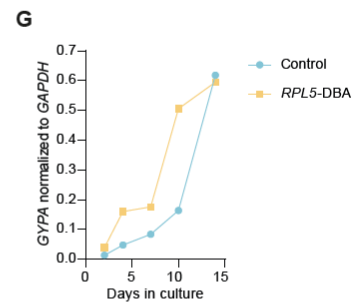
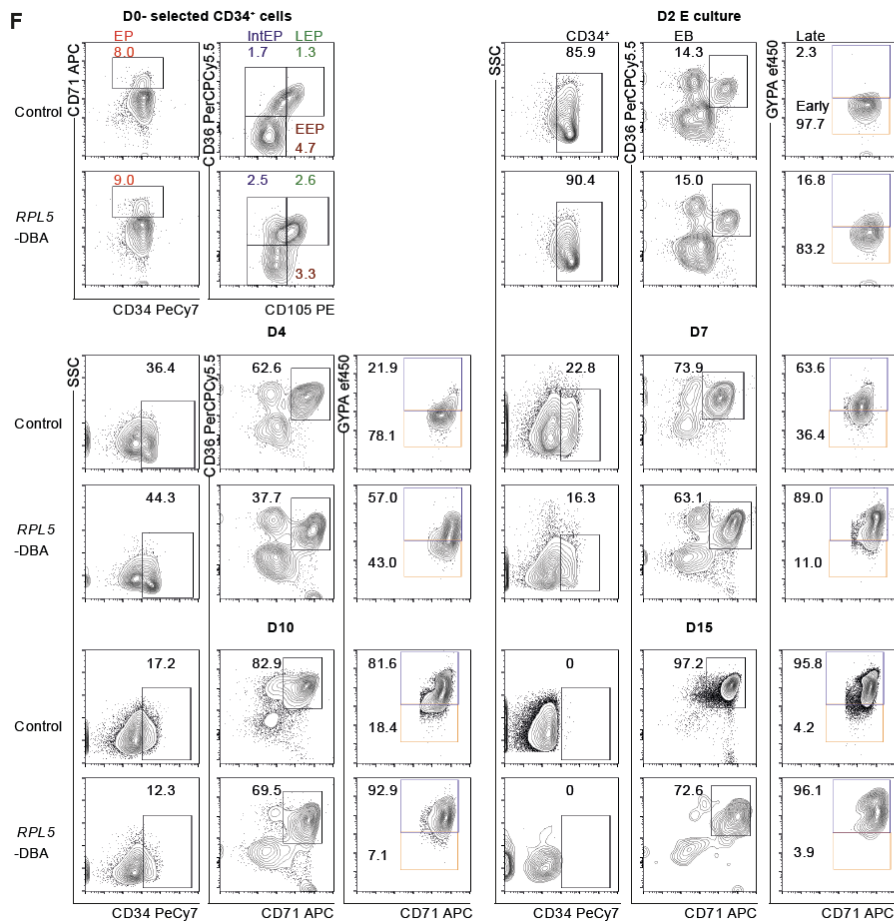
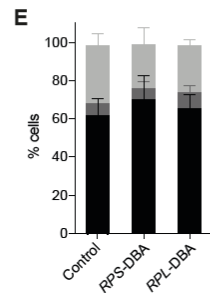
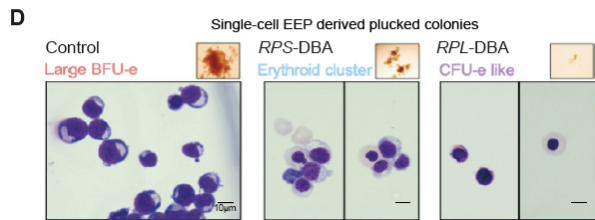
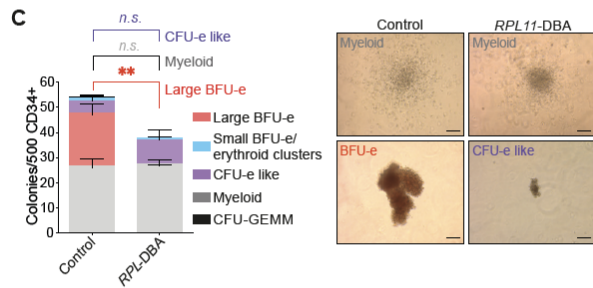
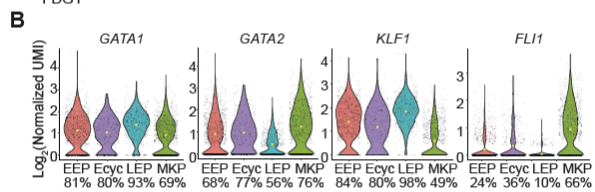
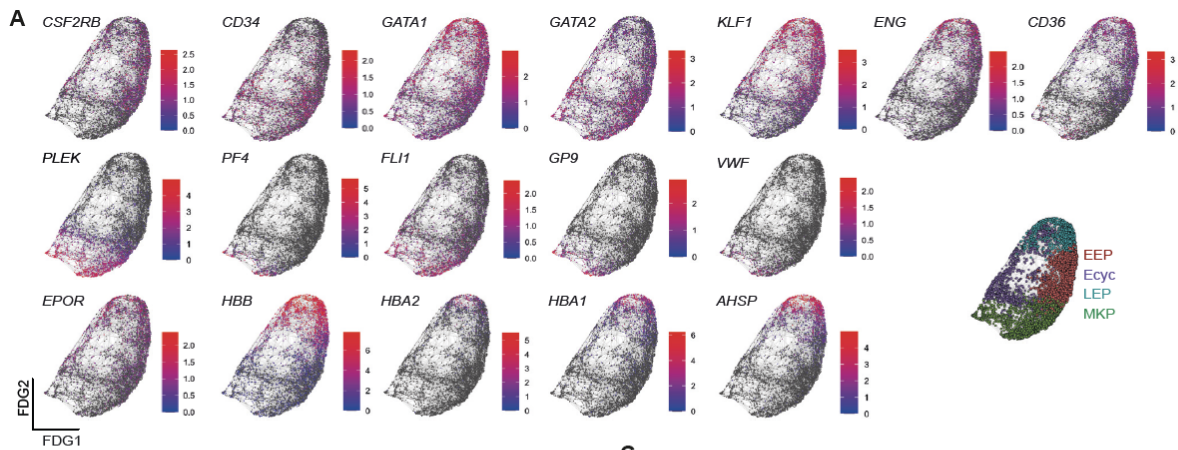


Fig. S4. Characterization of EP phenotype and function.

- A)** Expression of individual genes superimposed on FDG of all EP/MKP cells ($n=6380$) is shown, depicting a pattern of gene expression in normal mega-erythroid differentiation. Gray cells do not express the gene of interest. Color correlates with logarithmic-transformed expression as shown in color key.
- B)** Violin plots show expression of E/MK-related transcription factors in control EP/MKP subclusters ($n=2870$; 1050 EEP, 393 Ecyc, 479 LEP, 948 MKP). Yellow dot indicates mean expression and the fraction of cells expressing each gene is depicted on the x axis.
- C)** Number and morphology of erythroid and myeloid colonies, assessed at 14 days of culture of CD34⁺Lin⁻ cells. Cells were FACS-sorted from control and RPL-DBA bone marrow ($n=3$) in triplicate into methylcellulose permissive of erythroid and myeloid development. CFU- GEMM, colony-forming unit - granulocyte erythroid macrophage megakaryocyte. Scale bar, 100 μ m.
- D)** Cellular composition of single EEP-derived colonies plucked and cytopun on day 12 of culture is shown. BFU-e derived from control comprise nucleated, early EB. Erythroid clusters or CFU-e like colonies, derived from RPS-DBA or RPL-DBA EEP respectively, comprise fewer cells at a later stage of differentiation, from EB to anuclear reticulocytes. Lines within images show where empty space between cells has been cropped. Scale bar, 10 μ m.
- E)** Relative proportions of live (annexin V [AV]⁻ 4',6-diamidino-2-phenylindole [DAPI]⁻), early apoptotic (AV⁺DAPI⁻) and late apoptotic/necrotic (AV⁺DAPI⁺) cells are shown as determined on day 12 by flow cytometry, in control, RPS-DBA and RPL-DBA erythroid culture ($n=2$).
- F)** Dynamics of in vitro erythroid differentiation of control and RPL5-DBA bone marrow ($n=1$) are shown. EP frequencies are shown as percentage of total CD34⁺ cells on D0 and early and late EB as percentage of total CD71⁺CD36⁺ EB on Days 2, 4, 7, 10 and 15. GYPA, Glycophorin A; SSC, side scatter.
- G)** GYPA expression, normalized to GAPDH, during in vitro erythroid differentiation of control and RPL5-DBA bone marrow ($n=1$) was measured by RT-PCR in FACS-sorted CD71⁺ EB.
- H)** Mean Fluorescence Intensity (MFI) of GYPA is shown in CD71⁺ EB during in vitro erythroid differentiation of control and RPL5-DBA bone marrow ($n=1$).

Charts show mean \pm SEM of biological replicates. ** $P < 0.01$; *n.s.*, not significant. Groups were compared by a Student's t test (C).

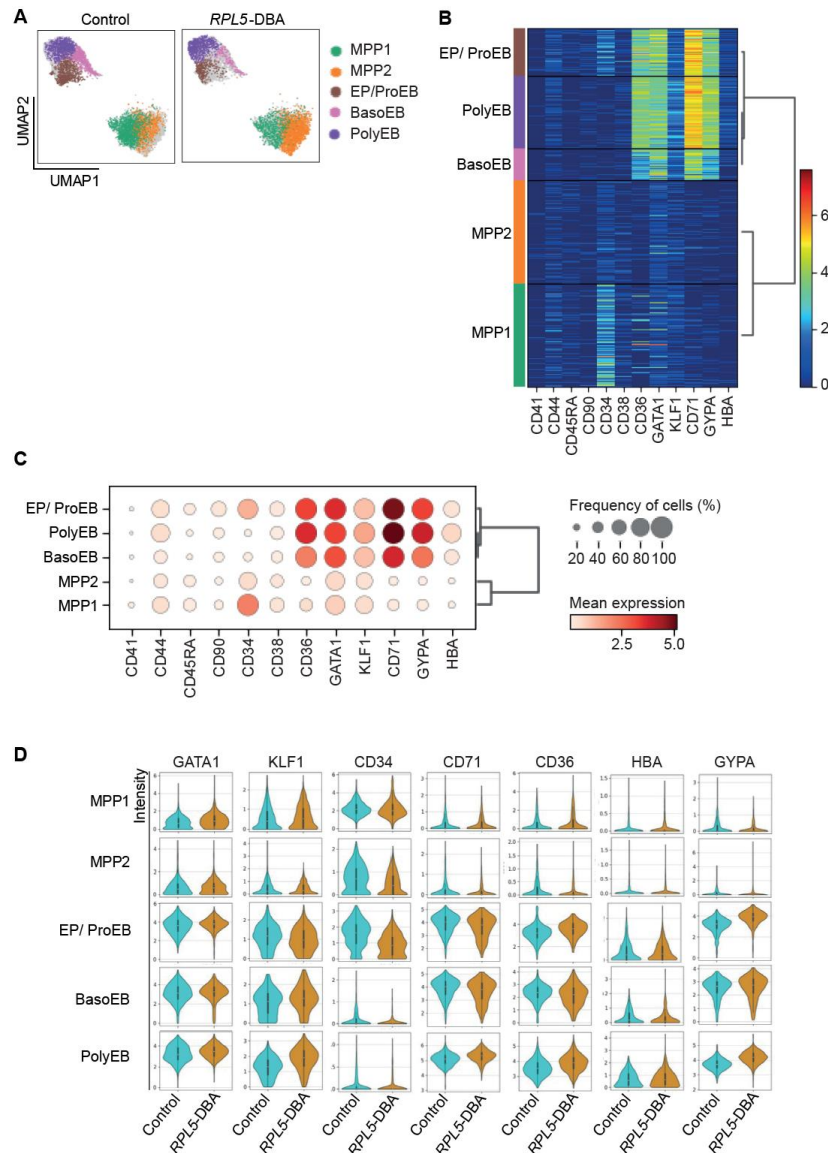


Fig. S5. Single-cell proteomics in bone marrow ex vivo reveals disordered differentiation in *RPL5-DBA*.

- A) UMAP embedding of 5 unsupervised Leiden clusters of single cell cytometry by time of flight (scCyTOF) proteomic data from control ($n=4138$; 1 donor) and *RPL5-DBA* BMMNCs ($n=2167$; 1 donor).
- B) A heatmap shows expression of cell surface and intracellular erythroid proteins measured by scCyTOF in 5 clusters (labeled on left). The major partition in the dendrogram is between MPP and EP/EB clusters.
- C) The bubble plot shows the frequency of cells (bubble size) and average expression (color scale) in each of 5 clusters that express cell surface and intracellular erythroid markers.
- D) Violin plots show the expression of cell surface and intracellular erythroid proteins in cell clusters as measured by scCYTOF in control and *RPL5-DBA* BMMNCs ($n=1$).

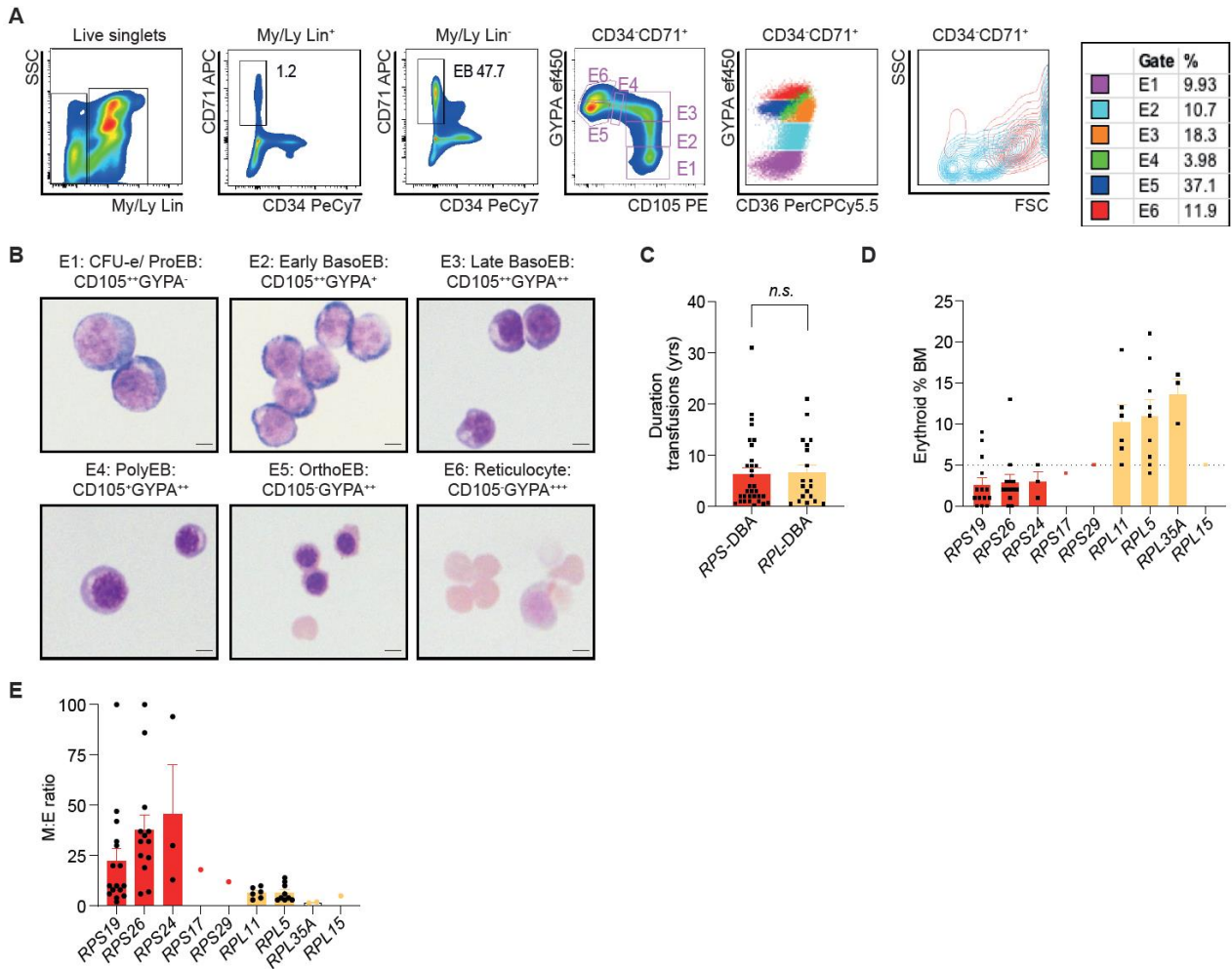


Fig. S6. Characterization of mature erythropoiesis in DBA.

- A)** Gating strategy for identification and prospective isolation of mature EB is shown. Shown are representative flow cytometry plots of normal BMMNCs. Percent is of parent population, which is indicated above plots. CD71⁺ cells comprise less than 2% of myeloid (My)/ lymphoid (Ly) lineage-positive compartment. My/Ly Lin antibodies comprise CD3, CD56, CD10, CD19, CD14, CD15 or CD16. Expression continuum of CD36 in 6 populations is shown. Table shows relative proportions of E1-E6, expressed as a percentage of total CD34⁺CD71⁺ EB. CFU-e/ProEB are CD105⁺⁺GYPA⁻, early BasoEB are CD105⁺⁺GYPA⁺, late BasoEB are CD105⁺⁺GYPA⁺⁺, PolyEB are CD105⁺GYPA⁺⁺, OrthoEB are CD105⁻GYPA⁺⁺, and reticulocytes are CD105⁻GYPA⁺⁺⁺, concordant with published data (39). APC, allophycocyanin; FSC, forward scatter; PE, phycoerythrin; PE-Cy7, phycoerythrin-cyanine7; PerCP-Cy5.5, peridinin-chlorophyll-protein complex-cyanine5.5.
- B)** CD34⁻Lin⁻CD71⁺ Live singlets were FACS-purified according to expression of CD105 and GYPA. Morphology of FACS-isolated and Hematoxylin & Eosin-stained EB subpopulations is shown. Scale bar, 5 μ m.

- C)** Duration of red blood cell transfusions (years) at time of bone marrow sampling from individuals with *RPS*-DBA ($n=32$) and *RPL*-DBA ($n=19$) is shown.
- D)** EB frequency is expressed as a percent of total nucleated cells in bone marrow aspirates from patients with DBA, according to genotype (*RPS19* $n= 14$, *RPS26* $n=13$, *RPS24* $n=3$, *RPS17* $n=1$, *RPS29* $n=1$, *RPL11* $n=6$, *RPL5* $n=9$, *RPL35A* $n=3$, *RPL15* $n=1$).
- E)** The ratio of frequency of myeloid to erythroid lineage cells (M:E ratio) in bone marrow aspirates from patients with DBA is shown, according to genotype.

Plots show mean \pm SEM of biological replicates. Variables were compared across genotypes using a Mann-Whitney U or a Kruskal-Wallis with Dunn's multiple comparisons test, as appropriate. *n.s.*, not significant.

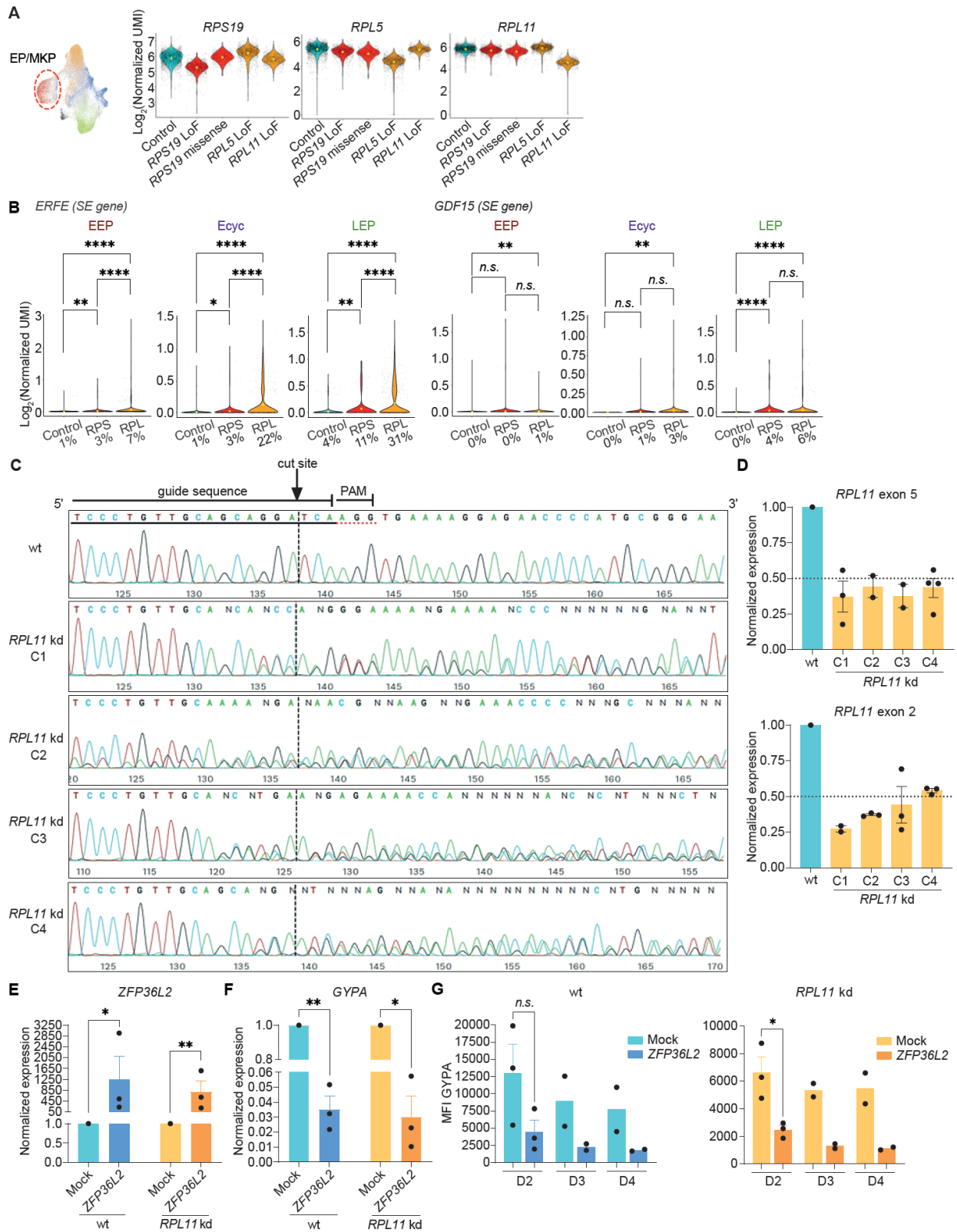


Fig. S7. DBA stress erythropoiesis and overexpression of *ZFP36L2* in wt and *RPL11* kd K562.

A) Expression of *RPS19*, *RPL5* and *RPL11* is shown in EP/MKP cluster cells from healthy control ($n=3$), *RPL5* loss of function (LoF; $n=2$), *RPL11* LoF ($n=1$), *RPS19* LoF ($n=2$) and *RPS19* missense mutation ($n=1$). Violin plots depict the mean expression (yellow dot) and its distribution (minimum to maximum). Fraction of cells expressing three genes is 100% for all groups.

- B)** Violin plots depict expression of *ERFE* and *GDF15* (stress erythropoiesis genes) at indicated stages.
- C)** Sanger sequencing traces (sense strand) of wild type (wt; representative of 6 clones) and 4 *RPL11*-knockdown (kd) K562 clones (termed C1-C4) are shown. Guide sequence, cut site and PAM (protospacer adjacent motif) are shown.
- D)** *RPL11* expression was measured by RT-PCR in wt and *RPL11* kd K562 clones ($n=4$), normalized to wt and *GAPDH*. Data points represent technical replicates of RNA harvested at distinct time points of culture.
- E)** *ZFP36L2* was measured by RT-PCR, in wt and *RPL11* kd K562 clones 2 days post lentiviral transduction with mock (empty vector) or *ZFP36L2*, normalized to mock and *GAPDH* ($n=3$).
- F)** *GYP A* was measured by RT-PCR, in wt and *RPL11* kd K562 clones 2 days post lentiviral transduction with mock or *ZFP36L2*, normalized to mock and to *GAPDH* ($n=3$).
- G)** MFI of *GYP A* was measured 2 to 4 days post lentiviral transduction with mock or *ZFP36L2* [$n=3$ (D2) or $n=2$ (D3 and 4)].

P values are indicated as ****P<0.0001; **P<0.01, *P<0.05, *n.s.*, not significant. Groups were compared by a Wilcoxon rank-sum test (**B**) or a paired Student's t test (**E**, **F**, and **G**).

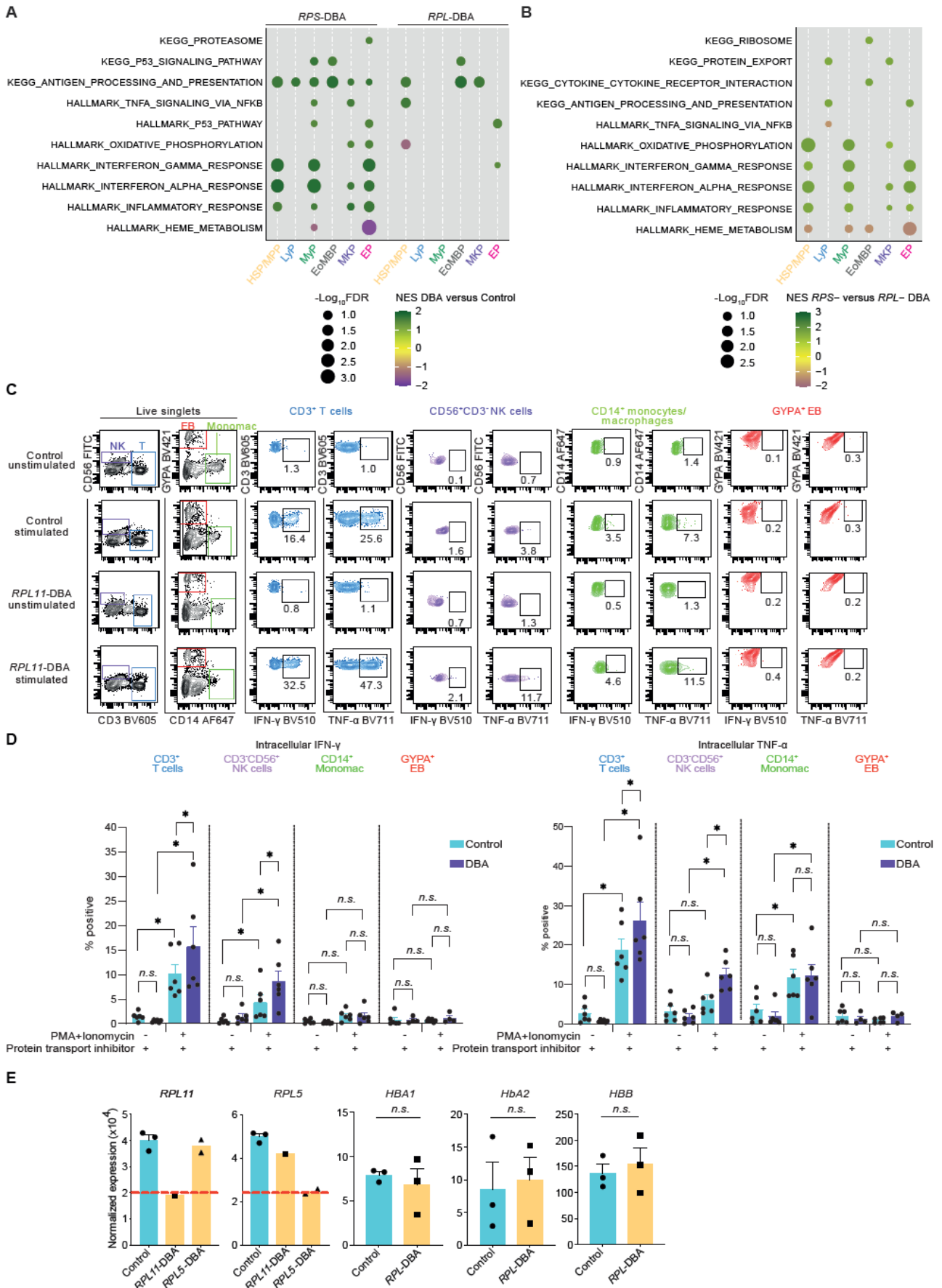


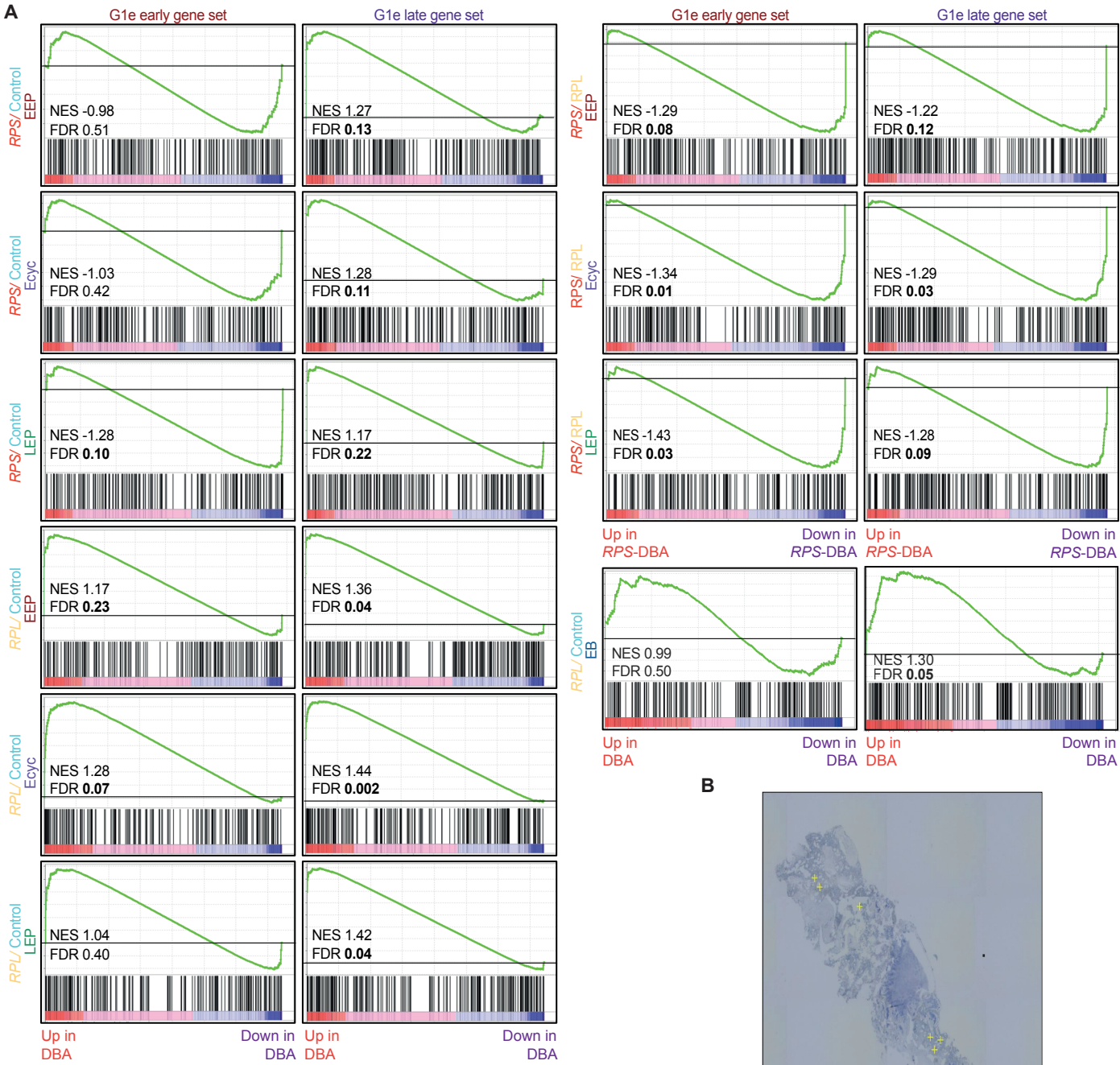
Fig. S8. Aberrant molecular signatures in DBA erythropoiesis.

A) Bubble plot showing normalized enrichment score (NES) and false discovery rate ($-\text{Log}_{10}$ FDR) of significantly enriched (FDR q value of <0.25) pathways of interest (y axis) upon

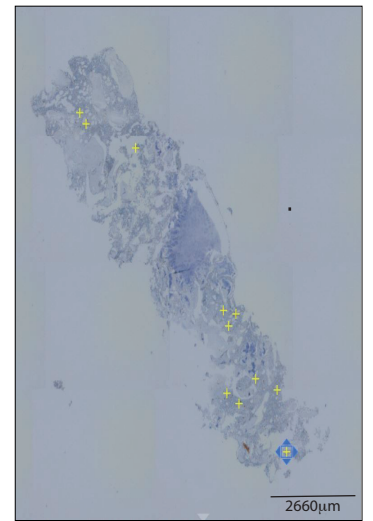
GSEA of all pre-ranked differentially expressed genes (DEG) between control and DBA HSPC cell types (x axis).

- B)** The bubble plot shows enriched pathways on GSEA of all pre-ranked DEG between *RPS*- and *RPL*-DBA HSPC cell types.
- C)** Intracellular TNF- α and IFN- γ , assessed by flow cytometry of bone marrow CD3⁺ T cells, CD3⁺CD56⁺ natural killer (NK) cells, CD14⁺ monocytes/macrophages and GYPA⁺ EB in control and *RPL11*-DBA BMMNCs ex vivo, following 5 hours incubation with PMA and ionomycin plus protein transport inhibitor (stimulated) or protein transport inhibitor alone (unstimulated). AF647, Alexa Fluor 647; BV421, Brilliant Violet 421; BV605, Brilliant Violet 605; BV711, Brilliant Violet 711; FITC, fluorescein isothiocyanate.
- D)** Intracellular TNF- α and IFN- γ in controls ($n=6$, including 2 samples from same donor stained independently) and DBA [$n=2$ *RPS19* (insufficient EB for assessment), $n=3$ *RPL5* and $n=1$ *RPL11*], following 5 hours incubation with PMA and ionomycin plus protein transport inhibitor (stimulated) or protein transport inhibitor alone (unstimulated).
- E)** Normalized expression of genes of interest, quantified by bulk RNA-seq in FACS-isolated stage-matched EB from 3 *RPL*-DBA (*RPL11*, $n=1$ and *RPL5*, $n=2$) patients, compared with 3 healthy controls. Red dashed line highlights 50% gene expression relative to control.

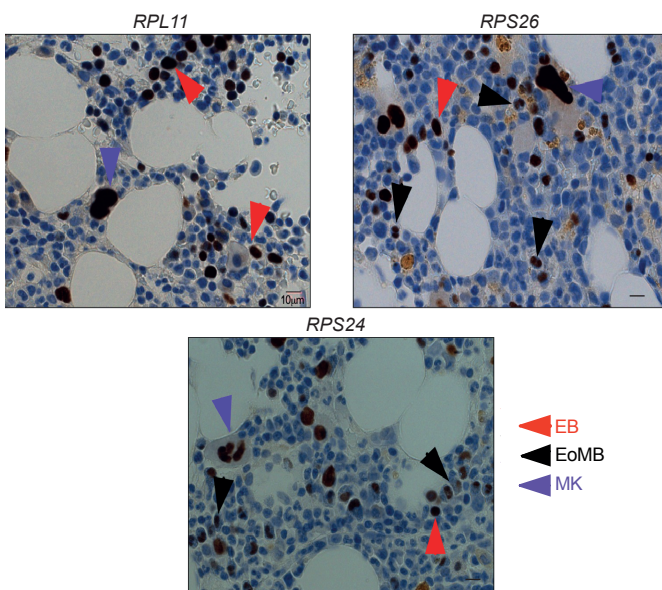
Plots show mean \pm SEM of biological replicates. * $P < 0.05$, *n.s.*, not significant. Groups were compared by a Wilcoxon matched- pairs signed-rank test (**D**) or a Mann-Whitney U test (**E**).



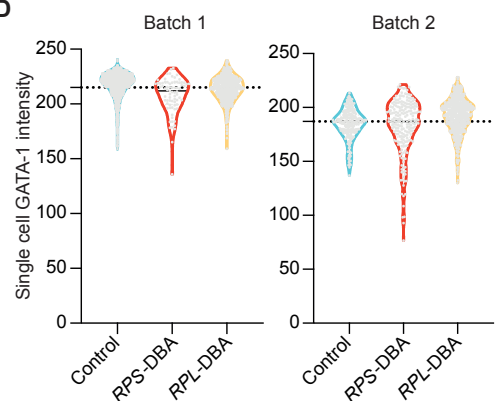
B



C



D



E

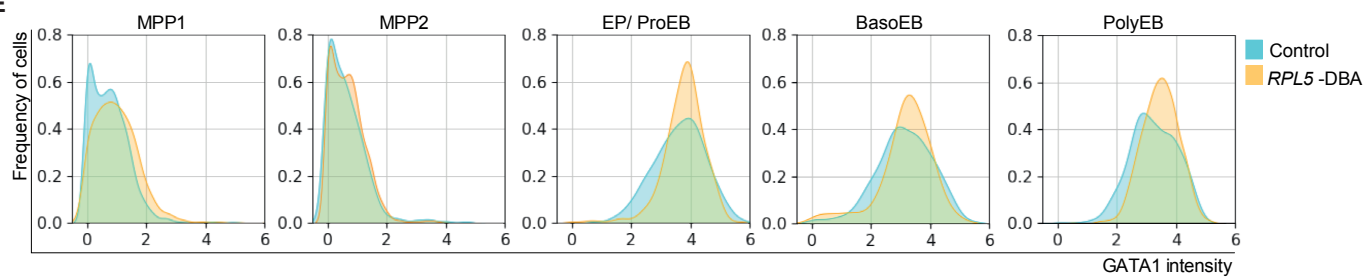


Fig. S9. GATA1 transcriptional activity and expression.

- A)** GSEA against GATA1 gene sets of pre-ranked DEG between control and DBA donors at distinct erythroid stages (scRNA-seq for EP and bulk RNA-seq for EB) are shown. NES and FDR q values are shown. Gene sets were defined as upregulated genes in the G1e cell line at two differentiation time points, termed early and late, after GATA1 activation (12, 49).
- B)** Representative image of bone marrow trephine biopsy section captured with the 5x objective of a Zeiss Axio Observer Inverted Widefield Microscope. Ten to 15 sites (marked with yellow crosses) were imaged in each section to ensure sampling of distinct, non-overlapping areas of tissue. Scale bar, 2660 μm .
- C)** Examples of GATA1 staining by IHC in bone marrow from *RPL11*-, *RPS26*-, and *RPS24*-DBA patients are shown. Scale bar, 10 μm .
- D)** Violin plots show the distribution of single cell GATA1 expression in EB from control, *RPS*-DBA, and *RPL*-DBA bone marrow. Batches refer to bone marrow sections imaged on different days. Distribution is from 5th percentile to 95th percentile. Dotted line shows mean expression of all samples in each batch.
- E)** Histograms show intracellular GATA1 expression in stage-matched MPP, EP, and EB clusters as measured by scCyTOF in control ($n=4138$; 1 donor) and *RPL*-DBA BMMNCs ($n=2167$; 1 donor).

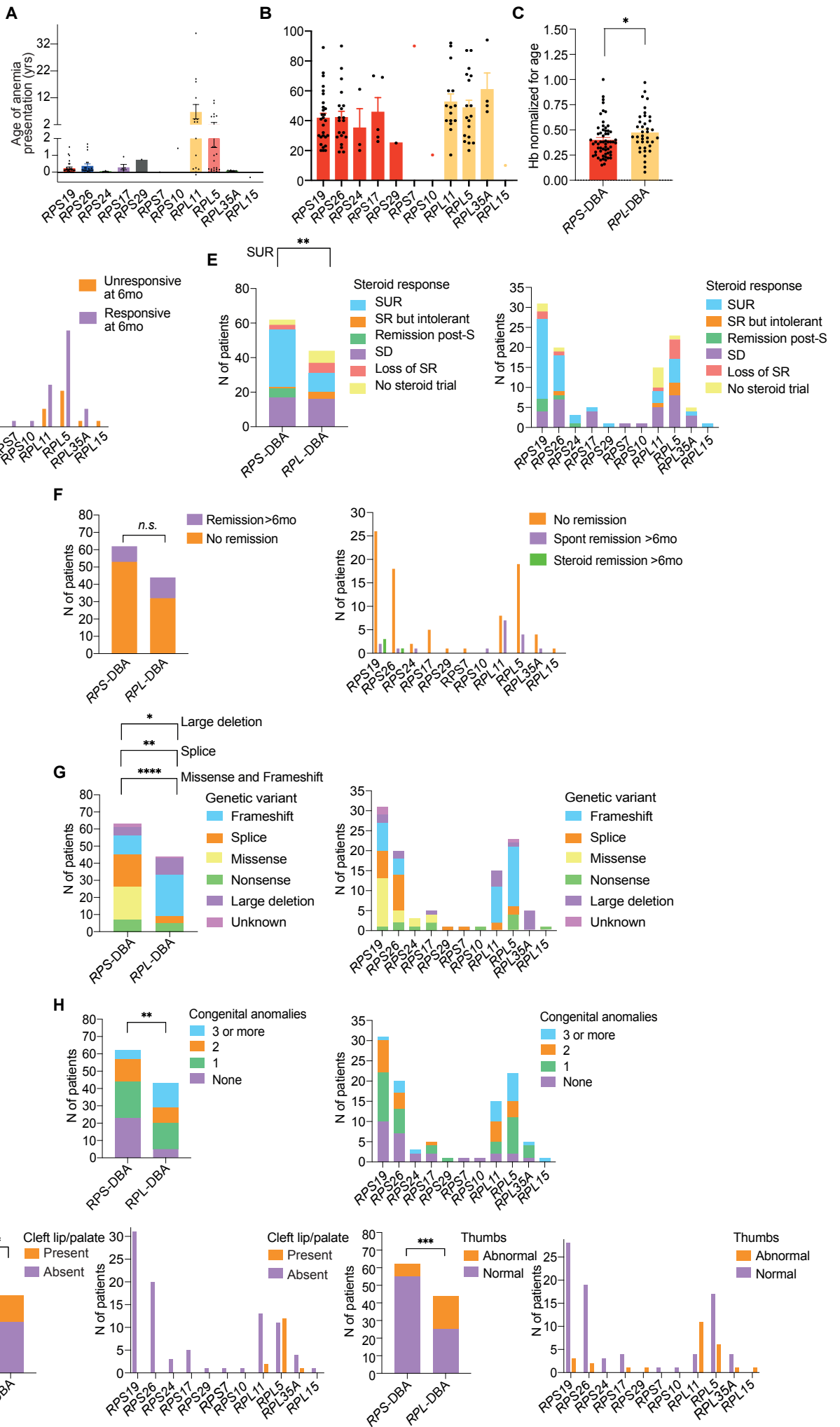


Fig. S10. Genotype-phenotype correlations in the United Kingdom (UK) DBA cohort.

- A) Age at presentation with anemia (years) is shown according to genotype (*RPS19* $n=31$, *RPS26* $n=20$, *RPS24* $n=3$, *RPS17* $n=5$, *RPS10* $n=1$, *RPS29* $n=1$, *RPS7* $n=1$, *RPL11* $n=15$, *RPL5* $n=23$, *RPL35A* $n=5$, *RPL15* $n=1$).
- B) Hemoglobin (Hb) concentration at presentation is shown, according to genotype.
- C) Hb at presentation, according to *RPS*-DBA ($n=59$) or *RPL*-DBA ($n=38$), was normalized for age by dividing by the lower limit of the age-specific normal range for each patient.
- D) Corticosteroid-responsive (transfusion-independent) status at 6 months (mo) is shown according to genotype (*RPS19* $n=29$, *RPS26* $n=19$, *RPS24* $n=3$, *RPS17* $n=5$, *RPS10* $n=1$, *RPS29* $n=1$, *RPS7* $n=1$, *RPL11* $n=10$, *RPL5* $n=22$, *RPL35A* $n=4$, *RPL15* $n=1$).
- E) Long-term corticosteroid responses according to *RPS* or *RPL* subgroup or specific genotype is shown. S, steroids; SR, steroid responsive; SUR, steroid unresponsive; SD, steroid-dependent.
- F) Remission more than 6 months is shown according to *RPS* or *RPL* subgroup or specific genotype.
- G) Type of genetic variant is shown according to *RPS* or *RPL* subgroup or specific genotype.
- H) The number of congenital anomalies is shown according to *RPS* ($n=62$) or *RPL* ($n=43$) subgroup or specific genotype.
- I) Congenital anomalies of the thumb/radius or cleft lip/palate is shown according to *RPS* or *RPL* subgroup or specific genotype (*RPS19* $n=31$, *RPS26* $n=20$, *RPS17* $n=5$, *RPS24* $n=3$, *RPS10* $n=1$, *RPS29* $n=1$, *RPS7* $n=1$, *RPL11* $n=15$, *RPL5* $n=22$, *RPL35A* $n=5$, *RPL15* $n=1$).

Samples sizes are $n=62$ for *RPS*-DBA and $n=44$ for *RPL*-DBA unless otherwise stated. Variables were compared across genotype using the Mann-Whitney U or Kruskal-Wallis with Dunn's multiple comparisons test, as appropriate. Fractions of patients were compared across genotypes using the Pearson chi-square test. All variables significant on univariate analysis were tested by multivariate regression and P values refer to the latter. **** $P<0.0001$; *** $P<0.001$; ** $P<0.01$; * $P<0.05$; *n.s.*, not significant.

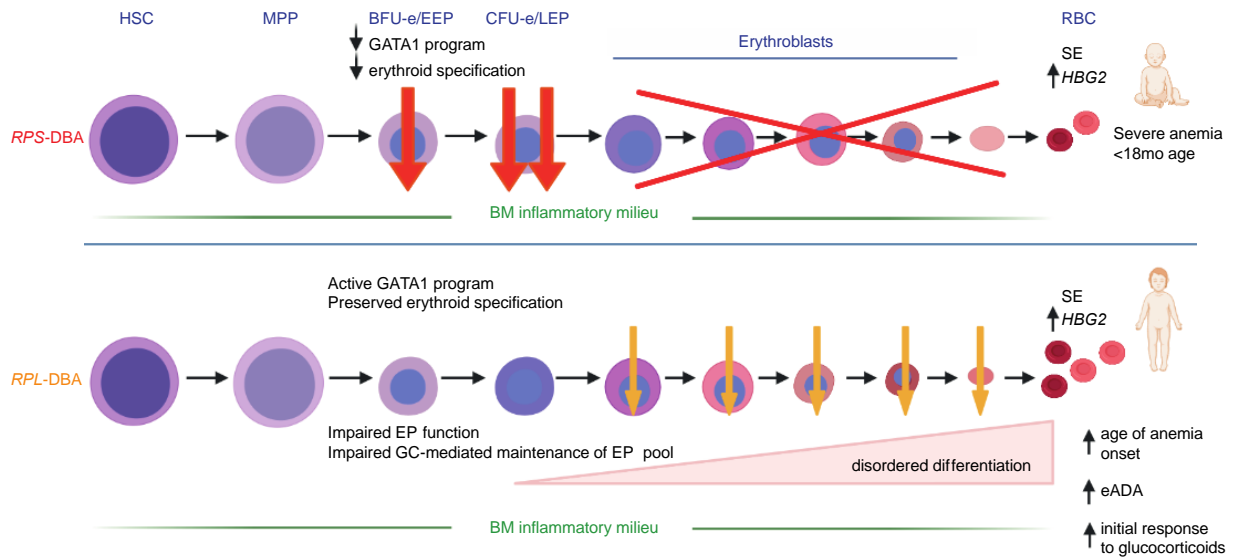


Fig. S11. Graphical summary.

A proposed model of *RPS*- vs *RPL*-DBA erythropoiesis summarizing the findings of this work.

Table S2. Pathogenic mutations and deletions in RP genes identified in all patients in the UK DBA cohort (pathogenic mutation identified in 106 of 161 patients). The Human Genome Organization Gene Nomenclature Committee nomenclature (7, 80) is used for DNA changes and proteins. ACGS criteria were used to assess pathogenicity, as described in the methods. There were 62 patients with *RPS*-genotype, including 2 multiplex families and 44 patients with *RPL*-genotype, including 3 multiplex families. Note that *GATA1* mutations were not identified in any patients in the UK cohort. Patients with VUS or no detected mutations were not included in genotype-phenotype analyses.

Gene DNA variant	Protein	N affected cases	N affected families, where >1 case
<i>RPS19</i> c.296_297delTG	p.?	1	
<i>RPS19</i> c.11delT	p.Thr5Leufs*2	1	
<i>RPS19</i> c.280C>T	p.Arg94*	1	
<i>RPS19</i> c.49G>C	p.Ala17Pro	1	
<i>RPS19</i> c.71+1G>T	p.?	1	
<i>RPS19</i> c.184C>T	p.Arg62Trp	1	
<i>RPS19</i> c.203_204dupG	p.Gly69Trpfs85*	1	
<i>RPS19</i> c.57delA	p.?	1	
<i>RPS19</i> c.412-2A>C	p.?	1	
<i>RPS19</i> c.296dupT	p.Ala100Glyfs*54	1	
<i>RPS19</i> c.3G>A	p.Met1?	3	3
<i>RPS19</i> allele deletion		1	
<i>RPS19</i> c.172+2T>G	p.?	1	
<i>RPS19</i> c.328delC	p.Leu1110*	1	
<i>RPS19</i> c.302G>C	p.Arg101Pro	1	
<i>RPS19</i> Int 2; int4 c.-152+1G>A; ex5-12del	p.?	1	
<i>RPS19</i> c.167G>T	p.Arg56Leu	1	
<i>RPS19</i> c.151-1G>T	p.?	1	
<i>RPS19</i> c.361C>G	p.Arg121Gly	2	1
<i>RPS19</i> c.3G>T	p.0?	1	
<i>RPS19</i> c.(?_1)(172+155_?) deletion exons 1-3	p.?	1	

<i>RPS19 c.156G>T</i>	p.Trp52Cys	1	
<i>RPS19 c.1-1G>T</i>	p.0?	1	
<i>RPS19 c.302 G>A</i>	p.Arg101His	1	
<i>RPS19 c.251_252delGA</i>	p.Arg84Lysfs*69	1	
<i>RPS19 c.356+1 G>A</i>	p.?	1	
<i>RPS19^a</i>		2	
<i>RPS26 c.176_177delTCinsAA</i>	p.Phe59*	1	
<i>RPS26 c.55C>T</i>	p.Gln9*	1	
<i>RPS26 c.259C> T</i>	R87*	1	
<i>RPS26 c.1A>G</i>	p.Met1 Val	1	
<i>RPS26 c.3+1G>A</i>	p.?	2	
<i>RPS26 c.6_9delAAAG</i>	p.Lys4Glufs*40	1	
<i>RPS26 c.3+1G>C</i>	p.?	1	
<i>RPS26 splice donor intron 1 c.3+1G>T</i>	p.?	4	
<i>RPS26 c.9_12delGAAA</i>	p.Lys4Glufs*40	1	
<i>RPS26 allele deletion</i>		2	2
<i>RPS26 c.30+1G>A</i>	p.?	1	
<i>RPS26 c.6_9delAAAG</i>	p.Lys4Glufs*40	1	
<i>RPS26 c.312+2T>A</i>	p.?	1	
<i>RPS26 c.3+2T>G</i>	p.?	1	
<i>RPS26 c.344T>C</i>	p.Met115Thr	1	
<i>RPS24 c.2T>G</i>	p.Met1Arg	1	
<i>RPS24 c.46C>T</i>	p.Arg16*	1	
<i>RPS24 c.1A>G</i>	p.0?	1	
<i>RPS17: c.3G>C</i>	p.?	1	
<i>RPS17 c.159T>G</i>	Y53*	2	1
<i>RPS17 allele deletion</i>		1	
<i>RPS17 c.1A>G</i>	p.?	1	
<i>RPS7 c.147+1G>T</i>	p.?	1	
<i>RPS29 c.63-3C>A</i>	p.?	1	
<i>RPS10 c.337C>T</i>	p.Arg113*	1	
<i>RPL11 allele deletion</i>		3	3
<i>RPL11 c.396+1G>T</i>	p.?	2	1

<i>RPL11 c.60_61delCT</i>	p.Cys21Serfs*33	2	2
<i>RPL11c.475_476delAA</i>	p.Lys159Argfs*12	1	
<i>RPL11 c.136-137insAG</i>	p.Thr47Argfs*42	1	
<i>RPL11 c.204delT</i>	p.?	1	
<i>RPL11 deletion intron exon</i>	p.0?	1	
<i>RPL11 c.202_203insG</i>	p.I67*	1	
<i>RPL11 c.44-45delTTinsCCCATC</i>	p.Lys15Profs*41	1	
<i>RPL11 c.58_59delCT</i>	p.Cys21Serfs*33	1	
<i>RPL11 deletion exons 5 and 6</i>		1	
<i>RPL5 c.172_173delAG</i>	p.Asp59Tyrf*53	1	
<i>RPL5 c.535C>T</i>	p.Arg179Ter	1	
<i>RPL5 c.367delG</i>	p.Val1123	1	
<i>RPL5 c.166-169del</i>	p.Asn57Glufs*12	1	
<i>RPL5 c.175_176delGA</i>	p.Asp59Tyrf*53	4	4
<i>RPL5 c.625_626insG</i>	p.?	1	
<i>RPL5 c.169_172delAACA</i>	p.Asn57Glufs*12	2	2
<i>RPL5 c.244C>T</i>	E82*	2	1
<i>RPL5 c.664C>T</i>	Q222*	1	
<i>RPL5 c.178_179delAT</i>	p.Ile60Hisfs*	1	
<i>RPL5 allele deletion</i>		1	
<i>RPL5 c.324+1G>C</i>	p.?	1	
<i>RPL5 c.190-1G>C</i>	p.?	1	
<i>RPL5 c.189delG</i>	p.Ile64LeufsTer6	1	
<i>RPL5^a</i>		2	
<i>RPL5 c.350delA</i>	p.Lys117Argfs*9	2	1
<i>RPL35A allele deletion: boundaries of deletion not established</i>		2	2
<i>3q microdeletion syndrome; RPL35A allele deletion</i>		2	2
<i>17.4Mb gain region 3q26.32 to q29 and loss 2.1Mb 3q29: RPL35A allele deletion</i>		1	
<i>RPL15 c.260G>A</i>	pTrp120*	1	

^aPathogenic variant reported but specific DNA change no longer available.

Table S3. Antibodies used for flow cytometry.

Marker	Supplier	Panel	Dilution	
Annexin V APC	BioLegend	EB	5 in 100	
Lin APC	BioLegend	HSPC/EP	3 in 100	
CD71 FITC	Life Technologies	HSPC/EP	5 in 100	
CD10 APC	BioLegend	HSPC/EP	3 in 100	
CD45RA allophycocyanin efluor 780 (APC-ef780)	Life Technologies	HSPC/EP	2 in 100	
CD34 PeCy7	Life Technologies	HSPC/EP/EB	1 in 100	
CD41a efluor 450 (ef450)	Life Technologies	EP	2 in 100	
CD38 AF700	Life Technologies	HSPC/EP	1 in 100	
CD123 BV605	BD Biosciences	HSPC/EP	8 in 100	
CD90 peridinin- chlorophyll-protein complex efluor 710 (PerCP-ef710)	Life Technologies	HSPC	2 in 100	
CD14 FITC	Life Technologies	EB	5 in 100	
CD15 FITC	Life Technologies		5 in 100	
CD16 FITC	Life Technologies		5 in 100	
CD10 FITC	Life Technologies		5 in 100	
CD2 FITC	Life Technologies		5 in 100	
CD3 FITC	Life Technologies		5 in 100	
CD19 FITC	Life Technologies		5 in 100	
CD61 FITC	Life Technologies		5 in 100	
CD56 FITC	Life Technologies		EB and IFN- γ /TNF- α	5 in 100
CD14 AF467	BioLegend		IFN- γ /TNF- α	3 in 100
CD3 BV605	BioLegend	IFN- γ /TNF- α	3 in 100	

IFN- γ BV510	BioLegend	IFN- γ /TNF- α	5 in 100
TNF- α BV711	BioLegend	IFN- γ /TNF- α	5 in 100
CD71 APC	Life Technologies	EB and K562	3 in 100
GYP A ef450	Life Technologies	EB and K562	1 in 100
CD36 PerCPCy5.5	BioLegend	EP/EB	2 in 100
CD105 PE	BioLegend	EP/EB	2 in 100
Live dead Brilliant Violet 510 (BV510)	BD Biosciences	HSPC/EP	1 in 1000
GATA1 PE	Cell Signaling Technology	GATA1/2	2 in 100
GATA2 FITC	R&D systems	GATA1/2	5 in 100
GYP A BV421	BD Biosciences	GATA1/2 and IFN- γ /TNF- α	0.5 in 100
PE Rabbit IgG	Cell Signaling Technology	GATA1/2	2 in 100
FITC normal IgG	R&D systems	GATA1/2	5 in 100
CD71 AF647	Invitrogen	GATA1/2	3 in 100

Table S4. Antibodies used for scCyTOF.

Label	Antibody	Clone	Source Cat#
89Y	CD41	HIP8	Fluidigm 3089004B
141Pr	CD235a/GYPA	HIR2	Fluidigm 3141001B
143Nd	CD45RA	HI100	Fluidigm 3143006B
149Sm	CD34	581	Fluidigm 3149013B
155Gd	CD36	5-271	Fluidigm 3155012B
156Gd	GATA1	D24E4	NEB/CST 4589BF
161Dy	CD90	5E10	Fluidigm 3161009B
165Ho	Kruppel Like Factor 1 (KLF1)	1B6A3	LS-Bio LS-C191841
166Er	CD44	BJ18	Fluidigm 3166001B
168Er	CD71	OKT-9	Fluidigm 3168014B
170Er	Hemoglobin A (HBA)	012	Creative Diagnostics DCABH-8054
172Yb	CD38	HIT2	Fluidigm 3172007B

Table S5. TaqMan assays used for RT-PCR.

Gene	ID
<i>GAPDH</i>	Hs02786624_g1
<i>ZFP36L2</i>	Hs00272828_m1
<i>RPL11</i>	Hs00831112_s1 (exon 2) Hs04183527_g1 (exon 5)
<i>GYPA</i>	Hs00266777_m1